國立中央大學
National Central University

水文與海洋科學研究所
Institute of Hydrological and Oceanic Sciences

International Symposium on Grids and Clouds 2016
13-18 March 2016, Academia Sinica, Taipei, Taiwan

ISGC 2016
Ubiquitous e-infrastructures and Applications

THE APPLICATIONS OF ADVANCED NUMERICAL SIMULATION ON THE TSUNAMI AND FLOODING HAZARD MITIGATION

DATE: 3/13 SUNDAY
3F, BUILDING FOR HUMANITIES AND SOCIAL SCIENCES, ACADEMIA SINICA, TAIPEI, TAIWAN.
128 ACADEMIA ROAD, SECTION 2, NANKANG, TAIPEI 115, TAIWAN

Tso-Ren Wu,吳祚任

Associate Professor and Director 副教授兼所長

Graduate Institute of Hydrological and Oceanic Sciences 水海所

National Central University 國立中央大學

tsoren@ncu.edu.tw

Tsunami Science Laboratory

海 嘯 科 學 研 究 室
TSUNAMI SCIENCE LABORATORY

ASGC
TWGrid

Abstract

- Moving boulders in the are frequently observed in the nature disasters, such as tsunamis, storm surges, river floods, and landslides. Resulted in violent impinging forces on the structures and sever local scours. The keys of the successful simulation are the technique that is able to solve the solid and fluid motions simultaneously, with the ambient fluids behave as high viscous non-Newtonian Bingham flows.
- In this presentation, we shall focus the discussions on solving the 3D Navier-Stokes (NS) equations with newly developed Discontinuous Bingham Fluid (DBM) model and two-way coupled moving-solid algorithm. The volume-of-fluid (VOF) method with Piecewise Linear Interface Calculation (PLIC) technique is adopted to describe the multiple phases in the fluids. Validations and Examples will be presented and discussed.

2011 Tōhoku earthquake and tsunami

（陳慧慈，2011）

Motivation
Huge Tsunami Scour Hole around the Buildings

Serious scouring problem during the tsunami inundation (Photo by Prof. Philip Liu)

Motivation
Tsunami Boulders were found in the Southern Taiwan

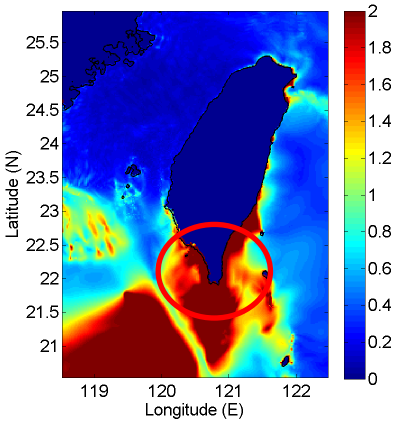

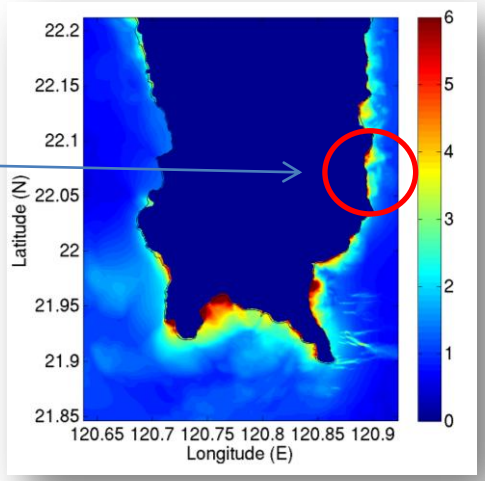

Motivation

One of the boulders is in a huge scour hole

The broken coral boulder implies an originally much bigger size and higher tsunami wave height

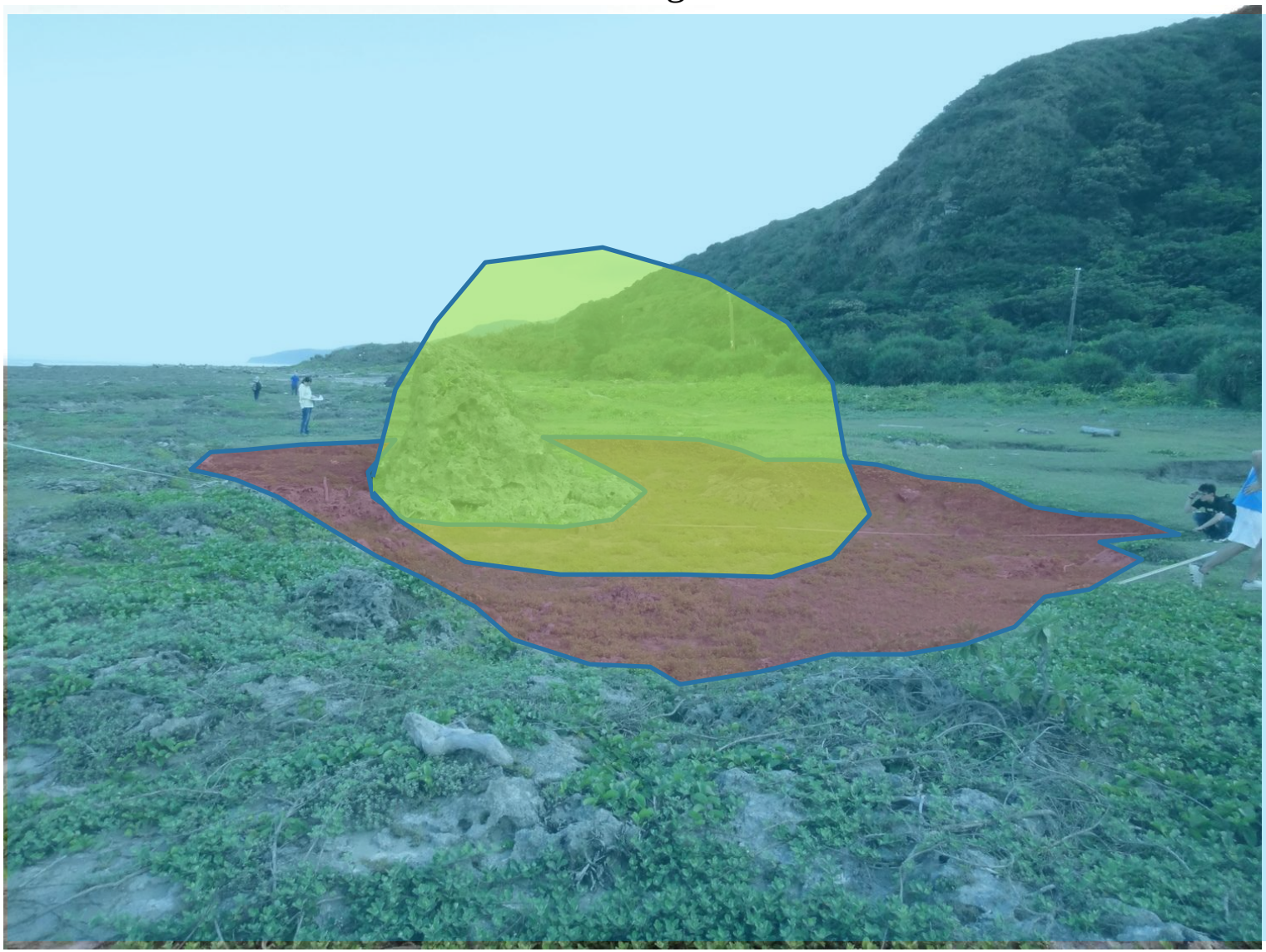

The failure of Shuang-Yuan Bridge in the event of 2009 Typhoon Morakot.

The undular waves indicate the soft reverbed and sever local scour around the bridge piles.

2009 莫拉克颱風強烈水流導致雙園橋斷裂

波狀水躍暗示床質鬆軟及橋墩周圍沖刷

Features of flood and boulder transportation

1. Because both Reynolds number and Froude number are involved, only 1:1 scale can be used. In other words, only numerical model is feasible.
2. Challenges:
    1. Breaking wave: VOF
    2. Turbulence: LES
    3. Drifting obstacles: Moving Solid
    4. Scouring: Discontinuous Bi-viscous Model
    5. Large and small scale tsunami modeling: COMCOT Coupling

Breaking wave modeling, Splash3D (史百力士3D)

We adopted the Splash3D numerical model to solve for the breaking wave problems (Wu, 2004; Liu et al., 2005). This model solves 3-dimensional incompressible flow with Navier-Stokes equations. The free-surface is tracked by Volume-of-Fluid (VOF) method. The domain is discretized by finite volume method (FVM). The turbulent effect is closed by large eddy simulation (LES) with Smagorinsky model.

Incompressible continuity equation:

$$\nabla \cdot \boldsymbol{u} = 0$$

Navier-Stokes Equation

$$\frac{\partial(\boldsymbol{u})}{\partial t} + \nabla \cdot (\boldsymbol{uu}) = -\frac{1}{\rho}\nabla P + \frac{1}{\rho}\nabla \cdot \tilde{\tau} + \boldsymbol{g} + \boldsymbol{F}_0$$

Splash: 飛濺

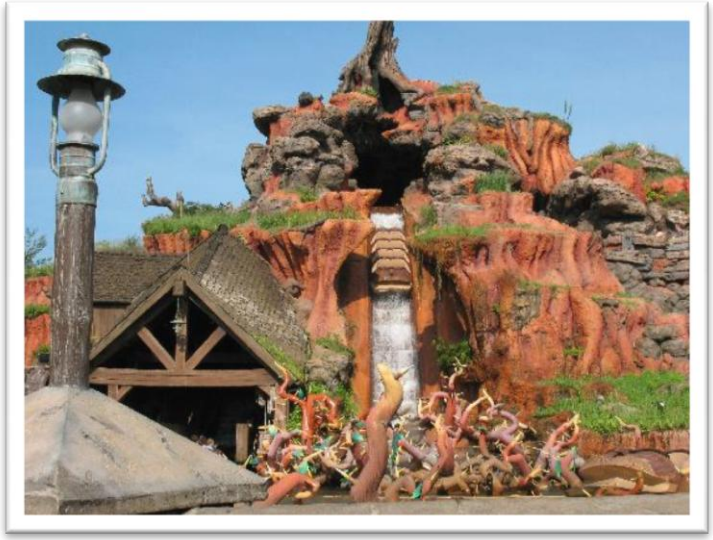

Disney Splash Mountain
迪士尼 史百力士山

$$\frac{\partial \rho}{\partial t} + \nabla \cdot (\rho \mathbf{u}) = 0$$

$$\frac{\partial (\rho \mathbf{u})}{\partial t} + \nabla \cdot (\rho \mathbf{u}\mathbf{u}) = -\nabla p + \nabla \cdot \tilde{\tau} + \mathbf{f}_B + \mathbf{f}_S + \mathbf{f}_D$$

$\mathbf{u}$ represents velocity, ρ density, p pressure, $\tilde{\tau}$ the shear stress tensor, $\mathbf{f}_B$ any body forces, and $\mathbf{f}_S$ any surface forces. $\mathbf{f}_D$ is a drag force used to describe flow in the presence of a diffuse solid boundary.

As we assume fluids to be Newtonian:

$$\tilde{\tau} = \mu(\nabla \mathbf{u} + \nabla^T \mathbf{u}) \tag{3.3}$$

Our implementation is on an unstructured hexahedral mesh, with the primary variables $\mathbf{u}$ and p located at cell centers. To assess solenoidality, we also calculate a velocity field $\mathbf{u}_f$ at cell face centroids.

As described above, we discretize Equation 3.2 to first order in time, and by introducing an interim "predicted" velocity $\mathbf{u}^\star$, divide the resulting equation in two:

$$\frac{\rho^{n+1}\mathbf{u}^\star - \rho^n\mathbf{u}^n}{\Delta t} = -\nabla\cdot(\rho\mathbf{u}\mathbf{u})^n + \nabla\cdot(\mu^{n+1}(\nabla\mathbf{u} + \nabla^T\mathbf{u})) + \mathbf{f}_S^{n+1} + \mathbf{f}_D^{n+1} - \nabla P^n + \mathbf{f}_B^n \tag{3.50}$$

$$\frac{\rho^{n+1}\mathbf{u}^{n+1} - \rho^{n+1}\mathbf{u}^\star}{\Delta t} = -\nabla\delta P^{n+1} + \mathbf{f}_B^{n+1} - \mathbf{f}_B^n \tag{3.51}$$

Equation 3.51 relates $\mathbf{u}^{n+1}$ to $\mathbf{u}^\star$; combining Equation 3.51 with Equation 3.12 yields:

$$\nabla\cdot\frac{\nabla\delta P^{n+1}}{\rho^{n+1}} = \nabla\cdot\left(\frac{\mathbf{u}^\star}{\Delta t}\right) \tag{3.62}$$

We solve Equation 3.62 for δP^{n+1} (using the techniques of Appendix C), and complete the timestep by evaluating $\mathbf{u}^{n+1}$ via Equation 3.51.

Divergences are calculated by summing over cell faces, and $\nabla\delta P_f$ is calculated from a stencil corresponding to that of the density interpolation to faces. Equation 3.51 is then used to calculate a solenoidal (to the precision required by the projection solution) face velocity field:

$$\mathbf{u}_f^{n+1} = \mathbf{u}_f^\star - \Delta t\left(\frac{\nabla\delta P_f^{n+1}}{\rho_f^{n+1}}\right) \tag{3.63}$$

3.2.1.1 Representing the Interface with Volume Fractions.

We solve Equation 3.1 for ρ^{n+1} using $\mathbf{u}_f^n$. We begin by defining a volume fraction f_k as the fraction of a cell volume V occupied by fluid k:

$$f_k = V_k / V \tag{3.13}$$

A cell density is related to the volume fractions via:

$$\rho = \sum f_k \rho_k \tag{3.14}$$

and Equation 3.1 may then be written as:

$$\frac{\partial (f_k \rho_k)}{\partial t} + \nabla \cdot (f_k \rho_k \mathbf{u}) = 0 \tag{3.15}$$

Since each ρ_k is constant, we obtain an evolution equation for the f_k:

$$\frac{\partial f_k}{\partial t} + \nabla \cdot (f_k \mathbf{u}) = 0 \tag{3.16}$$

Our volume tracking algorithm seeks discrete numerical solutions to

$$\frac{\partial f_k}{\partial t} + \mathbf{u} \cdot \nabla f_k = -f_k \nabla \cdot \mathbf{u} = 0\,, \tag{3.17}$$

where $\mathbf{u}$ is the flow velocity and f_k is the volume fraction of material k. (The final equality only holds in fluid regions that include no "void" material as described below, because the velocity field is not required to

be solenoidal in the vicinity of void.) Here we invoke a one-field approximation, as derived in [8]. Since f_k delineates the presence (or absence) of each fluid, f_k serves as a Heaviside function H for each material k. Equation 3.17 is therefore an evolution equation for the location of each fluid, with the volume fractions f_k discretely approximating H. The volume fractions f_k are bounded by $0 \leq f_k \leq 1$, where

$$f_k = \begin{cases} 1, & \text{inside fluid } k\,; \\ > 0, < 1, & \text{at the fluid } k \text{ interface}\,; \\ 0, & \text{outside fluid } k\,. \end{cases} \tag{3.18}$$

Since fluid volumes are volume-filling, volume fractions must sum to unity, $\sum_k f_k = 1$, throughout the domain. In seeking solutions to Equation 3.17, fluid *volumes* are marched forward in time as solutions to the volume integral of Equation 3.17 [10].

Volume of Fluid (VOF) method

The fluid density is presented in fluid fraction, and the transport equation is used to describe the fluid movement.

$$\frac{\partial \rho_m}{\partial t} + \nabla \cdot (\rho_m \boldsymbol{u}) = \frac{\partial \rho_m}{\partial t} + \boldsymbol{u}\frac{\partial \rho_m}{\partial x} + \boldsymbol{v}\frac{\partial \rho_m}{\partial y} + \boldsymbol{w}\frac{\partial \rho_m}{\partial z} = 0$$

$$\rho = \sum_m f_m \rho_m^0$$

$$\frac{\partial f_m}{\partial t} + \nabla(\boldsymbol{u}_i f_m) = 0$$

Piecewise linear interface calculation (PLIC)

$$\vec{N} \cdot \vec{x}_p - C_p = 0$$

$$F(C_p) = V_{tr}(C_p) - f_m * \forall \approx 0$$

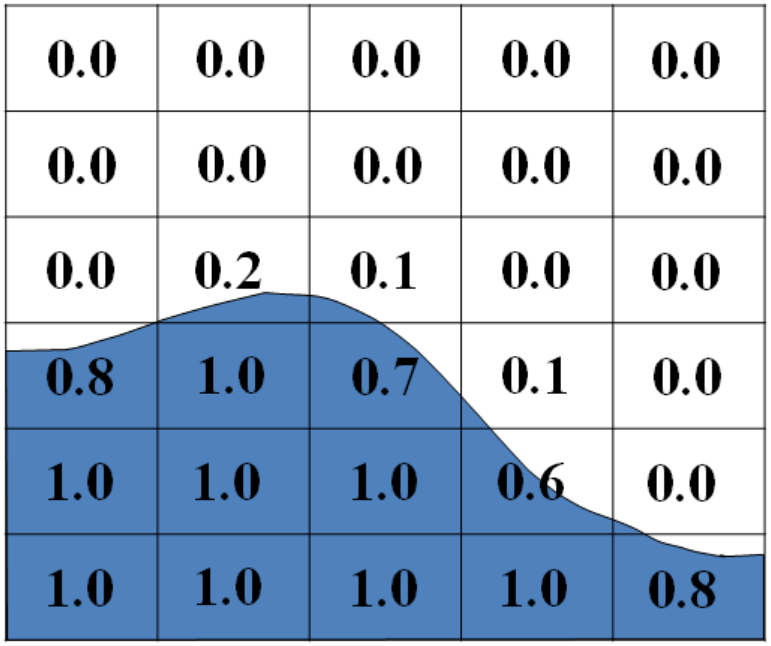

DEM and LiDAR topography input module and COMCOT boundary coupling module

DEM input

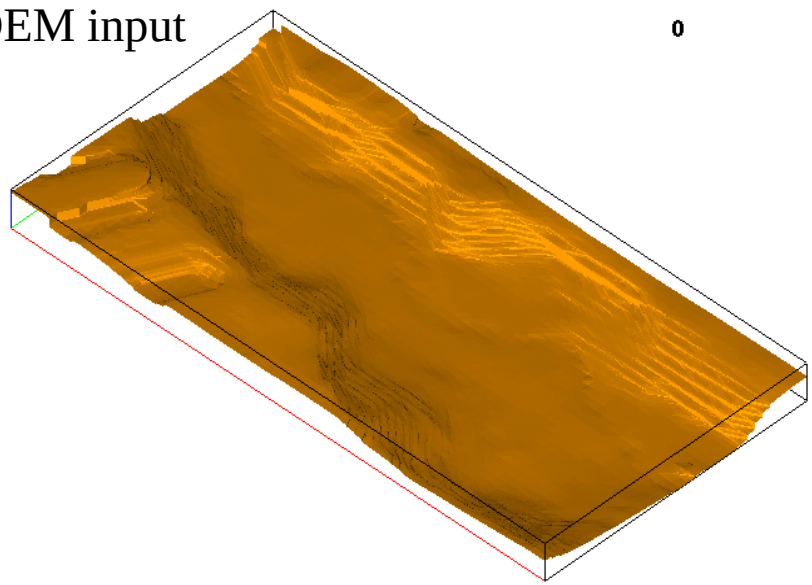

Topography of Toce River Valle

Partial-Cell treatment

$$\forall_{eff} = (1 - f_{solid})\forall = \theta\forall$$

$$\partial\frac{(\theta f_m)}{\partial t} + \nabla\cdot(\theta f_m V) = 0$$

LiDAR input

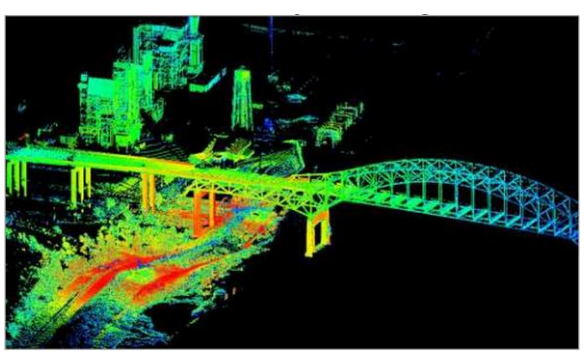

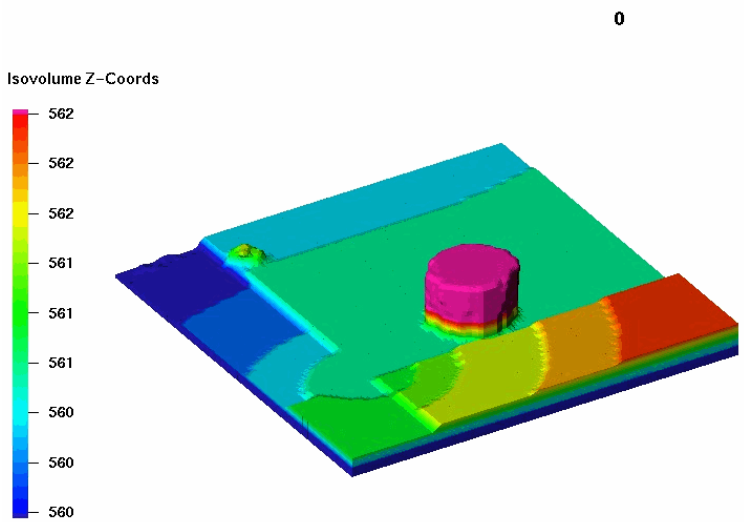

LES (Large Eddy Simulation) Filtering

A low-pass filtering operation is performed so that the resulting filtered velocity can be adequately resolved on a relatively coarse grid.

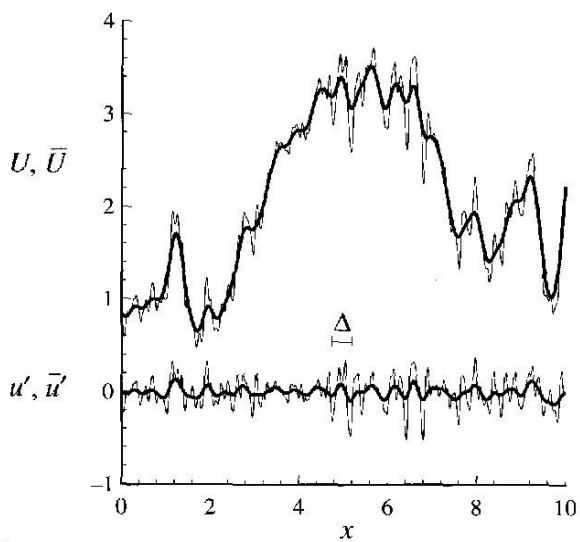

Fig. 13.2. Upper curves: a sample of the velocity field $U(x)$ and the corresponding filtered field $\bar{U}(x)$ (bold line), using the Gaussian filter with $\Delta \approx 0.35$. Lower curves: the residual field $u'(x)$ and the filtered residual field $\overline{u'(x)}$ (bold line).

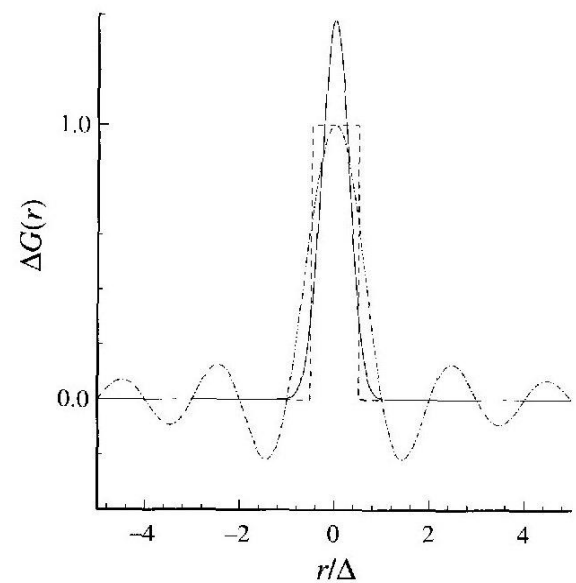

Fig. 13.1. Filters $G(r)$: box filter, dashed line; Gaussian filter, solid line; sharp spectral filter, dot dashed line.

Δ : the filter width

η : the radius

Filtered Conservation Equations

- Continuity equation:

$$\overline{\left(\frac{\partial U_i}{\partial x_i}\right)} = \frac{\partial \overline{U}_i}{\partial x_i} = 0$$

$$\frac{\partial u_i'}{\partial x_i} = \frac{\partial}{\partial x_i}\left(U_i - \overline{U}_i\right) = 0$$

- Conservation of Momentum:

$$k_r \equiv \frac{1}{2}\tau_{ii}^R$$

$$\tau_{ij}^r \equiv \tau_{ij}^R - \frac{2}{3}k_r\delta_{ij}$$

the anisotropic residual-stress tensor is:

$$\tau_{ij}^r \equiv \tau_{ij}^R - \frac{2}{3}k_r\delta_{ij}$$

$$\overline{p} \equiv \overline{P} + \frac{2}{3}k_r$$

$$\frac{\partial \overline{U}_j}{\partial t} + \frac{\partial \overline{U_i U_j}}{\partial x_i} = \nu \frac{\partial^2 \overline{U}_j}{\partial x_i \partial x_i} - \frac{1}{\rho}\frac{\partial \overline{P}}{\partial x_j}$$

$$\because \overline{U_i U_j} \neq \overline{U}_i \overline{U}_j$$

$$\text{Let } \tau_{ij}^R \equiv \overline{U_i U_j} - \overline{U}_i \overline{U}_j$$

$$\frac{\overline{D}\,\overline{U}_j}{\overline{D}t} = \nu \frac{\partial^2 \overline{U}_j}{\partial x_i \partial x_i} - \frac{1}{\rho}\frac{\partial \overline{p}}{\partial x_j} - \frac{\partial \tau_{ij}^r}{\partial x_i}$$

$$\text{where } \frac{\overline{D}}{\overline{D}t} \equiv \frac{\partial}{\partial t} + \overline{\mathbf{U}} \cdot \nabla$$

Smagorinsky Model

$$\tau_{ij}^{r} = -\nu_t \left(\frac{\partial \bar{u}_i}{\partial x_j} + \frac{\partial \bar{u}_j}{\partial x_i} \right) = -2\nu_t \bar{S}_{ij}$$

$$\nu_t = \ell_S^2 \bar{\mathbf{S}} = (C_S \Delta)^2 \bar{\mathbf{S}}$$

ℓ_S : Smagorinsky length scale

C_S : Smagorinsky coefficient

Δ : filter width

$$\bar{\mathbf{S}} \equiv \left(2\bar{S}_{ij} \bar{S}_{ij} \right)^{1/2}$$: the characteristic filtered rate of strain

$$\Delta = (\Delta x_1 \times \Delta x_2 \times \Delta x_3)^{1/3}$$

Model Validation 1: Dam-break bore impinging a square cylinder

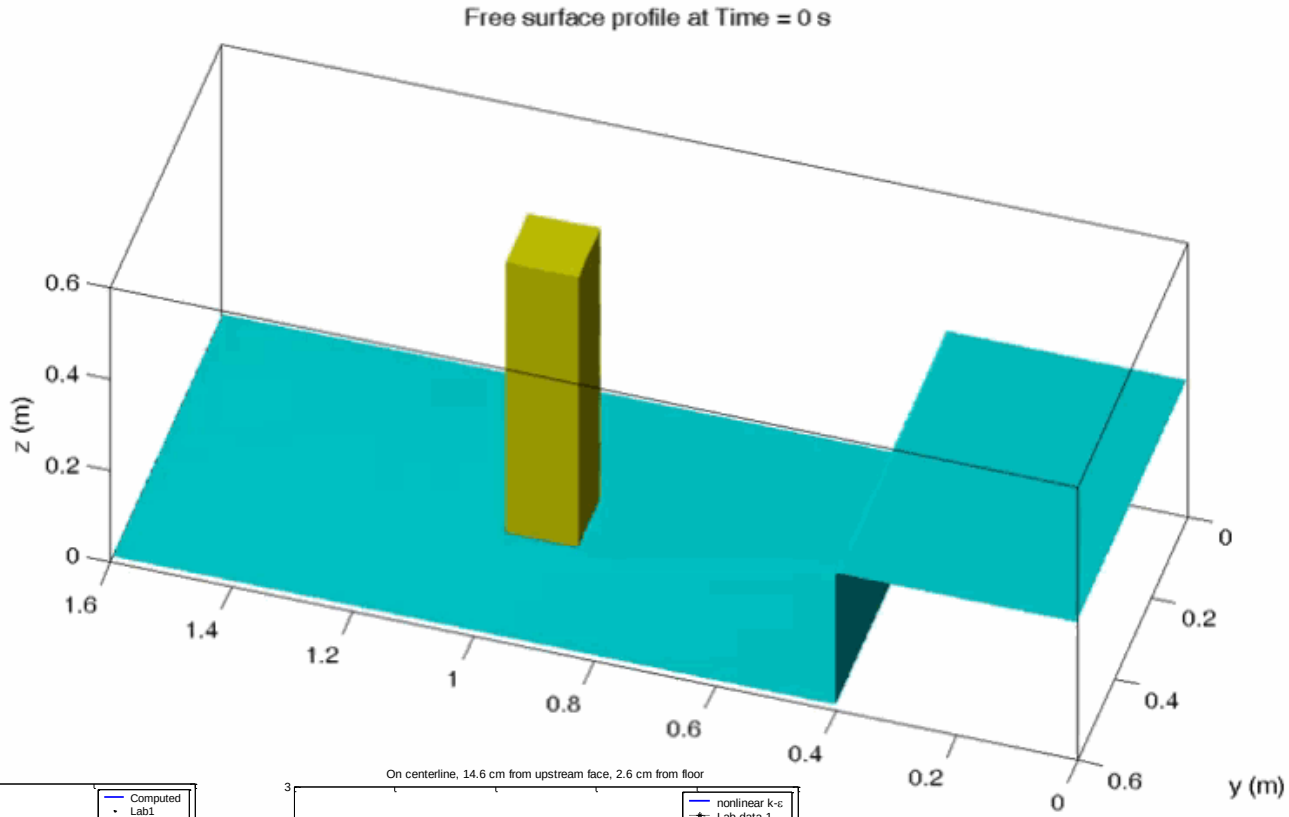

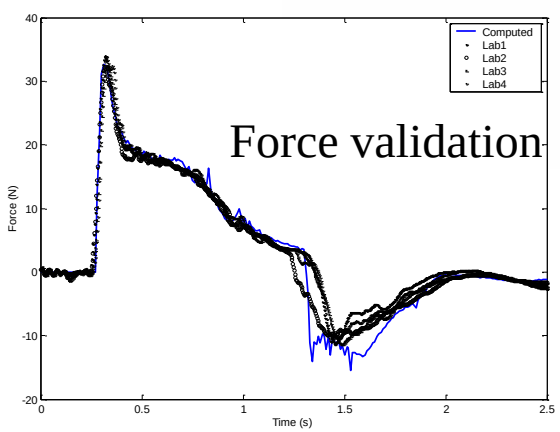

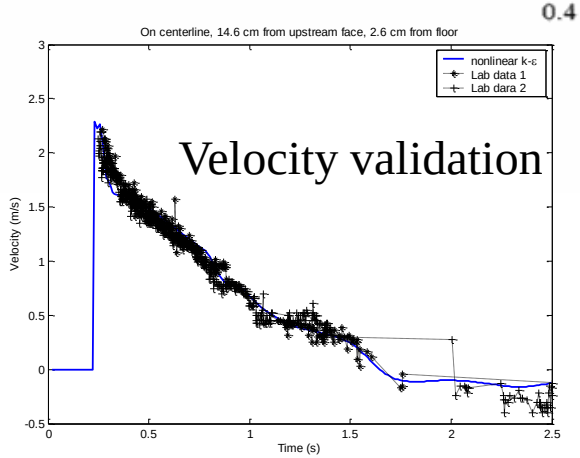

Pollutants

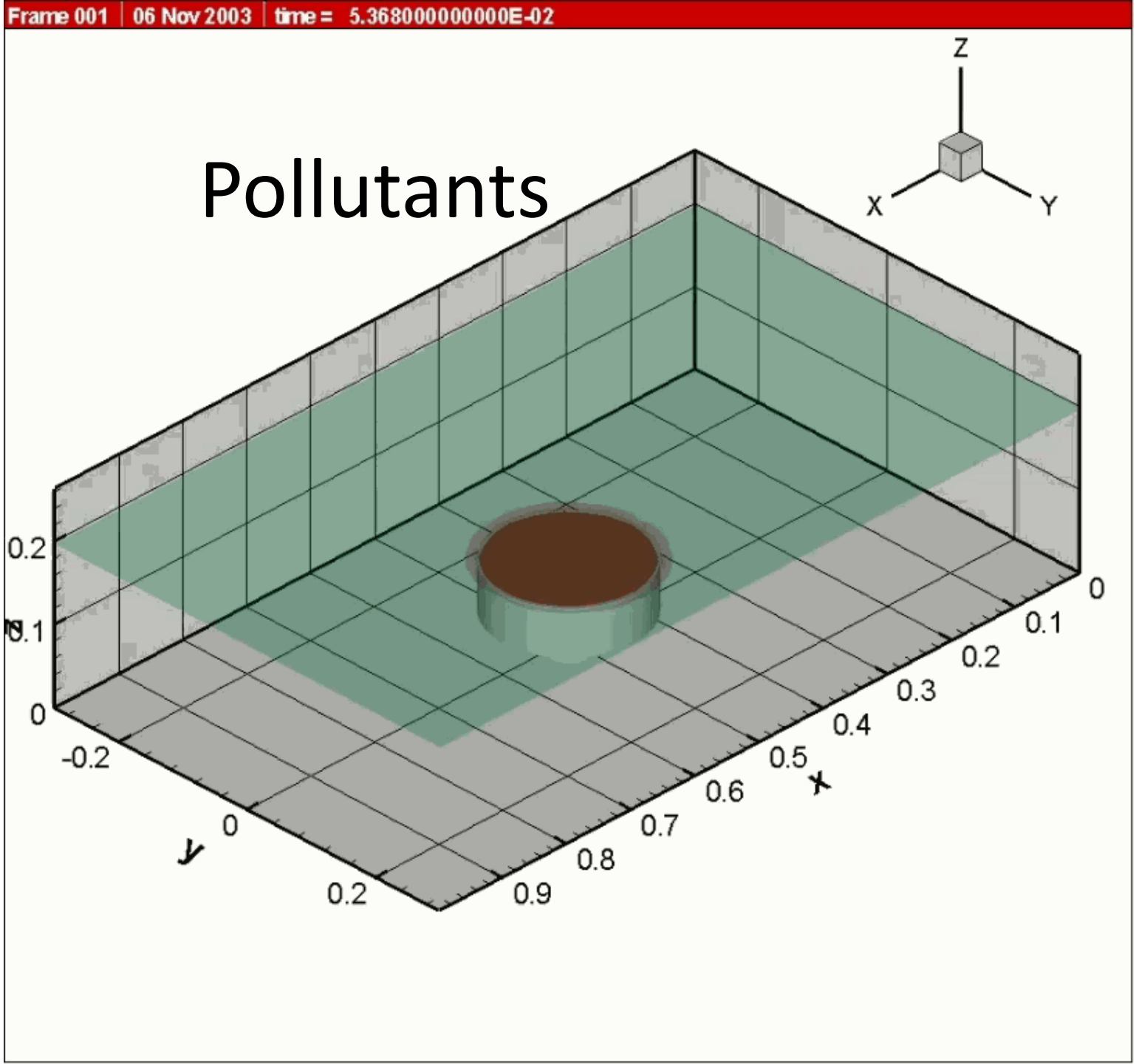
Frame 001 | 06 Nov 2003 | time = 5.368000000000E-02
Z
X
Y
0.2
0.1
0
-0.2
0
0.2
y
0
0.1
0.2
0.3
0.4
0.5
0.6
0.7
0.8
0.9
x

Wave + Current + Truss
Surface Elevation and Dynamic Pressure

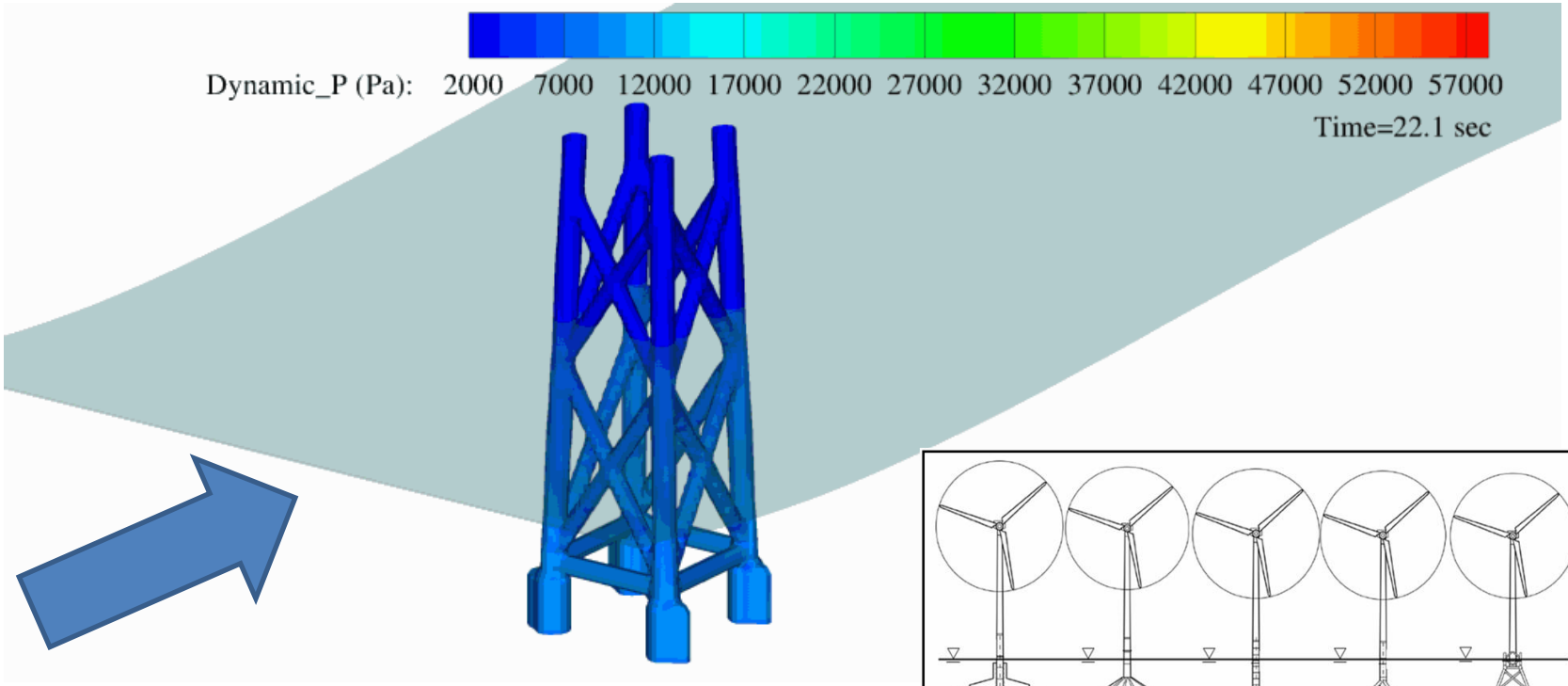

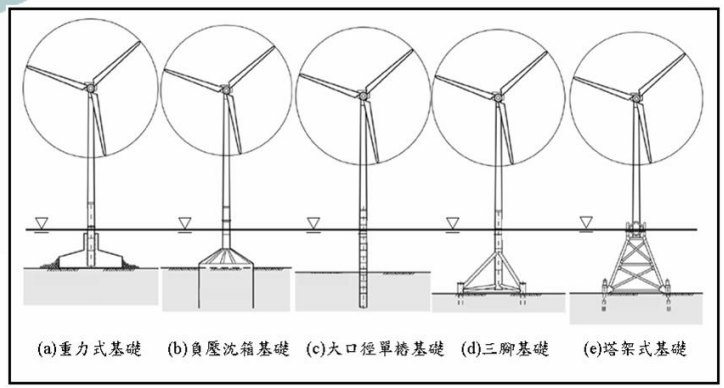

Surface Velocity Magnitude

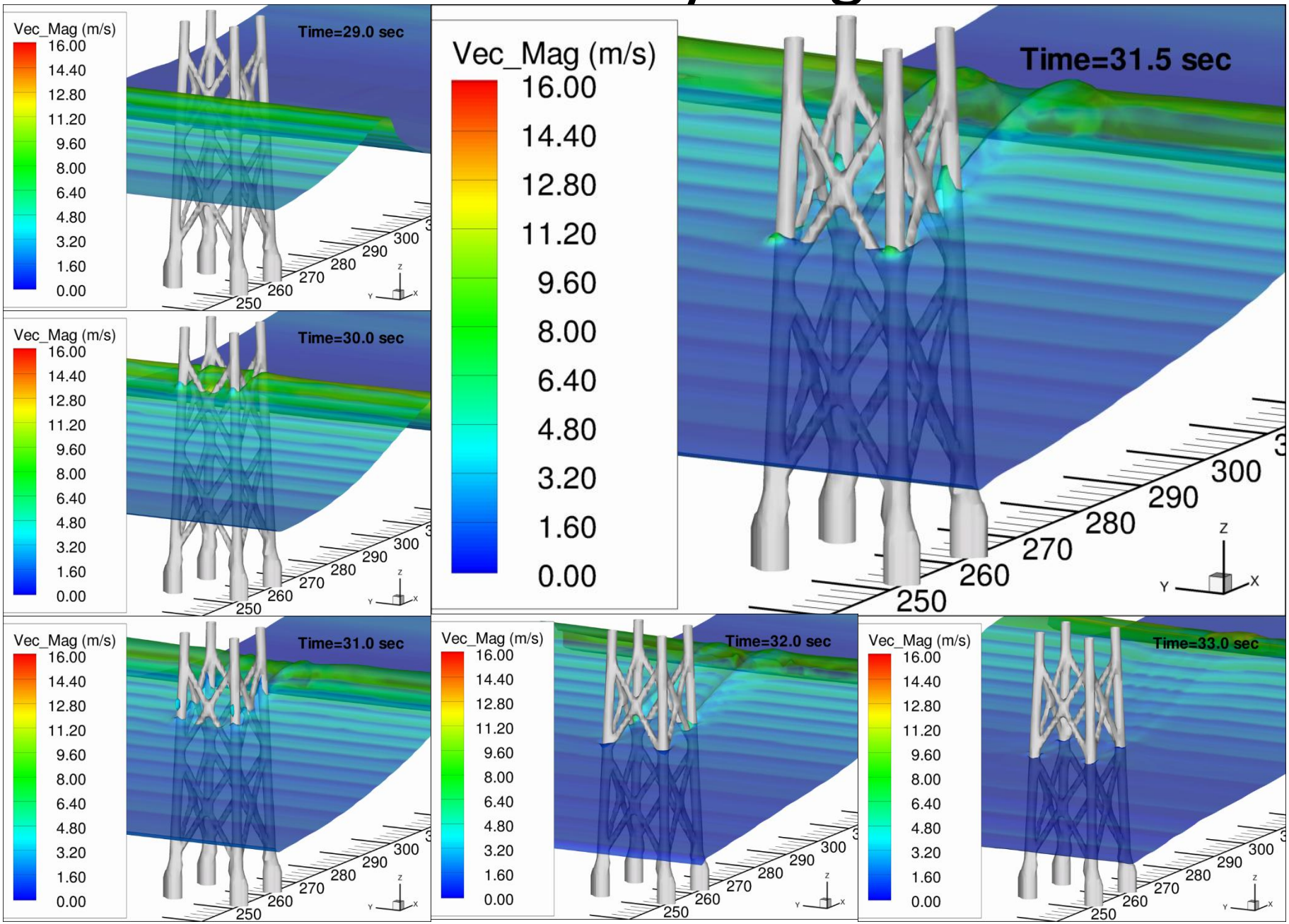

Application: Sloshing Problem

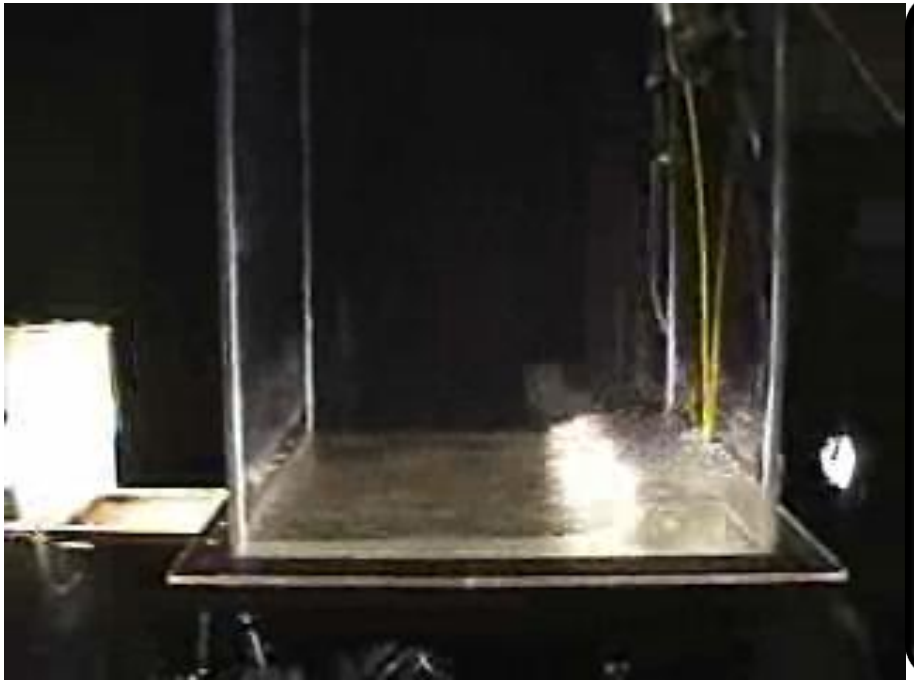

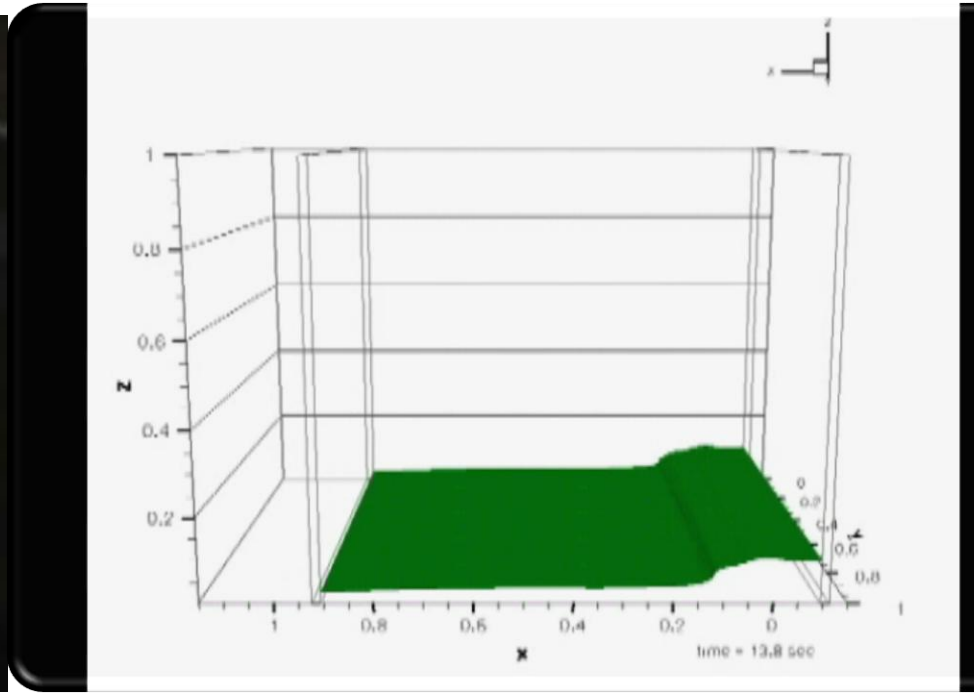

Sloshing Problem

2015 Nepal Earthquake, Swimming pool.

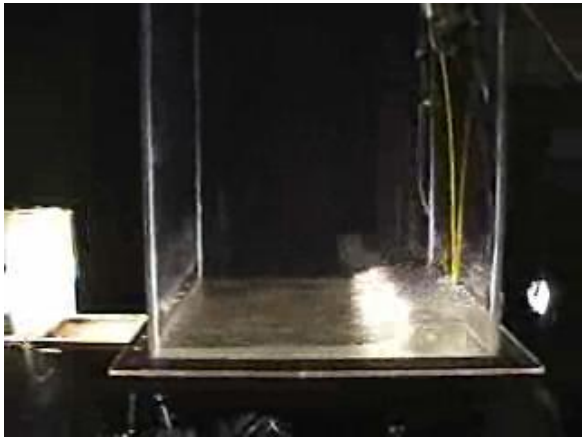

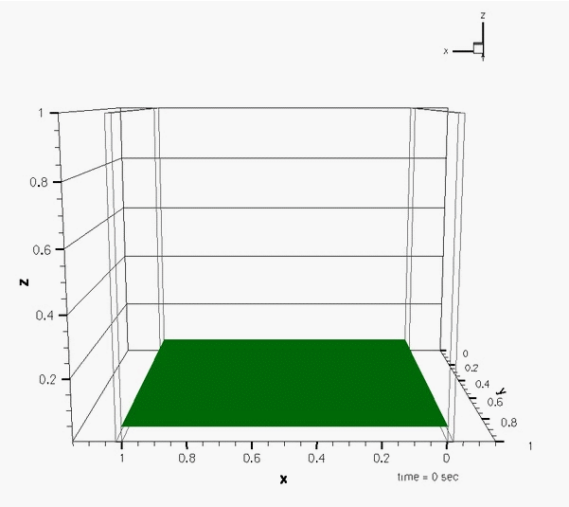

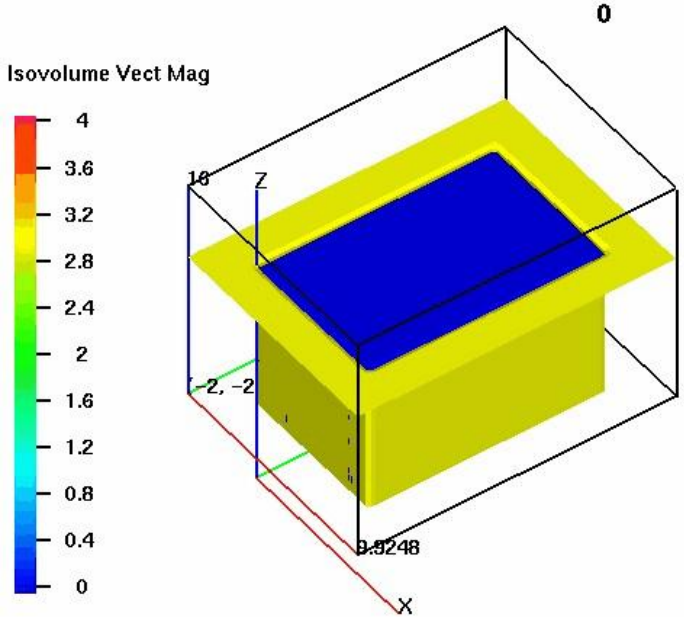

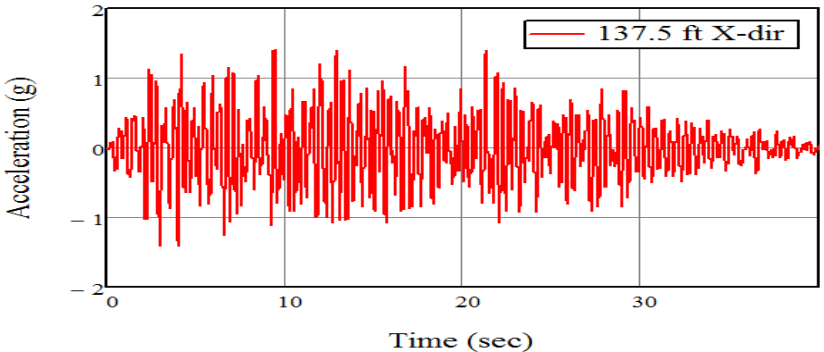

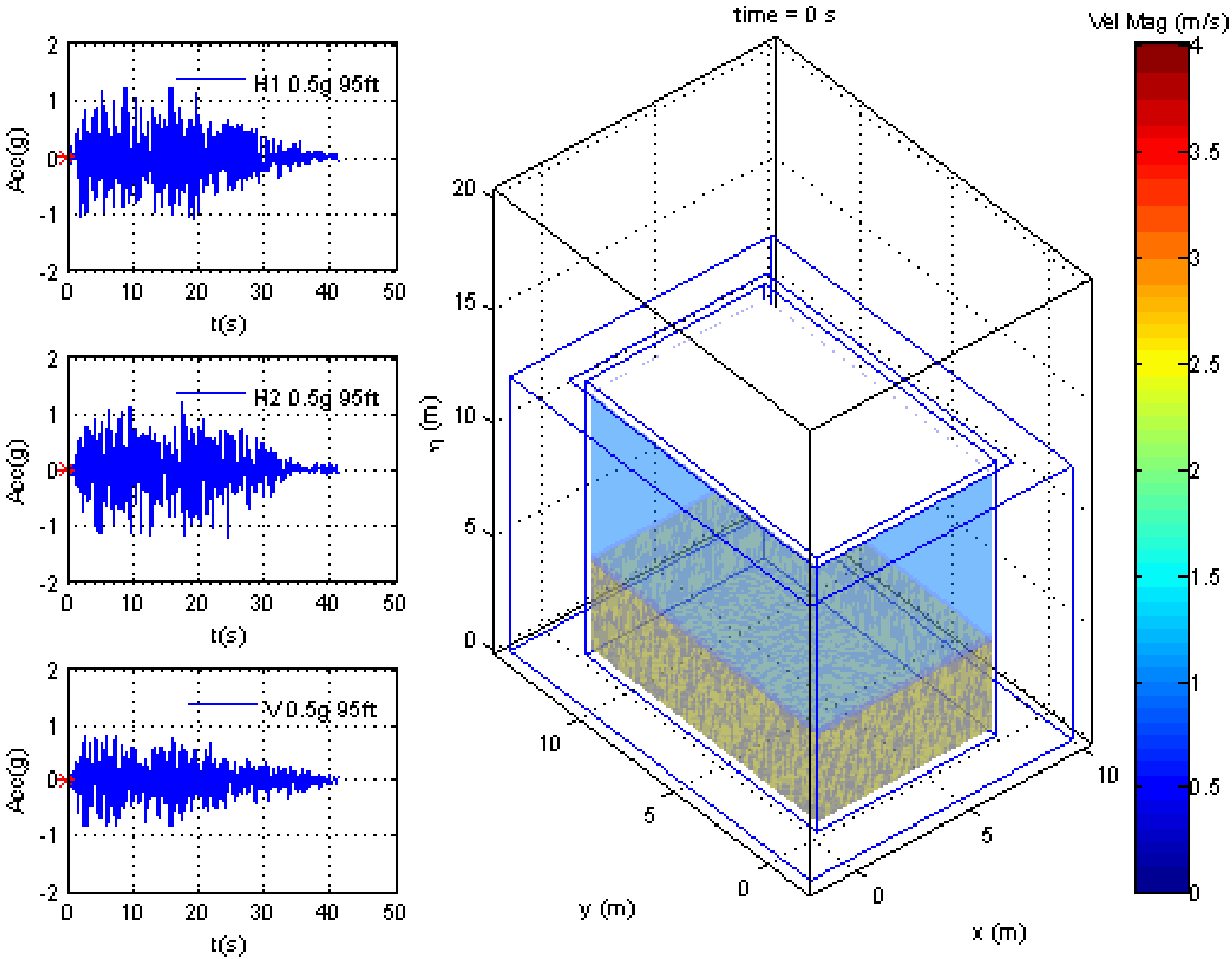
H1 0.5g 95ft
H2 0.5g 95ft
V 0.5g 95ft
Acc(g)
t(s)
time = 0 s
Vel Mag (m/s)
η (m)
y (m)
x (m)

Potential tsunami impact on the Nuclear Power Plant (NPP) No.3 in Taiwan.

Splash3D Coupled with the result of 2D COMCOT tsunami model

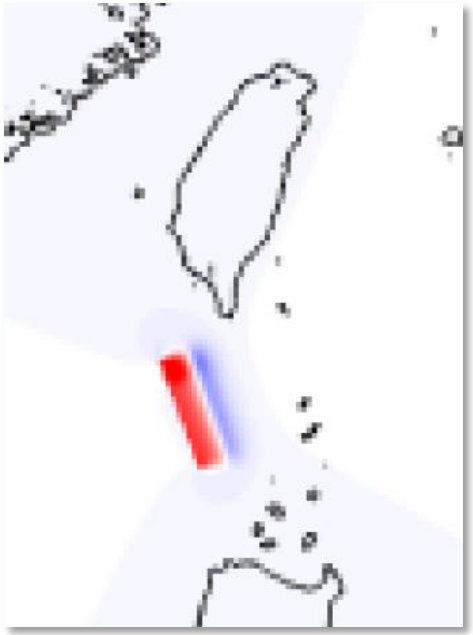

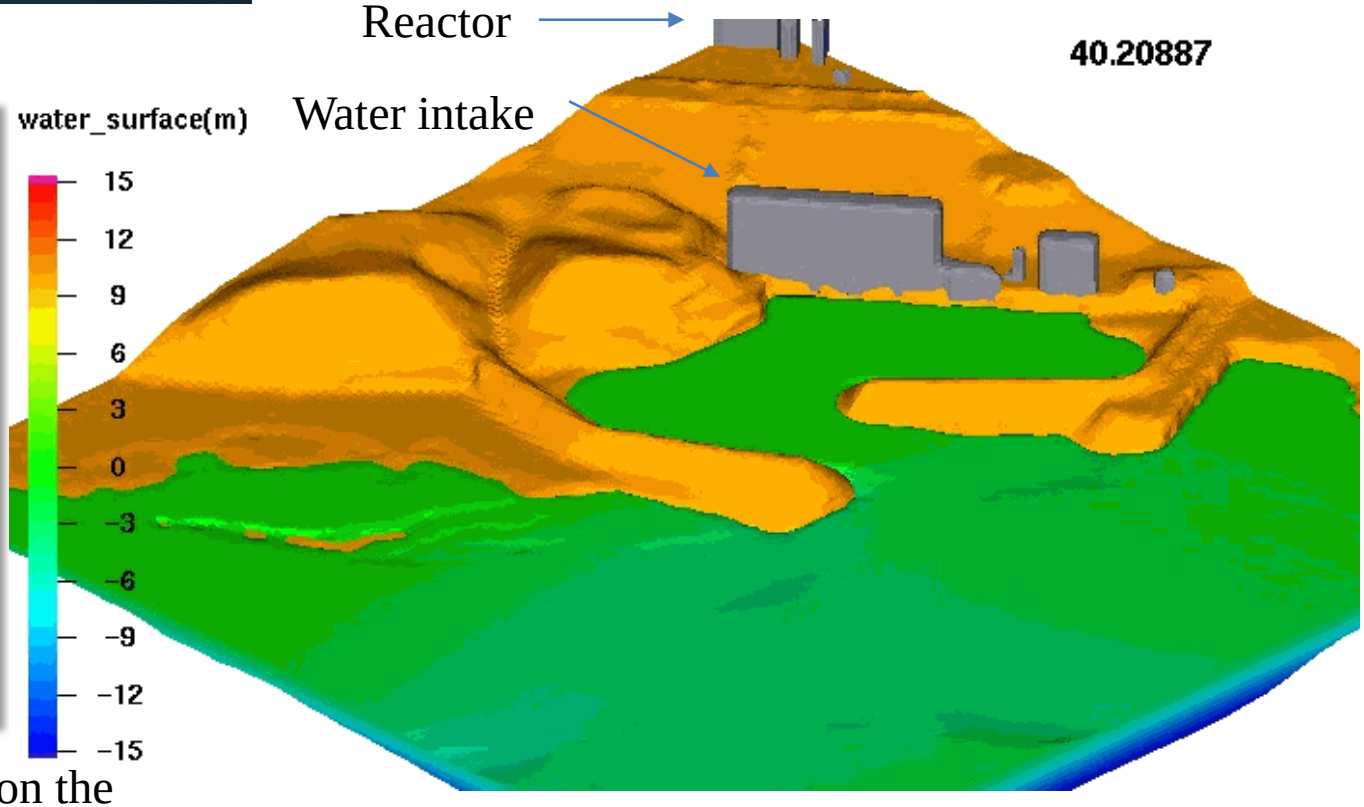

Scenario tsunami source on the northern Manila Trench

E-IBM (Efficient Immersed Boundary Method)

$$\frac{\partial \rho}{\partial t} + \nabla \cdot (\rho \mathbf{u}) = 0$$

$$\frac{\partial (\rho \mathbf{u})}{\partial t} + \nabla \cdot (\rho \mathbf{u}\mathbf{u}) = -\nabla P + \nabla \cdot \tilde{\tau} + \mathbf{f}_B$$

$$\frac{\rho^{n+1}\mathbf{u}^* - \rho^{n+1}\mathbf{u}^*}{\Delta t} = -\nabla \cdot (\rho \mathbf{u}\mathbf{u})^n - \nabla P^n + \nabla \cdot \left(\mu^{n+1}\left(\nabla \mathbf{u} + \nabla^{\mathrm{T}}\mathbf{u}\right)\right) + \mathbf{f}_B^n$$

$$\frac{\rho^{n+1}\mathbf{u}^{**} - \rho^{n+1}\mathbf{u}^*}{\Delta t} = -\nabla \delta P^{**} + \mathbf{f}_B^{n+1} - \mathbf{f}_B^n$$

$$\nabla \cdot \frac{\nabla \delta P^{**}}{\rho^{n+1}} = \nabla \cdot \left(\frac{\mathbf{u}^*}{\Delta t} + \frac{\mathbf{f}_B^{n+1}}{\rho^{n+1}} - \frac{\mathbf{f}_B^n}{\rho^{n+1}} \right)$$

$$\mathbf{u}^{**} = \mathbf{u}^* - \Delta t \left(\frac{\nabla \delta P^{**} - \mathbf{f}_B^{n+1} + \mathbf{f}_B^n}{\rho^{n+1}} \right)$$

Loop until $\left(\mathrm{abs}\left(\mathbf{u}^{n+1} - \mathbf{u}_s\right) < \mathrm{tolerance}\right)$

$$\mathbf{f}_s^{n+1} = \rho^{n+1} \left(\frac{\mathbf{u}_s^{n+1} - \mathbf{u}^{**}}{\Delta t} \right)$$

$$\frac{\rho^{n+1}\mathbf{u}^{n+1} - \rho^{n+1}\mathbf{u}^{**}}{\Delta t} = -\nabla \delta P^{n+1} + \mathbf{f}_B^{n+1} - \mathbf{f}_B^n + \mathbf{f}_s^{n+1}$$

$$\nabla \cdot \frac{\nabla \delta P^{n+1}}{\rho^{n+1}} = \nabla \cdot \left(\frac{\mathbf{u}^{**}}{\Delta t} + \frac{\mathbf{f}_B^{n+1}}{\rho^{n+1}} - \frac{\mathbf{f}_B^n}{\rho^{n+1}} + \frac{\mathbf{f}_s^{n+1}}{\rho^{n+1}} \right)$$

$$\mathbf{u}^{n+1} = \mathbf{u}^{**} - \Delta t \left(\frac{\nabla \delta P^{n+1} - \mathbf{f}_B^{n+1} + \mathbf{f}_B^n - \mathbf{f}_s^{n+1}}{\rho^{n+1}} \right)$$

End Loop

Pressure Integration

- Considering non-streamline obstacles, the normal force (Pressure force) is one or two order of magnitudes greater than the shear stress on obstacle. The obstacle shear stress can be ignored.
- Sum the pressure force on the solid surface to obtain the net force on the solid.
- The virtual pressure sensor (VPS) arrays are installed on each solid surface.

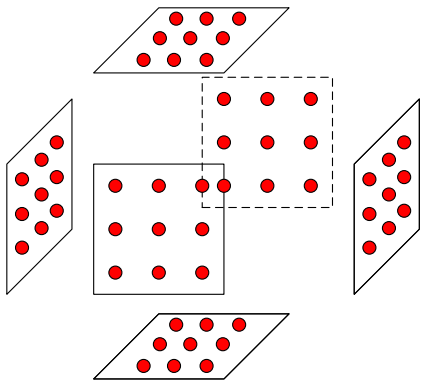

VPS arrays are installed on each solid surface

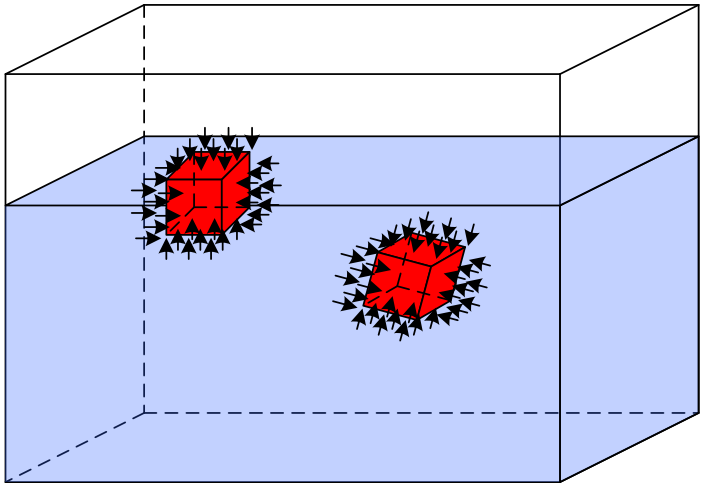

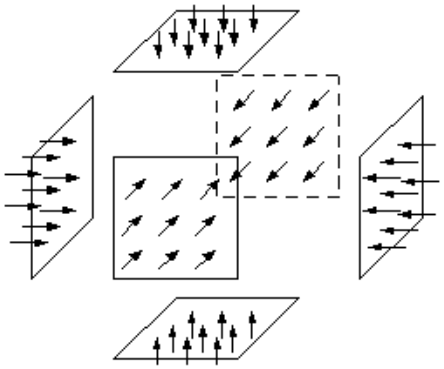

Surface pressure can be obtained from VPS arrays

Floating Obstacle

Numerical setup of the floating bodies.

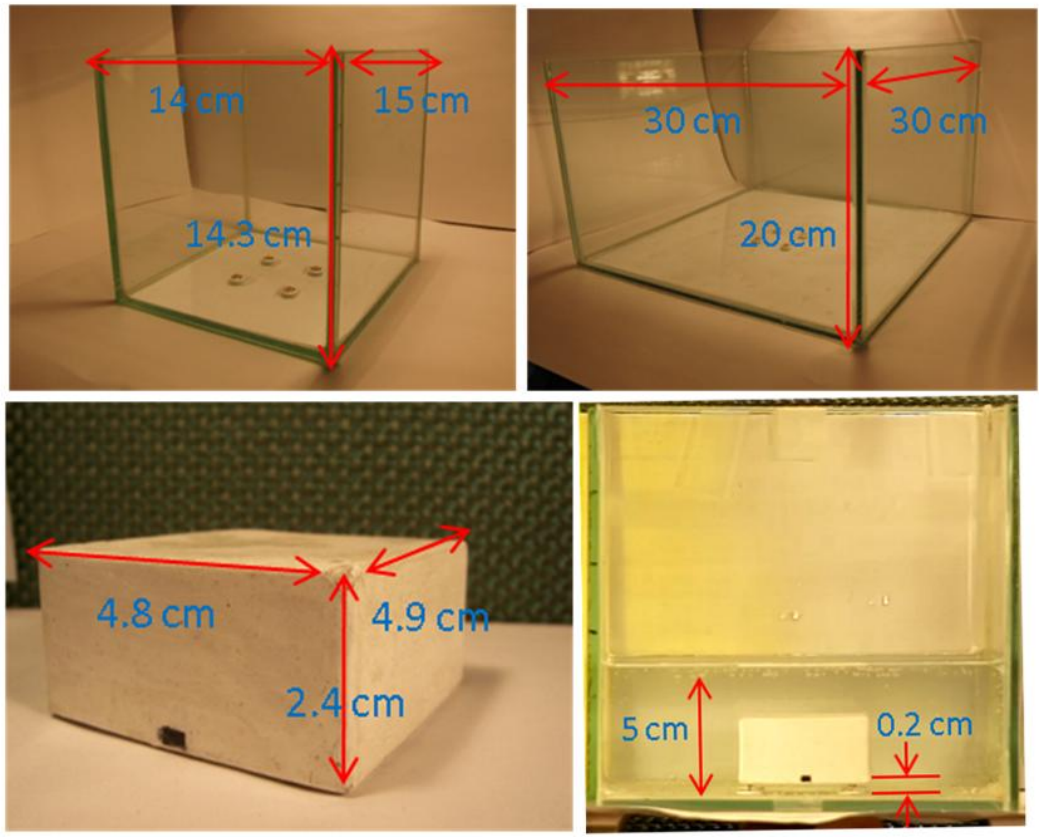

tank size (cm)	14 x 15	30 x 30
cell	45 x 42 x 28	55 x 55 x 28
coordinate (cm)	X (0.0, 15.0) Y (0.0, 14.0) Z (0.0, 7.0)	X (0.0, 30.0) Y (0.0, 30.0) Z (0.0, 7.0)
Simulation time	1.2 sec	
Calculation time (CPU time)	0.17 hours	1.5 hours

The photos with dimension of the small tank (upper left) and the large tank (upper right). The floating box is made of wood (lower right). A small black dot is painted on it to trace the floating trajectory. The still water depth is 5 cm. The box is initially elevated 0.2 cm by four pins. (Lower left).

Simulation on a Floating Obstacle

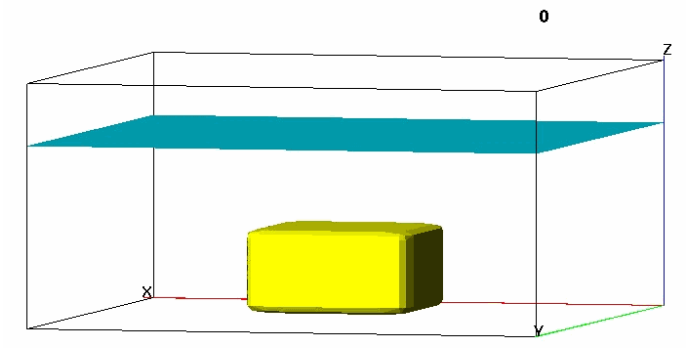

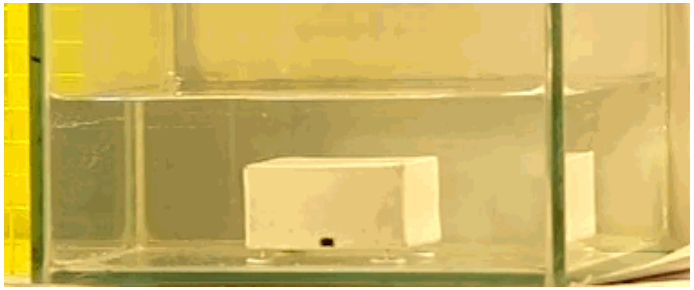

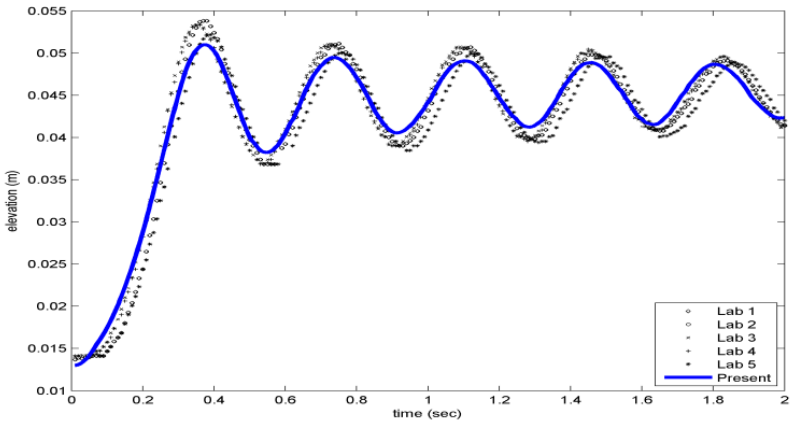

（莊美惠製）

- 渠槽大小：15 × 14 cm、30 × 30 cm
- 網格大小：0.33 × 0.33 × 0.25 cm
- 楔形體：4.8 × 4.9 × 2.4 cm
- 變動條件：渠槽大小

Rotation: the Magnus Effect

$$\omega_y = 100 \ \left(rad/s\right)$$

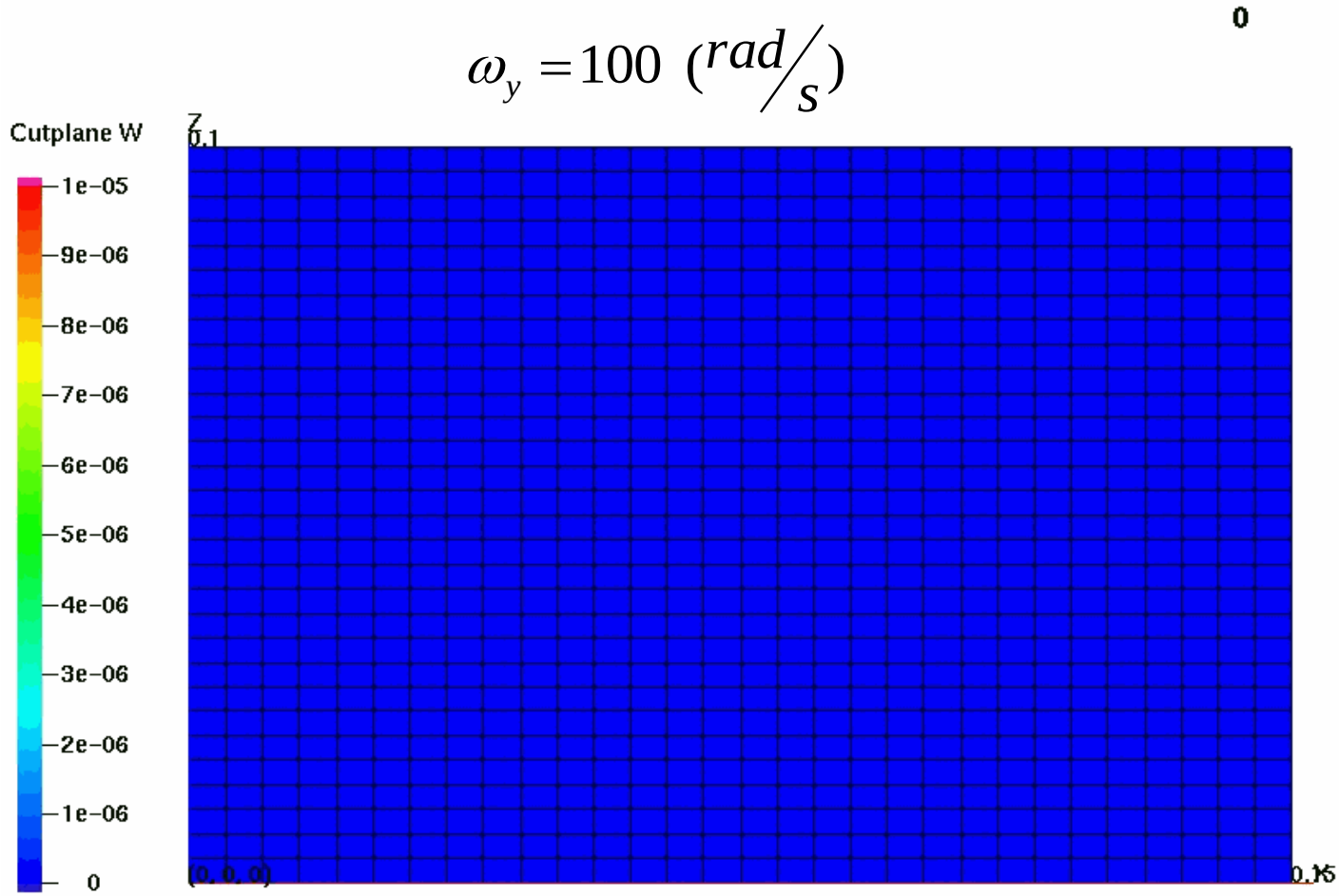

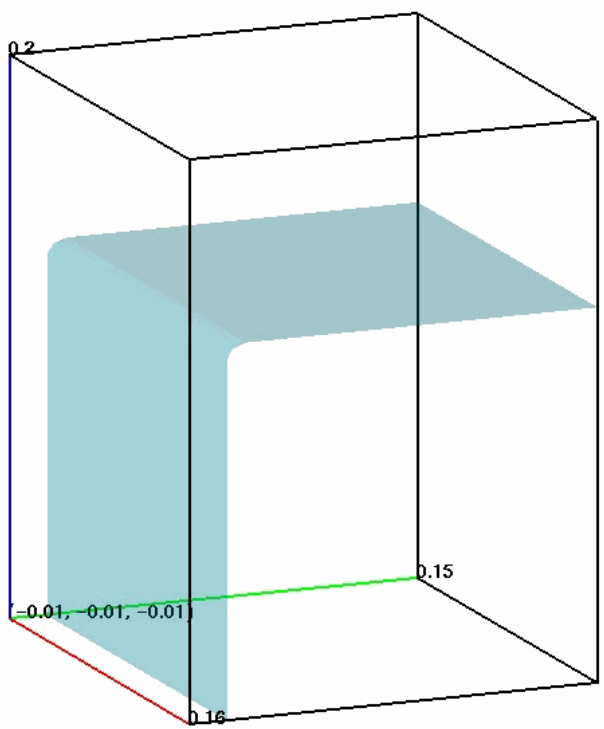
0.2
0.15
(-0.01, -0.01, -0.01)
0.16

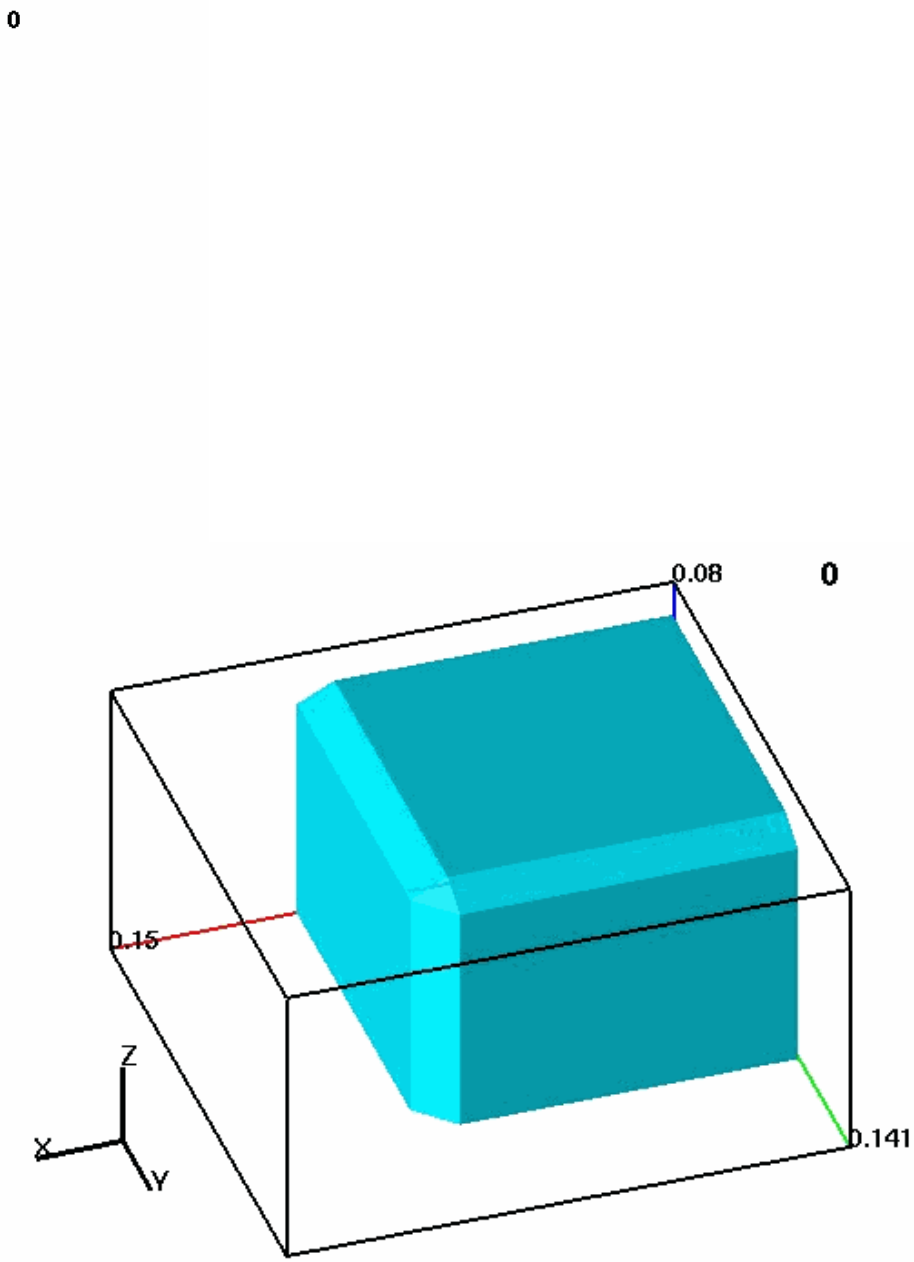
0
0.08
0
0.15
Z
X
Y
0.141

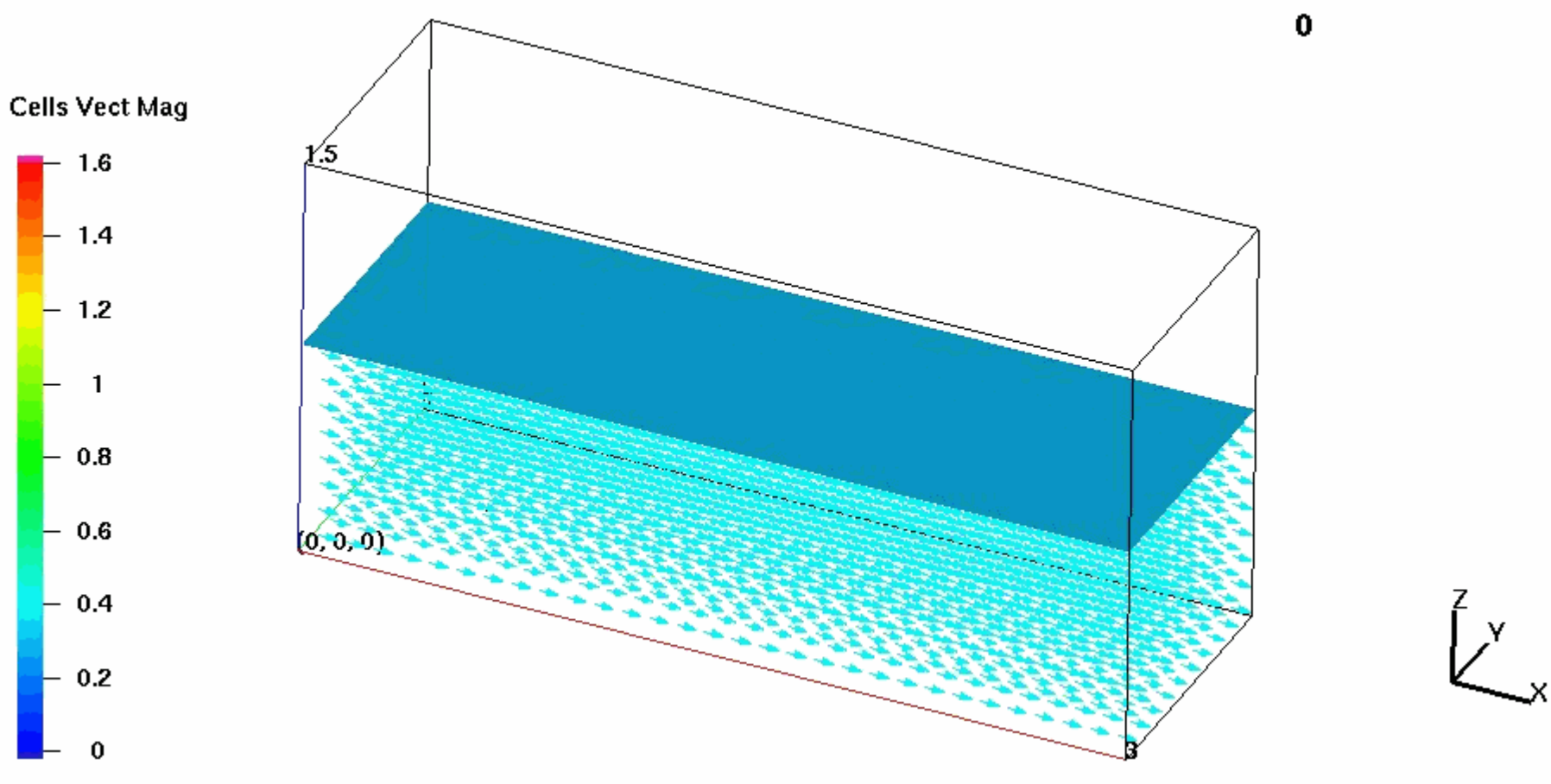
0
Cells Vect Mag
1.6
1.4
1.2
1
0.8
0.6
0.4
0.2
0
1.5
(0, 0, 0)
3
Z
Y
X

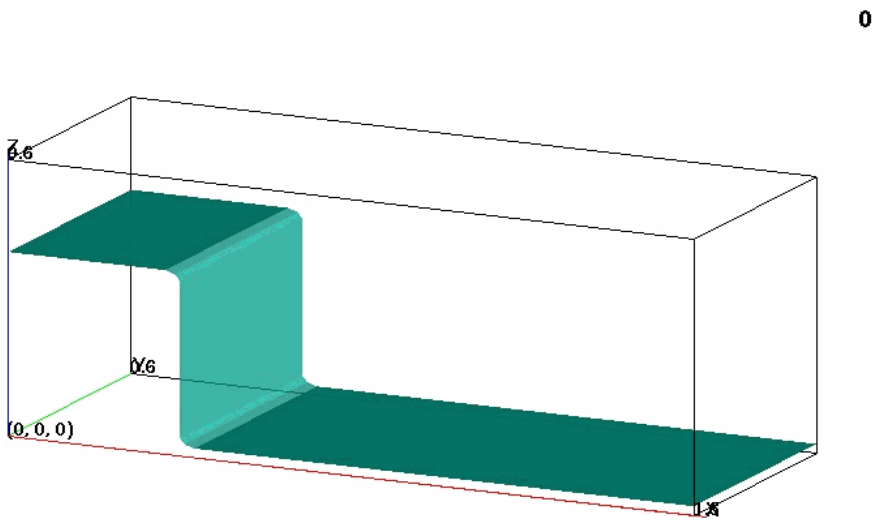
0
Z
0.6
Y
0.6
(0, 0, 0)
X

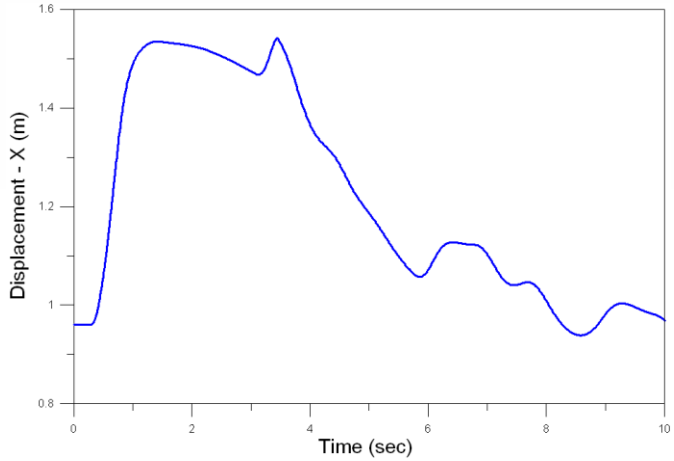
Displacement - X (m)
1.6
1.4
1.2
1
0.8
0
2
4
6
8
10
Time (sec)

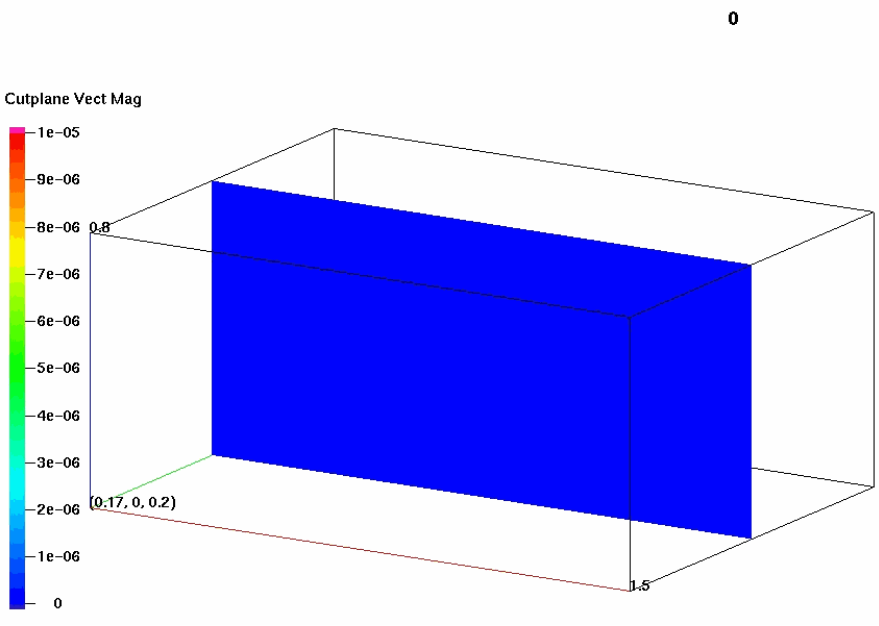

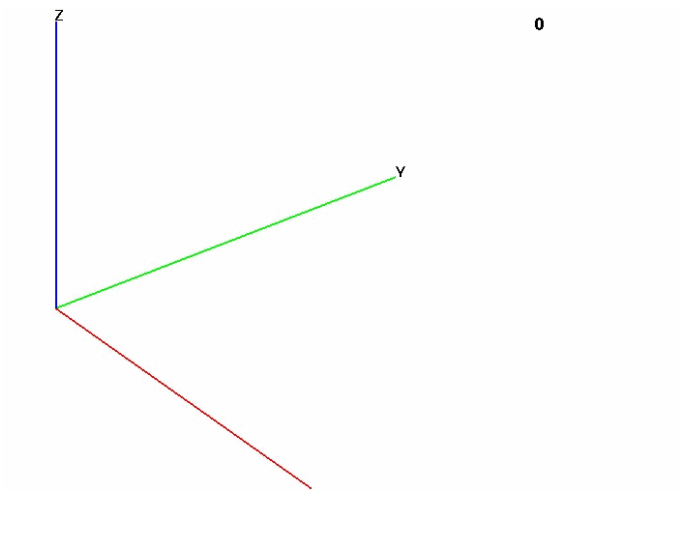

速度場剖面(y=0.5m)

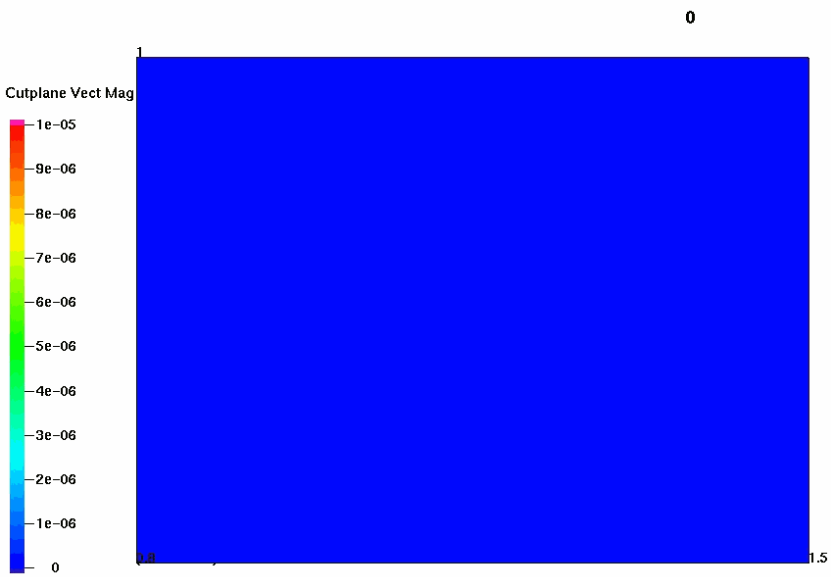

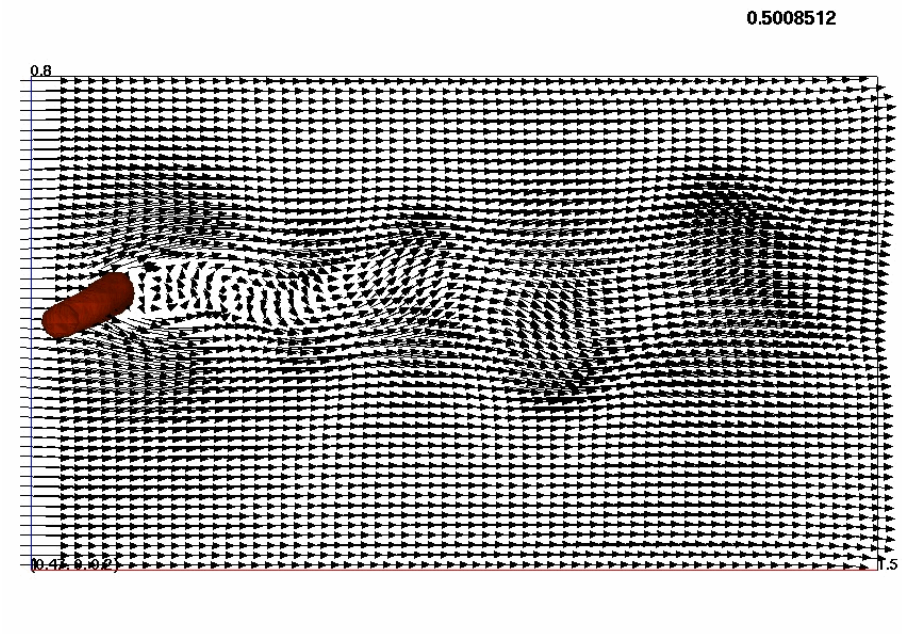

速度場俯視圖(z=0.525m)

E-IBM

(Efficient Immersed Boundary Method)

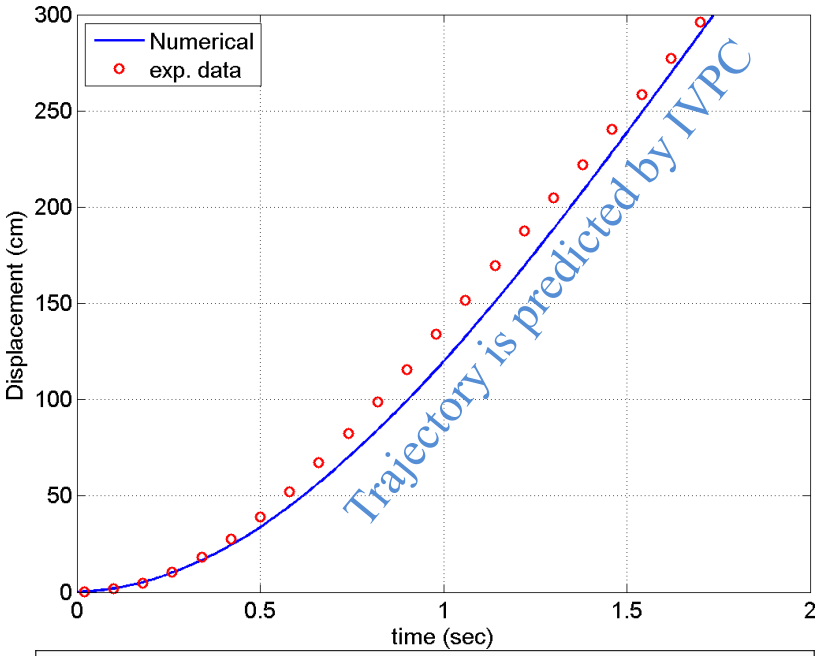

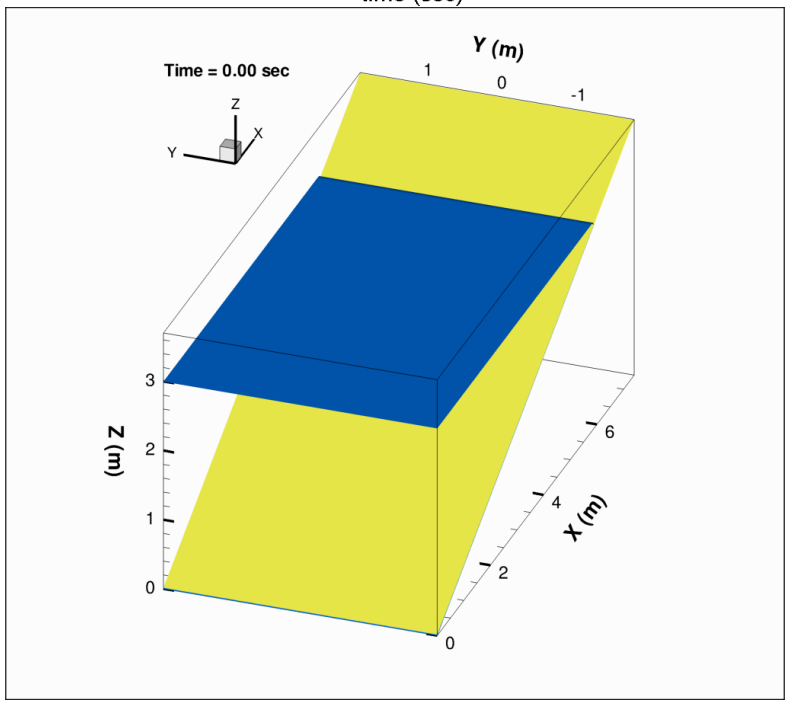

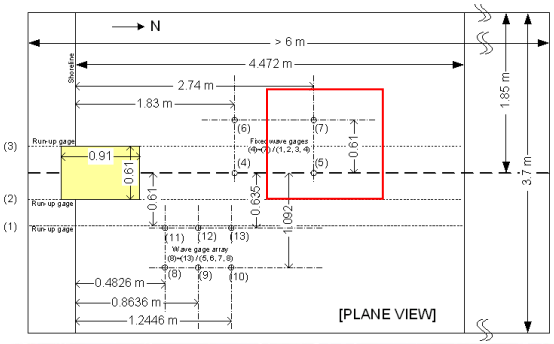

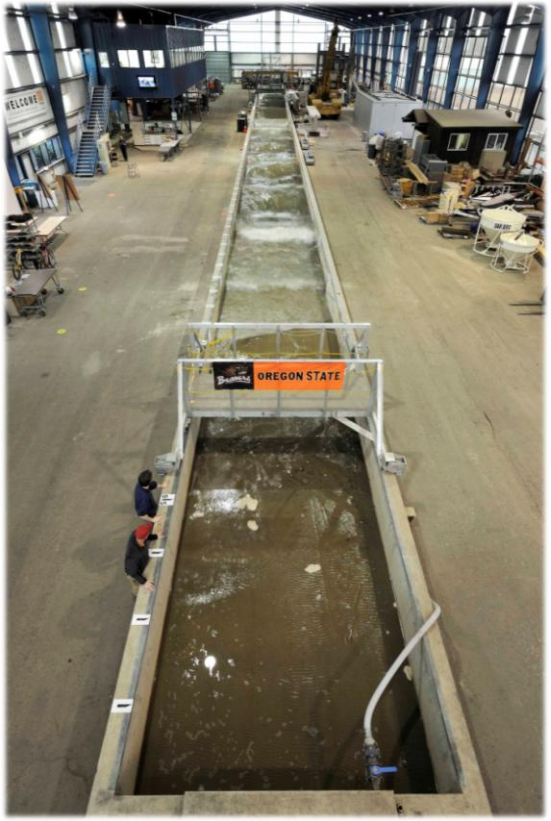

(OSU‘s O.H. Hinsdale Wave Research Lab之Large Wave Flume)

-- exp. Data
— two-way couple

#05

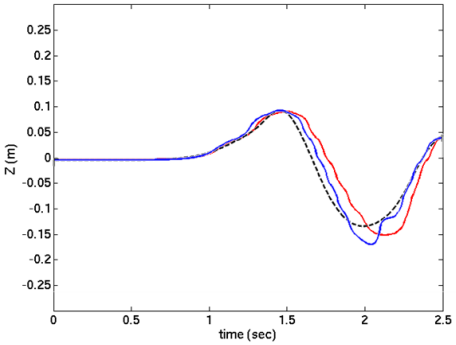

#07

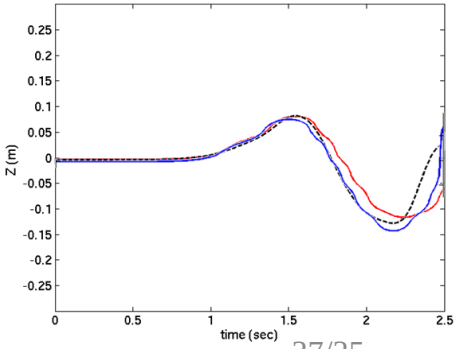

Example 1

- Parameters

➢ L1=L3=0.0125m

➢ R1=R3=0.0075m

➢ Beta=60°

➢ Density1=1300kg/m³

➢ Flud Grid =30x30x60

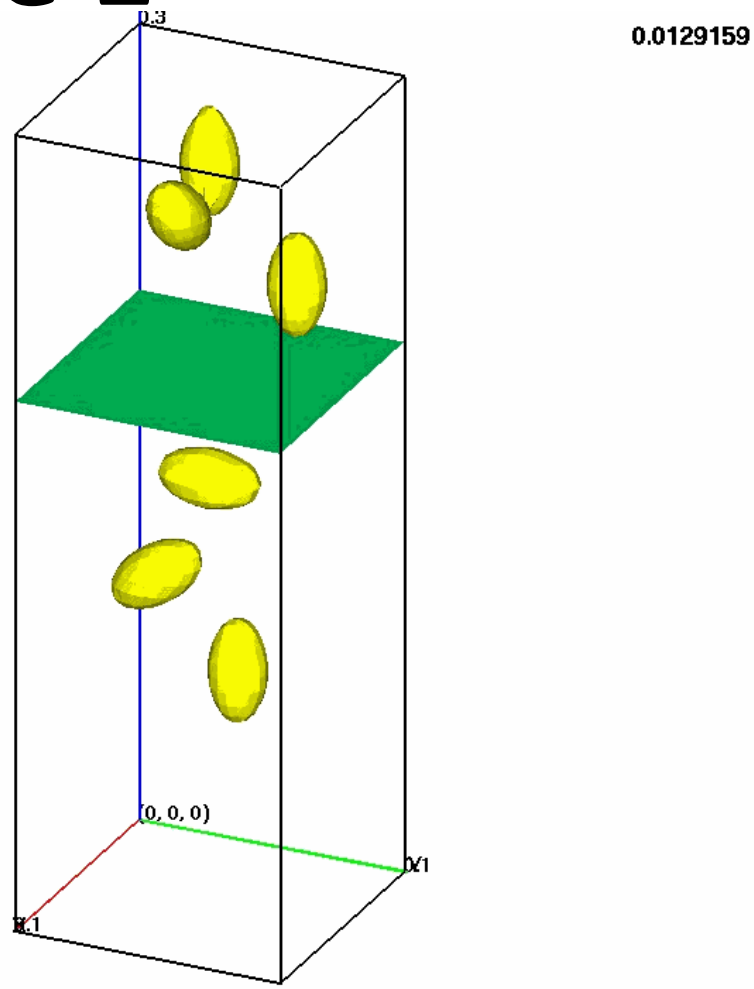

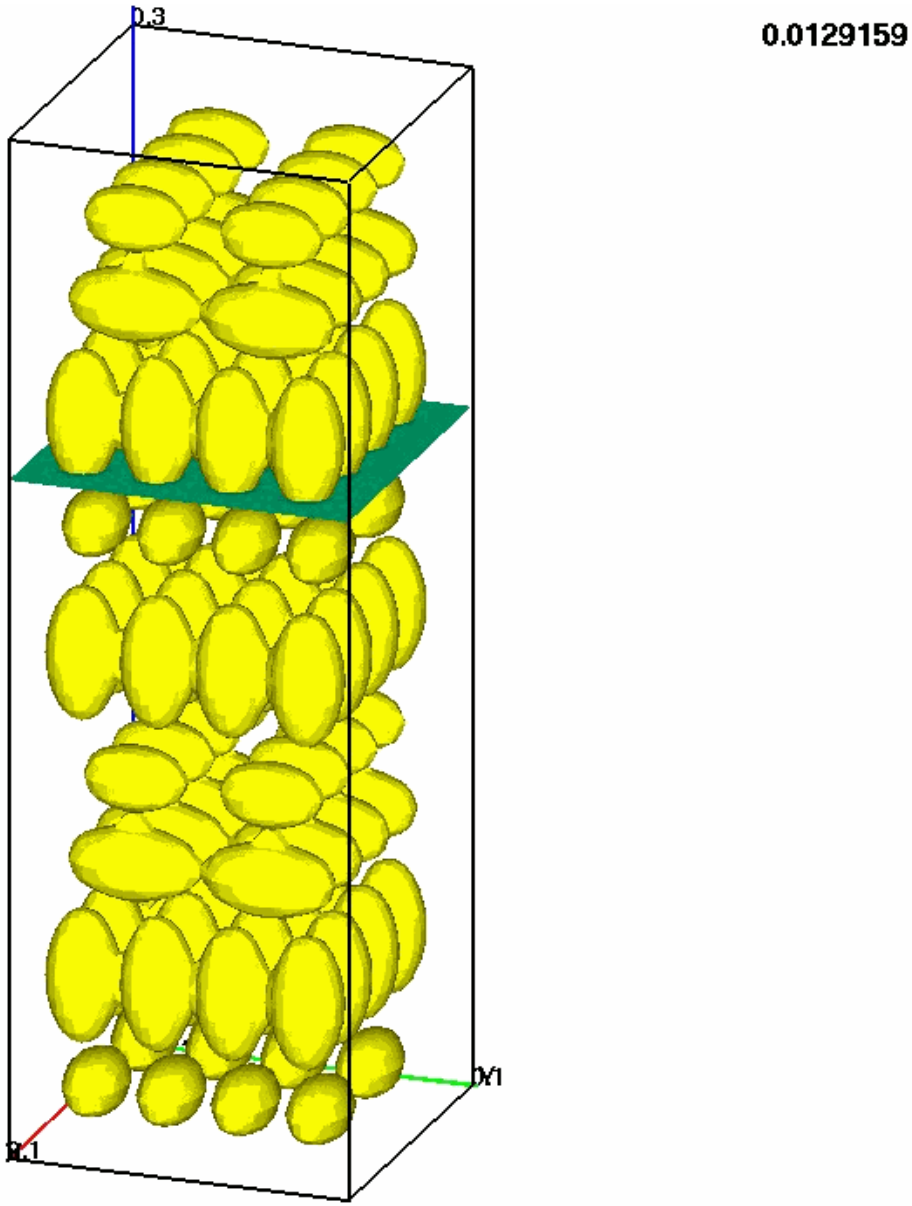
0.3
0.0129159
0.1
0.1

How do people solve the scour problems?

1. Empirical or Semi-empirical Formulae

- Lacey's formula (1930)

Clear Water Contraction Scour Equation

Compute the average depth in the contracted cross section including contraction scour with Equation 9-18.

$$y_2 = 0.2138 \left(\frac{Q_2^2}{D_{50}^{2/3} W_2^2} \right)^{3/7}$$

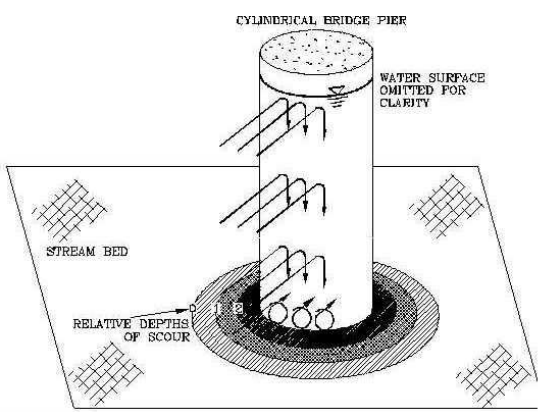

However, Big Differences on the Predicted Scour Depth

Local scour at abutments: A review

Table 3. Scour depths estimated using equations of different investigators.

Investigator	d_s (m)
Melville (1992)	4·00
Lim (1997)	4·03
Froehlich (1989)	3·88
Richardson *et al* (2001)	8·90
Oliveto & Hager (2002)	9·90
Dey & Barbhuiya (2004b)	5·90

http://onlinemanuals.txdot.gov/txdotmanuals/hyd/bridge_scour.htm

The Modern Scour Models:
CCHE3D model (State of the art, so far.)

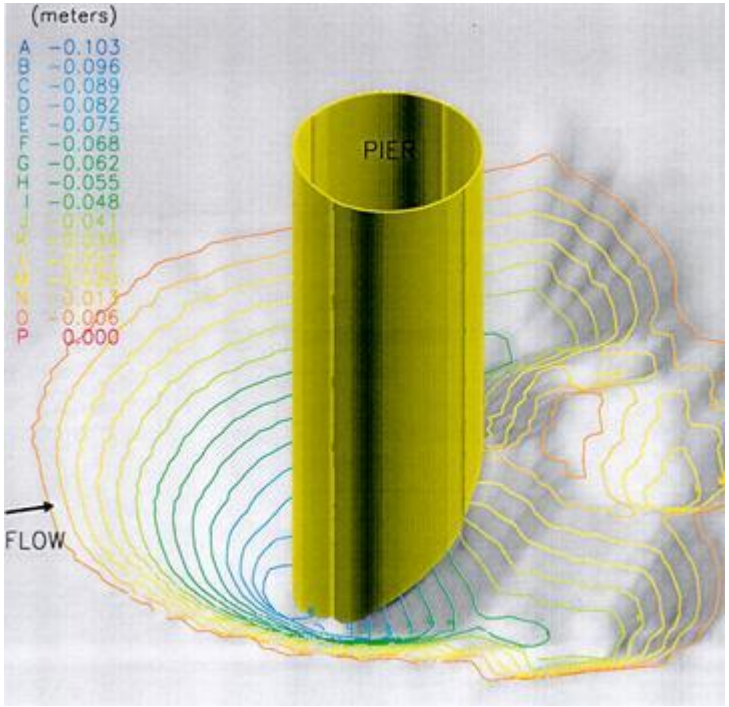

Local Scour around a Bridge Pier Simulated by CCHE3D Model

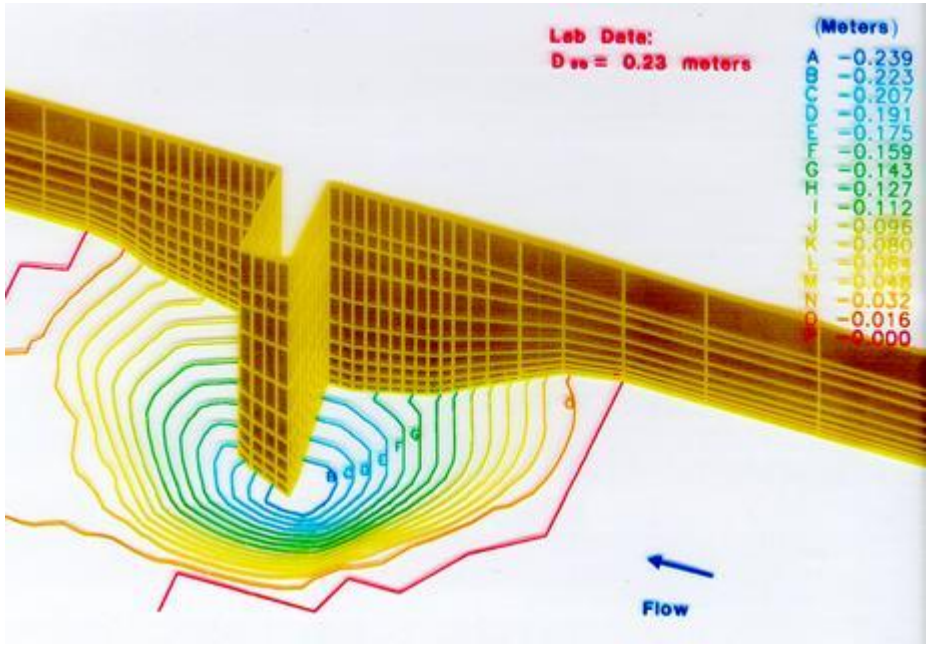

Local Scour around a Spur-Dyke Simulated by CCHE3D Model

http://www.ncche.olemiss.edu/content/research/sedimentgroup/simulation_of_local_scour.htm

Flat free-surface assumption, one-layer sediment

However, it requires too many empirical coefficients for the Sediment Transport Theory

List of symbols

B	channel or flume width;
b_d	width of cylindrical pier experiencing the same drag as that on abutment;
b_s	width of analogous pier;
C_D	drag coefficient of sediment particles;
D	pier diameter;
d, d_{50}	median diameter of sediment particles;
d_{16}	16% finer particle diameter;
d_{50a}	$d_{\max}/1{\cdot}8$;
d_{84}	84% finer particle diameter;
$\hat{d}_l$	ratio of scour depth at abutment to scour depth in equivalent long contraction;
$d_{\max}$	maximum particle size of a nonuniform sediment;
d_s	equilibrium scour depth in uniform sediment;
d_{st}	scour depth at time t;
$\mathrm{F_d}$	$U/(\Delta g d)^{0{\cdot}5}$, densimetric Froude number;
$\mathrm{F_r}$	$U/(gh)^{0{\cdot}5}$, approaching flow Froude number;
$\mathrm{F_{rc}}$	$U_c/(gh)^{0{\cdot}5}$, approaching flow Froude number corresponding to critical velocity;
f_1	Lacev's slit factor, $1{\cdot}76d^{0{\cdot}5}$;
g	gravitational acceleration;
h	approaching flow depth;
h^*	flow depth in floodplain;
$K_{1,2}$, $k_{1,2}$	coefficients;
K_d	particle size factor;
K_G	channel geometry factor;
K_{hl}	flow depth – abutment length factor;
K_I	flow intensity factor;
K_s, K_s^*	abutment shape factor and adjusted abutment shape factor respectively;
K_θ, K_θ^*	abutment alignment factor and adjusted abutment alignment factor respectively;
K_σ	function depending on σ_g;
L_R	reference length $l^{2/3}h^{1/3}$;
l	transverse length or protrusion length of abutment;
l^*	width of floodplain;
M	discharge ratio;
m	coefficients depending on bed sediment size;
N, N^*	Manning roughness coefficients for main channel and for floodplains respectively;
N_s	shape number;
T	time to equilibrium scour depth;
T_R	dimensionless time, $t(\Delta g d)^{0{\cdot}5}/LR$;
T^*	time when $d_t = 0{\cdot}632 d_s$;
t	time;
U	average approaching flow velocity;
U_a	$0{\cdot}8U_{cn}$;
U_c	critical velocity for sediment particles;
U_{cn}	critical velocity for armour particle size d_{50a};
u, v, w	time-averaged velocity components in (x, y, z) or (θ, r, z);
$\hat{u}$	u/U;
u_*	shear velocity of approaching flow;
u_{*c}	critical shear velocity for sediment particles;
u_{*cn}	critical shear velocity for armour particle size d_{50a};
$\hat{v}$	v/U;
$\hat{w}$	w/U;
w_s	settling velocity of sediment particles;
X	$\theta_c^{-0{\cdot}375}\,\mathrm{F_d^{0{\cdot}75}}(d/h)^{0{\cdot}25}[0{\cdot}9(l/h)^{0{\cdot}5}+1]$;
$\hat{x}$	x/l;
x, y, z	Cartesian coordinates;
$\hat{y}$	y/l;
$\hat{z}$	z/l;
α	$1 - l/B$, opening ratio;
Δ	$s - 1$;
ϕ_s	side slope angle of scour hole;
η_{1-3}	coefficients;
θ, r, z	cylindrical polar coordinates;
θ_a	angle of attack;
θ_c	$u_{*c}^2/(\Delta g d)$, shield's entrainment function;
θ_t	turning angle between bottom streamline and main flow direction, $1{\cdot}485\,\mathrm{F_r^{0{\cdot}13}}(l/h)^{0{\cdot}06}$;
ρ, ρ_s	mass densities of water and of sediment particles respectively;
σ_g	geometric standard deviation;
τ_o	bed shear stress of approaching flow;
τ_c	critical shear stress of sediment particles;
τ_{cont}	shear stress due to contraction;
$\hat{\tau}_{cont}$	τ_{cont}/τ_o, bed shear stress due to contraction;
τ_{nose}	bed shear stress at nose region of abutment;

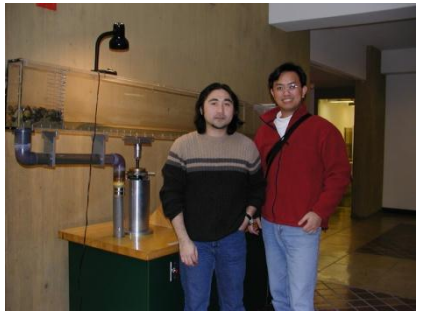

(2002 at Cornell)

Schematic of Discontinuous Bi-viscous Model (DBM)

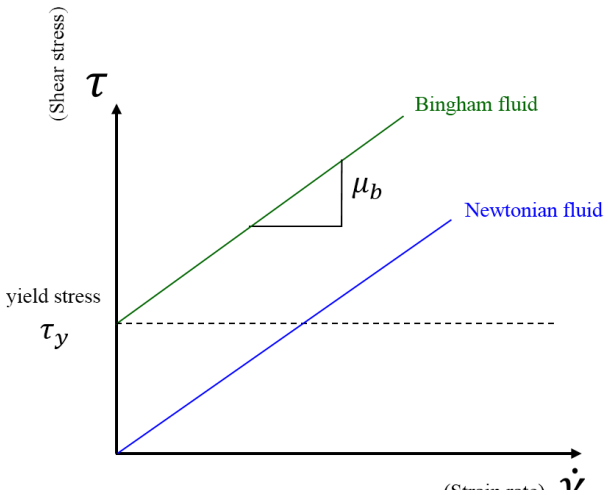

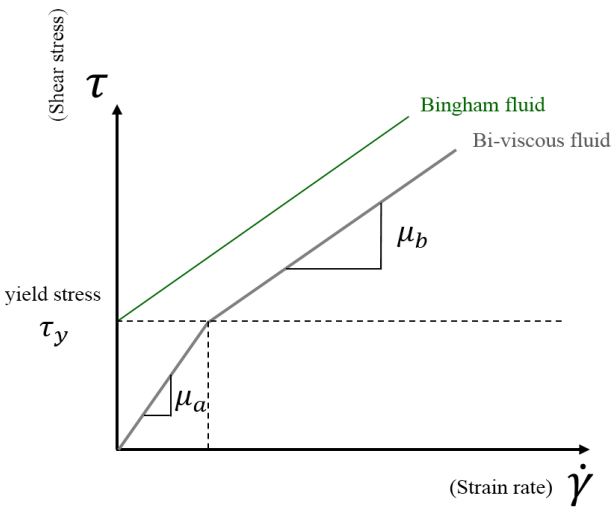

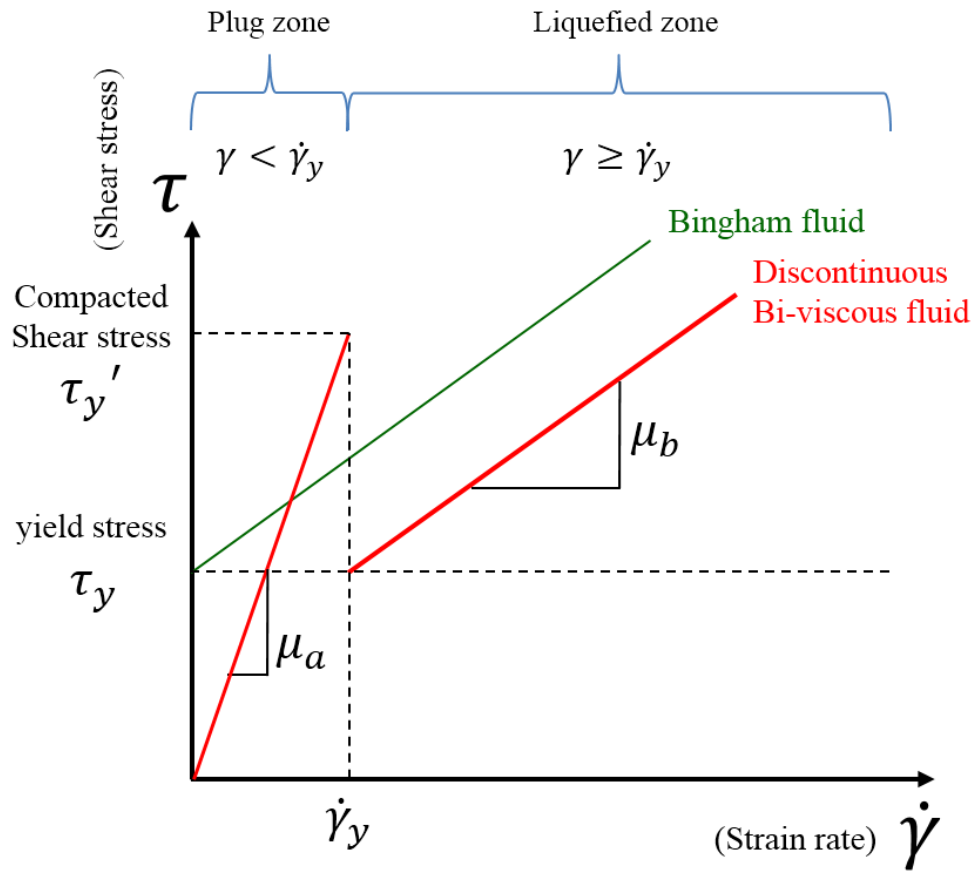

牛頓流體、賓漢流體、非連續雙黏性流體之流變圖

- Loose structure without tamping:
  Angle = Angle of repose
- 未夯實，結構鬆散：
  角度為安息角

- Tight structure after tamping or settlement:
  Angle > Angle of repose
- 夯實後，結構緊實，角度大於安息角

(Chinatimes)

Discontinuous Bi-viscous Model (DBM)
Equations of Rheology

$$\tau = \mu\left(\bar{D}\right)\bar{D}$$

$$\mu\left(\bar{D}\right) = \begin{cases} \mu_\infty & \text{,if } \bar{D} > \bar{D}_y \\ \mu_B + \dfrac{\tau_0}{\sqrt{\dfrac{1}{2}\bar{D}:\bar{D}}} & \text{,if } \bar{D} \le \bar{D}_y \end{cases}$$

$$\bar{D} = \dot{\gamma}_{ij} = \frac{\partial \dot{u}_i}{\partial x_j} + \frac{\partial \dot{u}_j}{\partial x_i}$$

Only 4 unknown variables: $\bar{D}_y \quad \mu_\infty \quad \mu_B \quad \tau_0$

BM vs DBM

Bi-viscous Model (BM)

$\tau_0 = 1000.0\ (Pa)$

$\mu_b = 50.0\ (Pa \cdot s)$

$\mu_\infty = 2.e3\ (Pa \cdot s)$

$ssc = 0.5\ (1/s)$

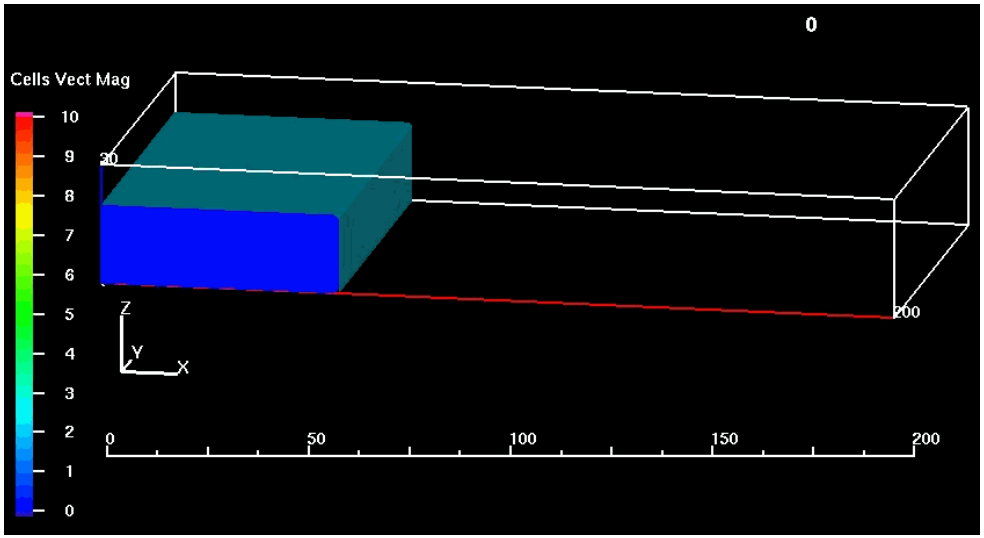

Discontinuous Bi-viscous Model (DBM)

$\tau_0 = 1000.0\ (Pa)$

$\mu_b = 50.0\ (Pa \cdot s)$

$\mu_\infty = 1.e8\ (Pa \cdot s)$

$ssc = 0.5\ (1/s)$

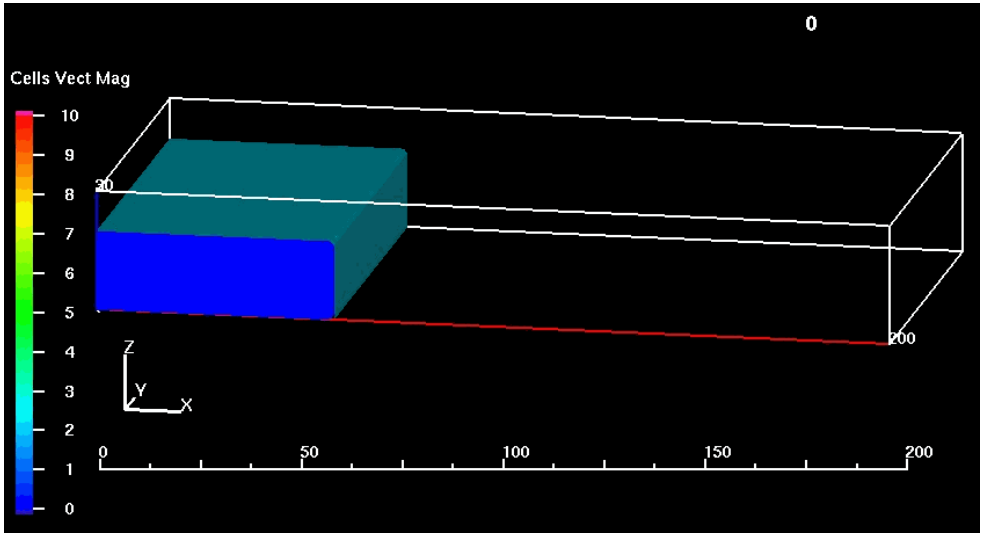

The development of Slip surface can be seen clearly

Simulation on the Sand Sliding Down by DBM

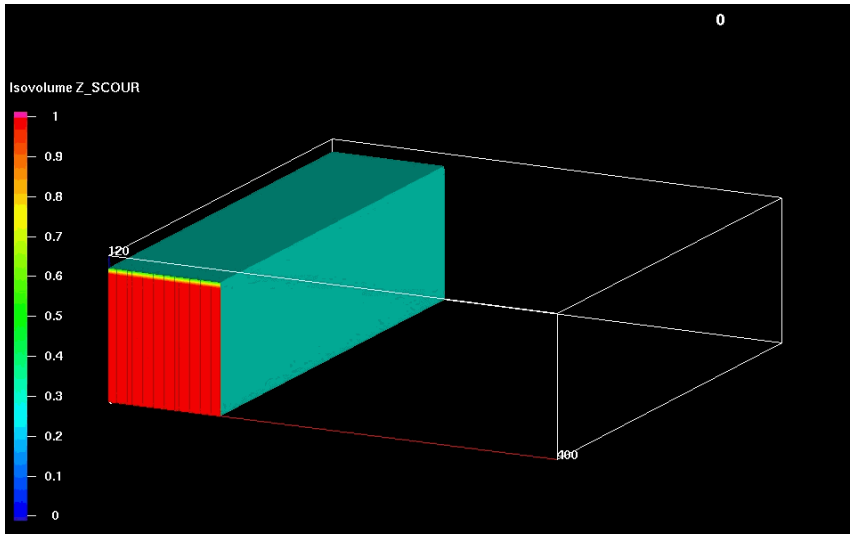

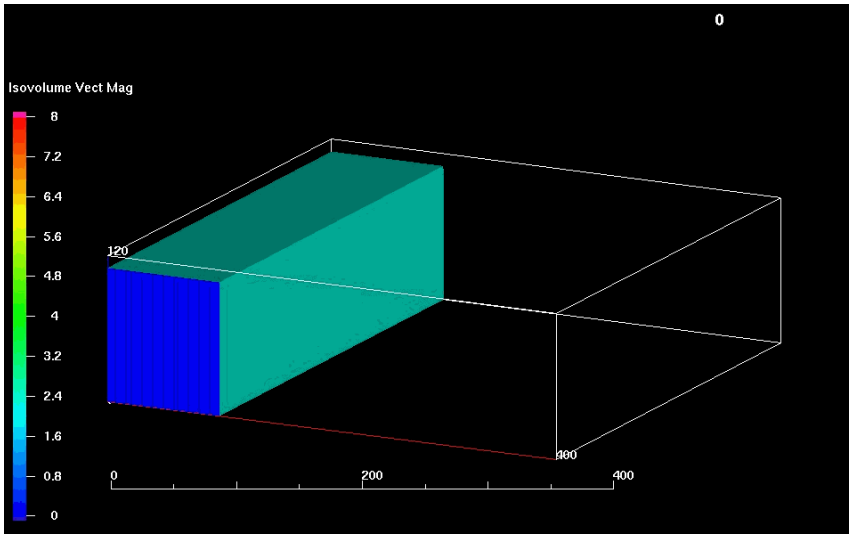

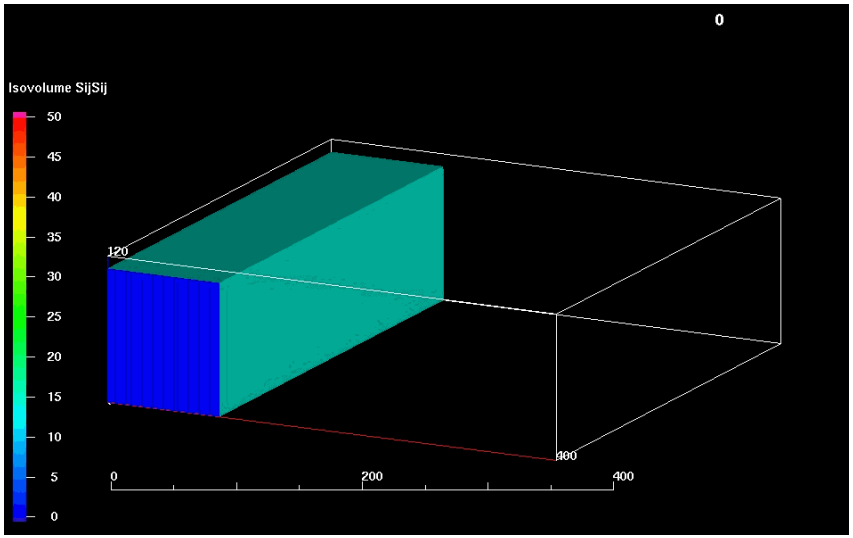

1. Pressure Gradient Channel Flow (Bird et al. 1983)

Newtonian Fluid

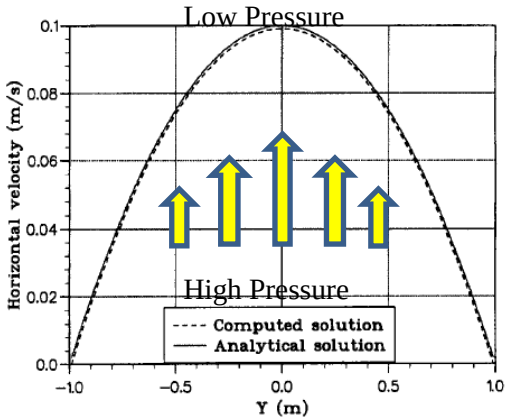

FIG. 2. Comparison between Computed and Analytical Velocity Profiles for Newtonian Fluid

Bingham Fluid

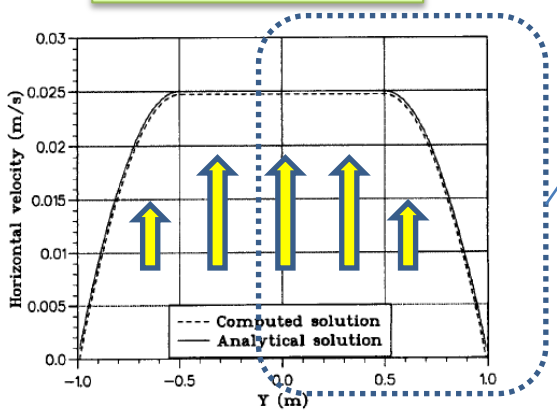

FIG. 3. Comparison between Computed and Analytical Velocity Profiles for Bingham Fluid

Analytical Solution of Bingham Fluid in a Channel

$$u(y) = \frac{(P_0 - P_L)B^2}{2\mu_B L}\left[1-\left(\frac{y}{B}\right)^2\right] - \frac{\tau_0 B}{\mu_B}\left(1-\frac{y}{B}\right) \qquad y_0 \le y \le B$$

$$u(y) = u(y_0) = u_M \qquad 0 \le y \le y_0$$

(Accurate turning point)

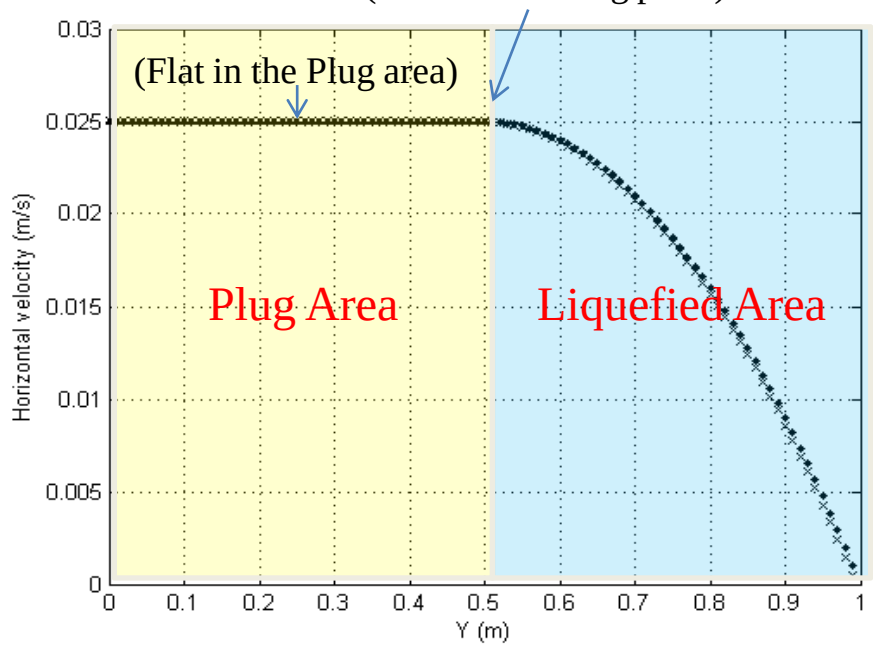

$\mu_B = 5.0\ \text{Pa}\cdot\text{s}$ $\quad \tau_0 = 0.5\ \text{Pa}$

$$\mu_\infty = 1e6\ \text{Pa}\cdot\text{s}$$

2. Spreading of Bingham fluid on an inclined plane

Liu and Mei (1989) 推導出斜板上之賓漢流理論解，並與同時進行之實驗結果相符。

Experiment settings

Length : 332 cm Width : 7.62 cm Height : 15.24 cm

θ: 1.47°

Material : Kaolinite mixed with tap water

ρ: 1.106 g/cm^3

τ_0 : 0.875 Pa

μ: 0.034 $Pa \cdot S$

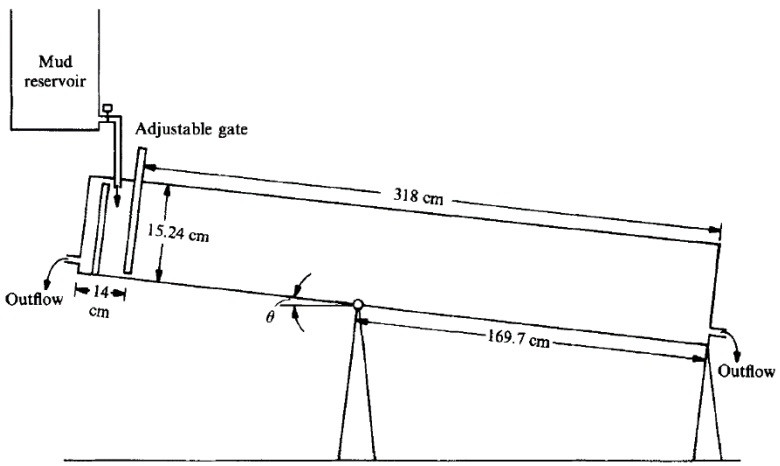

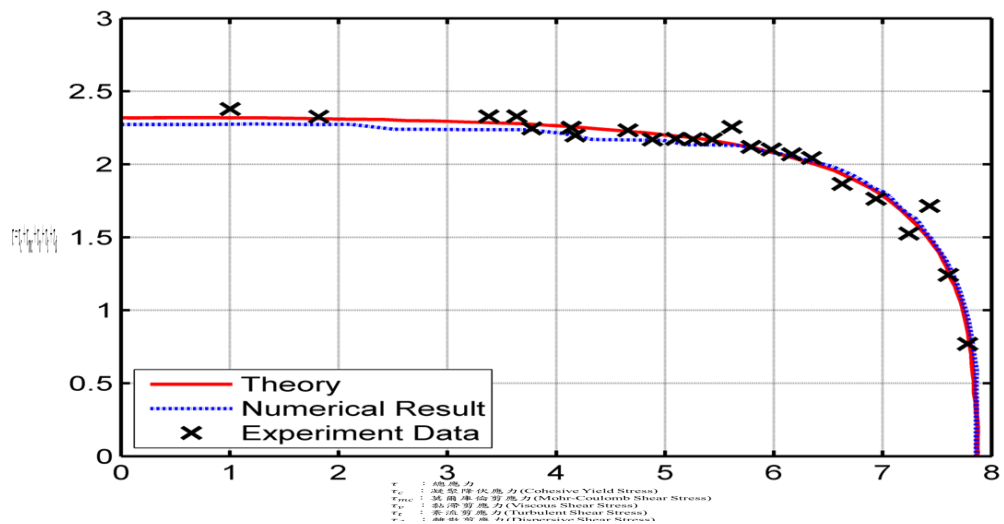

Experimental set-up for gravity currents down a dry bed

3. Failure of Gypsum Tailings Dam East Texas, 1966

Jeyapalan (1983):

Initial Height of Dam : 11 m

Material : Gypsum Tailings

Bed Slope : 0°

Properties of Tailings :

$\rho = 1400.0\ kg/m^3$

$\tau_0 = 1000.0\ Pa$

$\mu = 50.0\ Pa \cdot S$

Mu_max=1.e6, ss_c=0.2

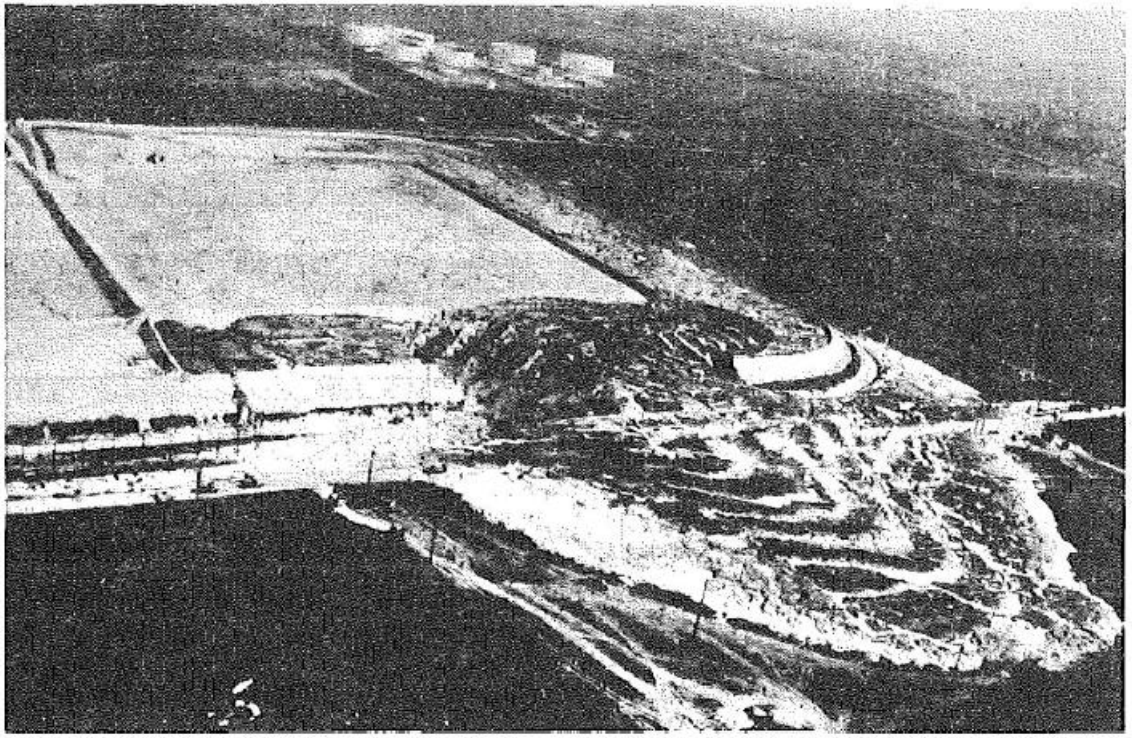

Flow of Liquefied Tailings from Gypsum Tailings Impoundment (1966)

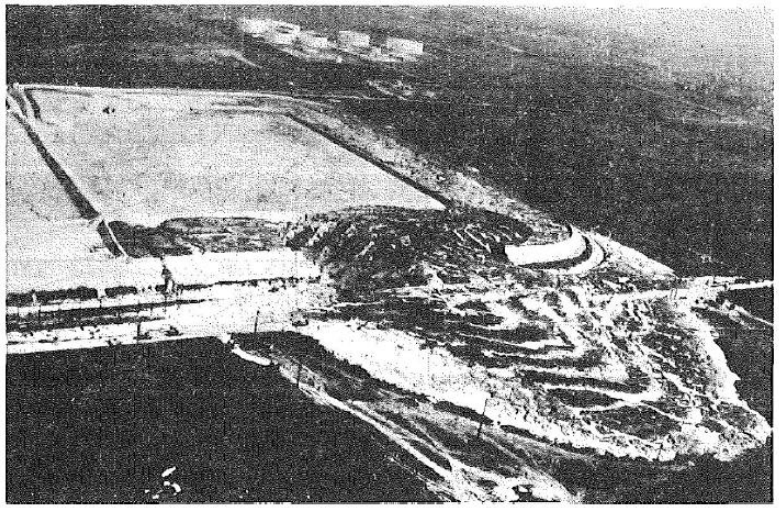

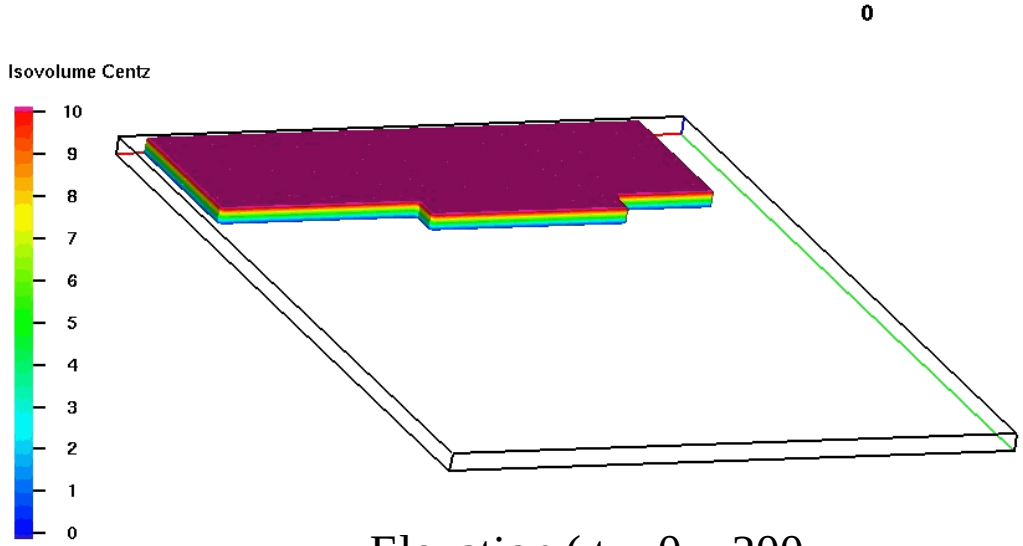

Elevation (t = 0 ~ 200 s)

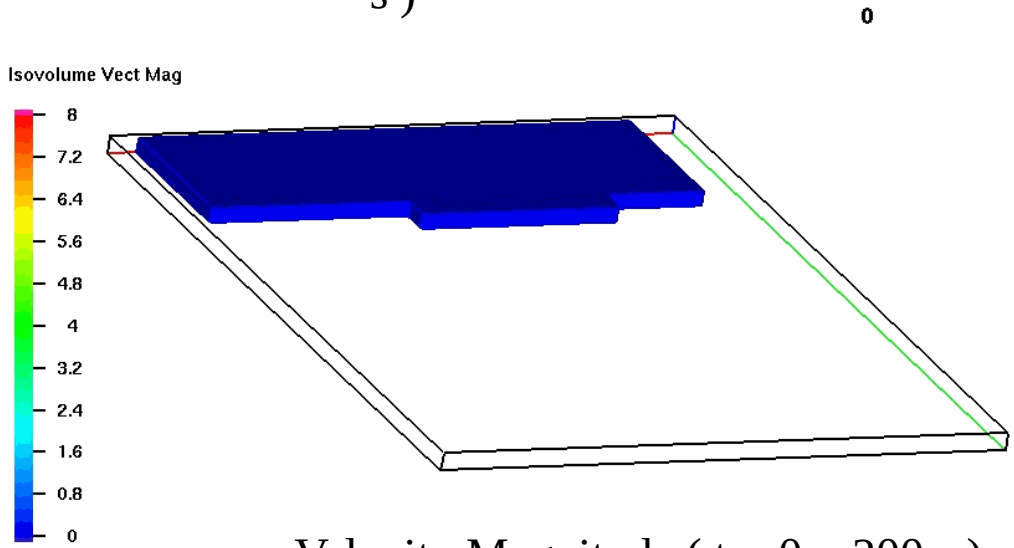

Velocity Magnitude (t = 0 ~ 200 s)

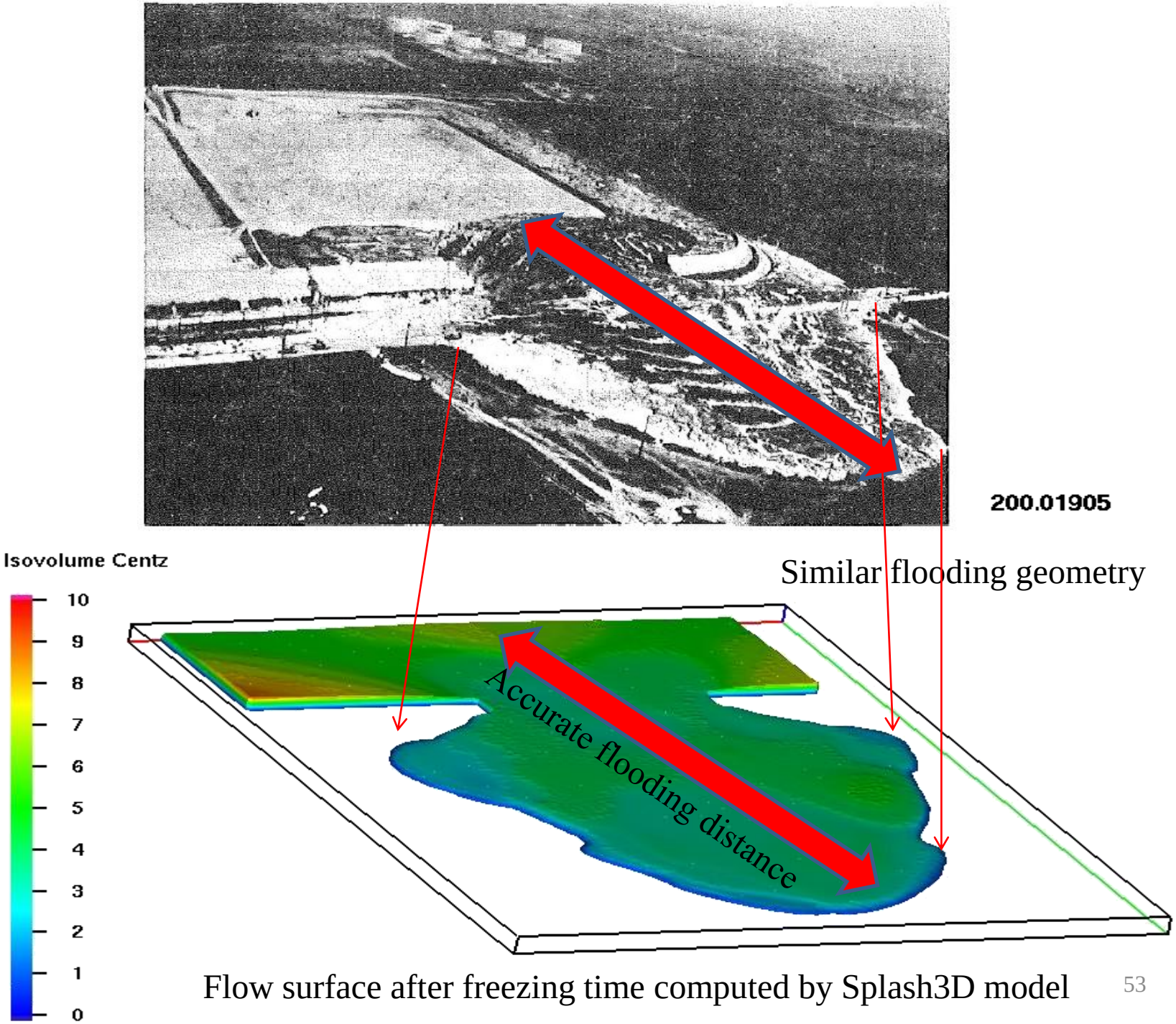

Flow surface after freezing time computed by Splash3D model

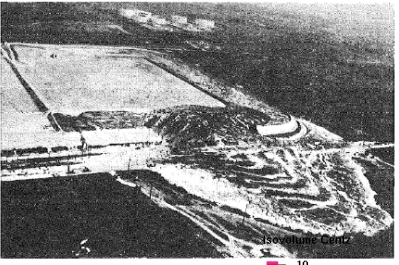

Bingham

Discontinuous Bingham (DBM)

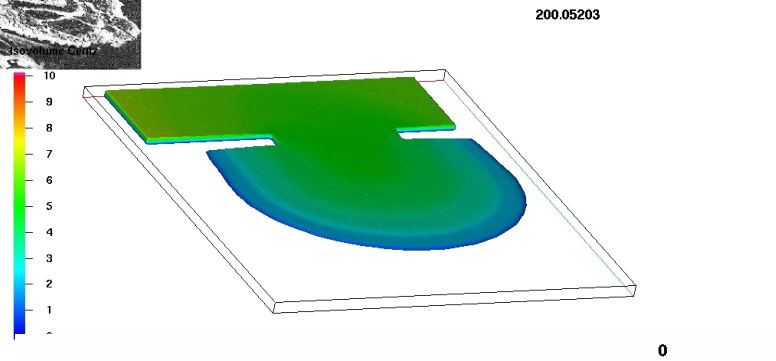

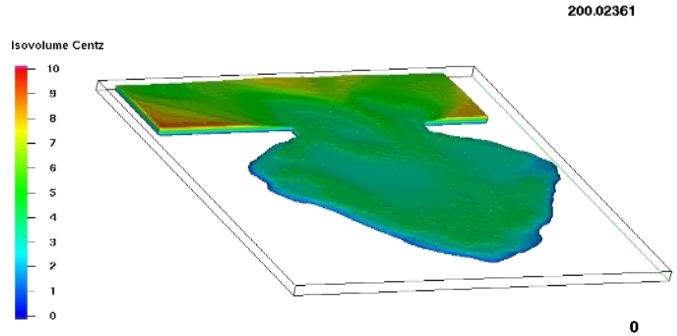

高程
(t = 0 ~ 20

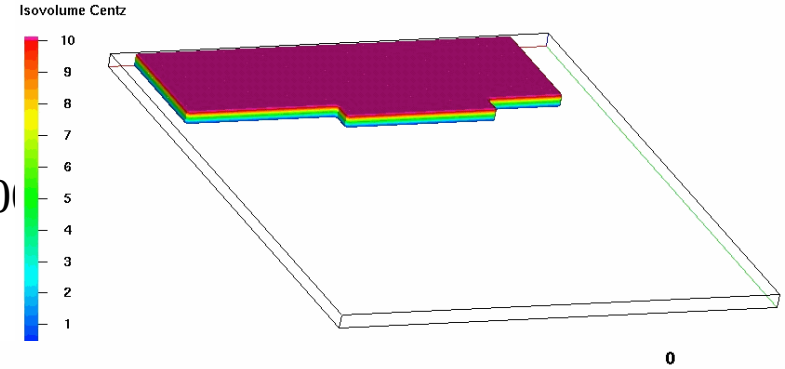

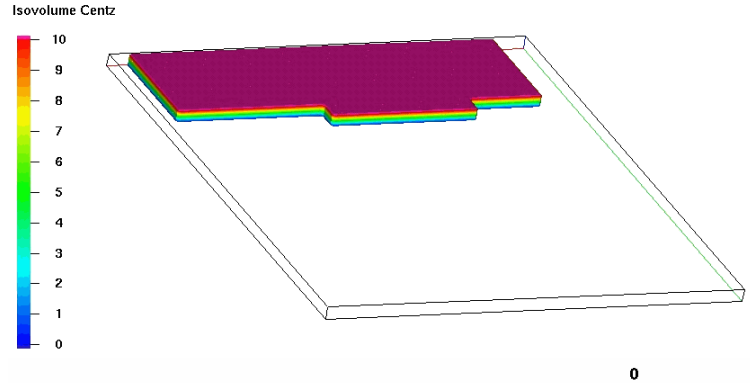

絕對流
(t = 0 ~ 2

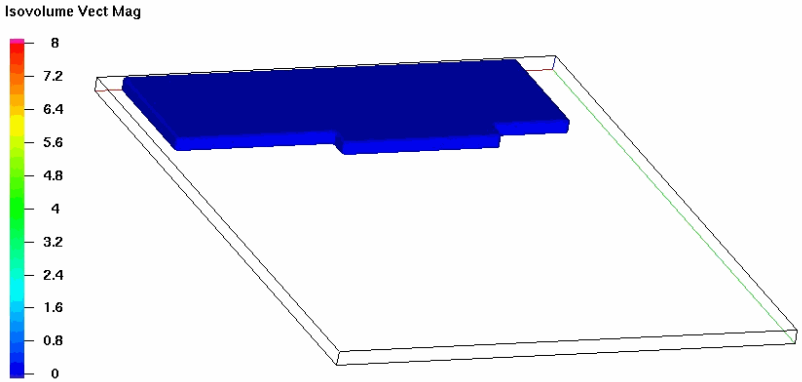

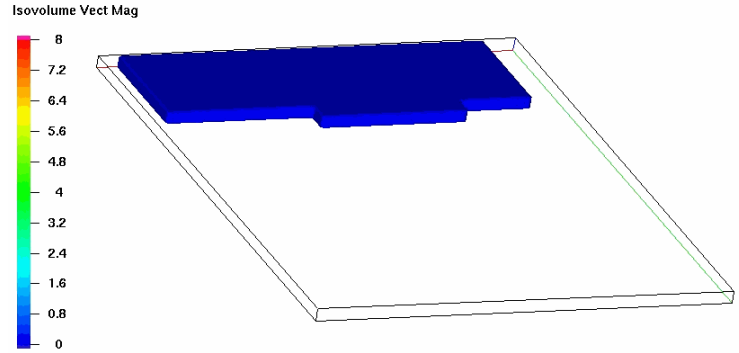

Result Competition

	Inundation distance（m）	Freezing time（s）	Mean velocity（m/s）
Observed values	300	60-120	2.5-5.0
Theoretical results from charts	550	132	4.2
Result using TFLOW（Jeyapalan, 1983）	470	85	5.5
Result computed by Pastor et al.（2004）	170	≅120	1.4
Result computed by Chen（2006）	200	≅120	1.7
Result using Splash3D model	310	≅130	2.4

4. Local scour around the semi-circular cylinder

- Scour hole

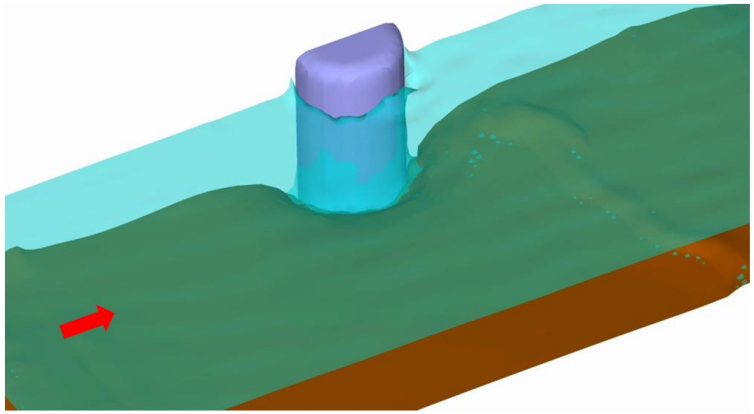

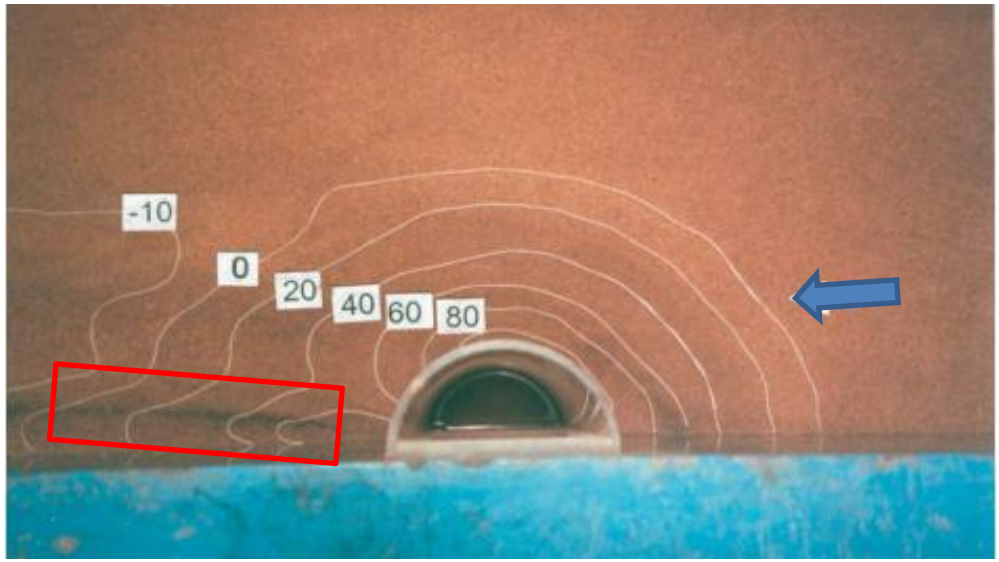

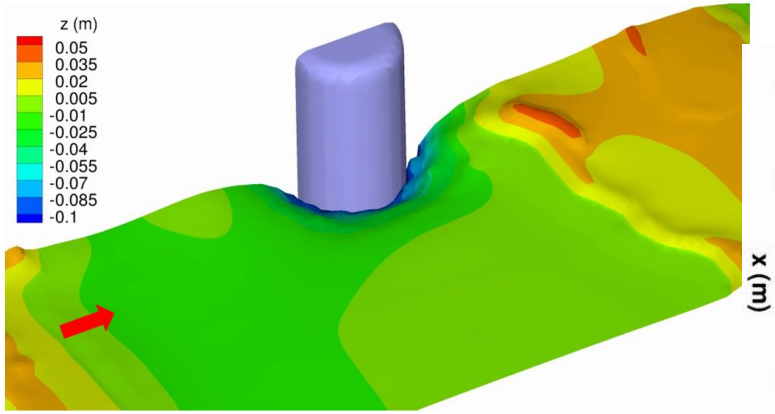

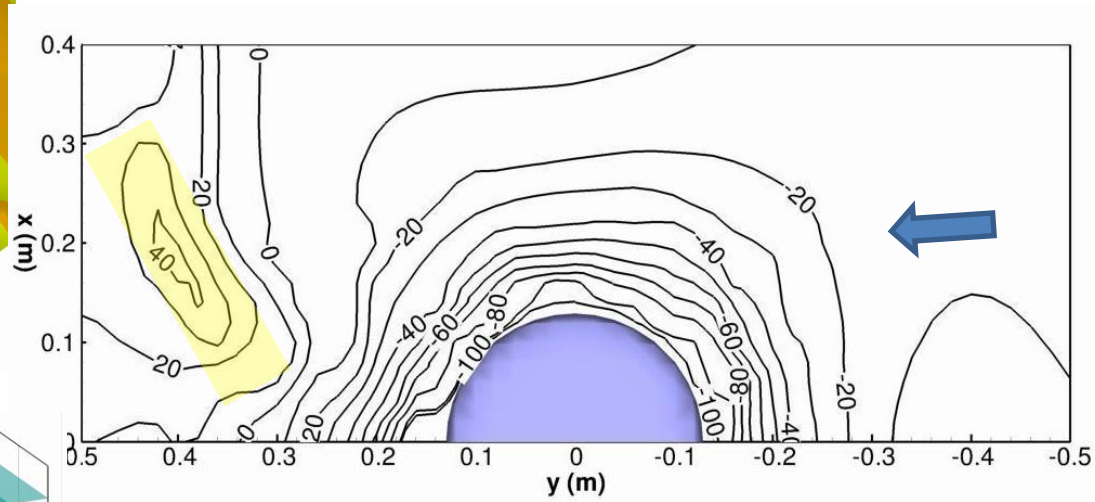

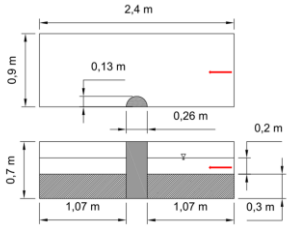

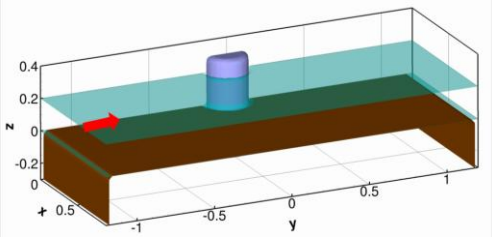

Compare with the experimental data done by Dey and Barbhuiya (2005) (Uupper) (mm)

Rheology of Grains

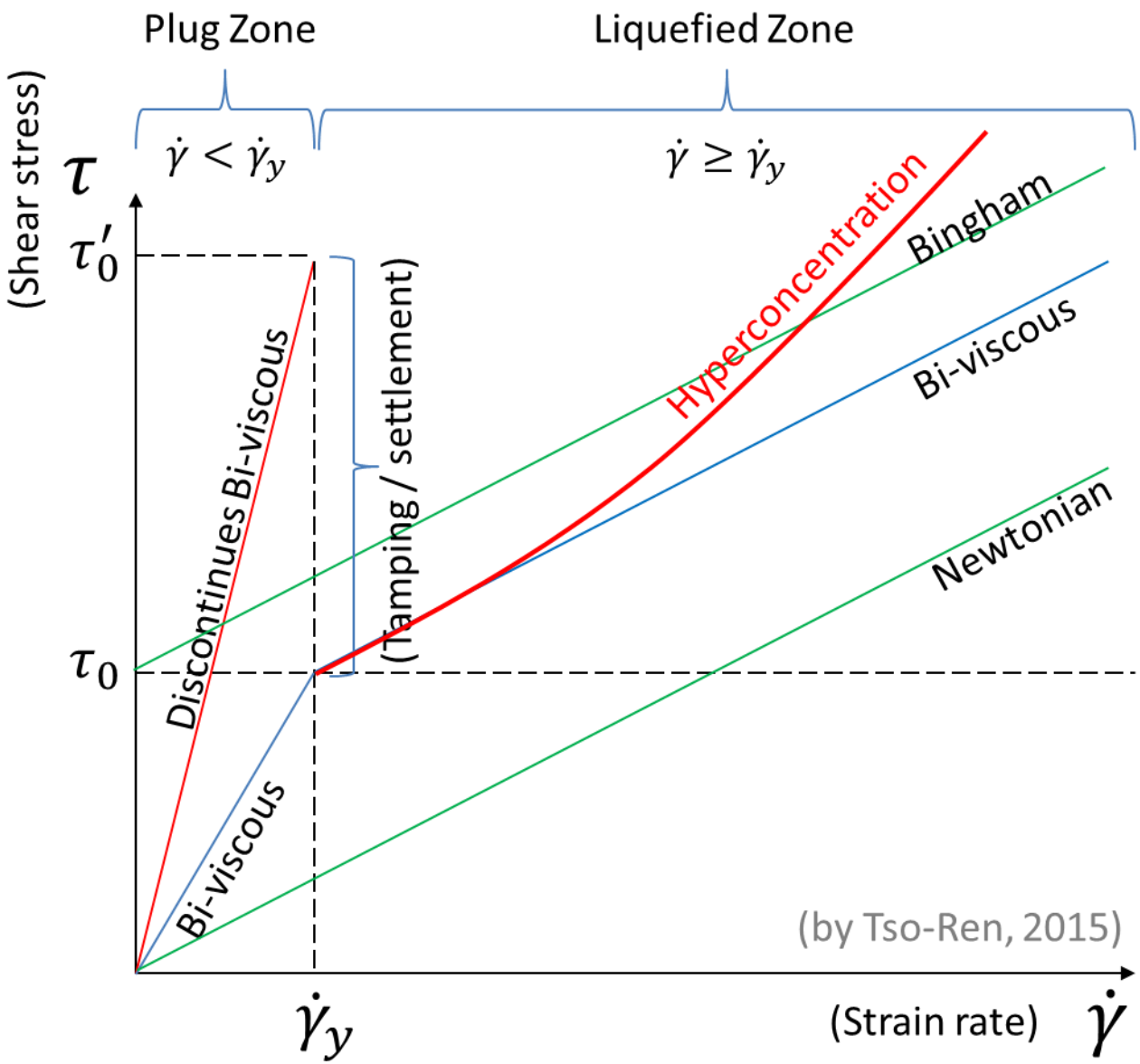

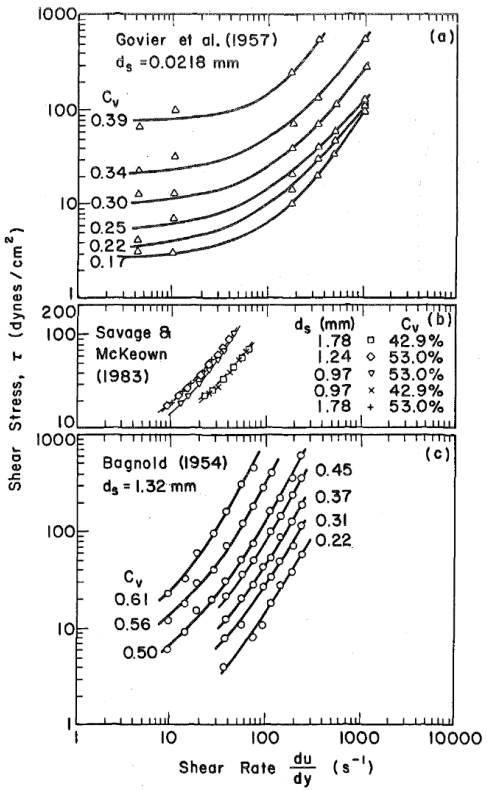

FIG. 1. Rheograms for Three Data Sets: Govier et al. (1957); Savage and McKeown (1983); and Bagnold (1954)

Snapshot of the experiment：

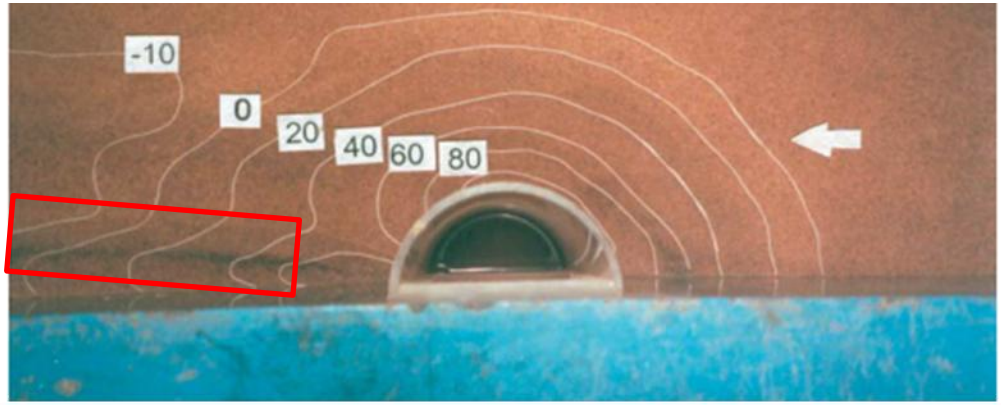

Numerical result without particle collision term：

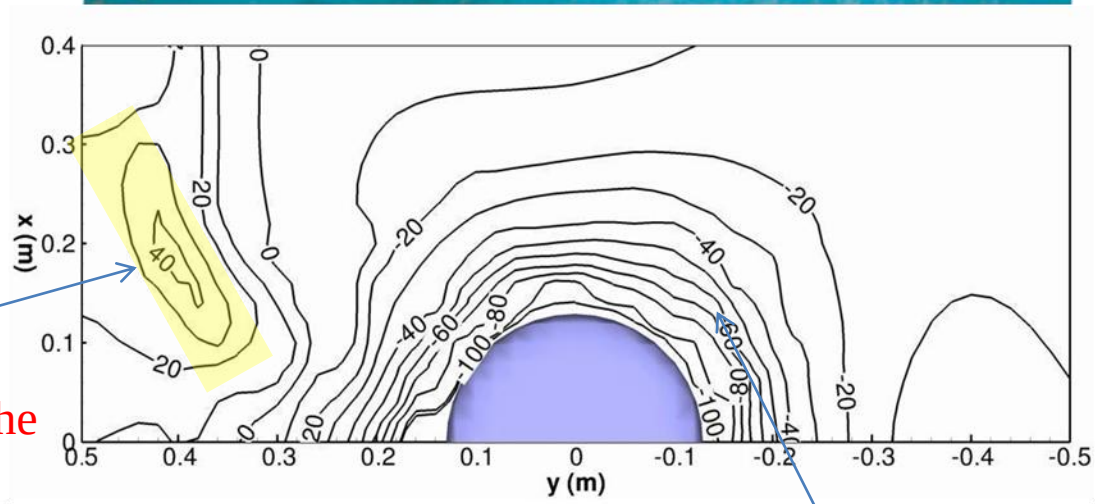

Significant improvement in the wake area

Numerical result with practical collision term：

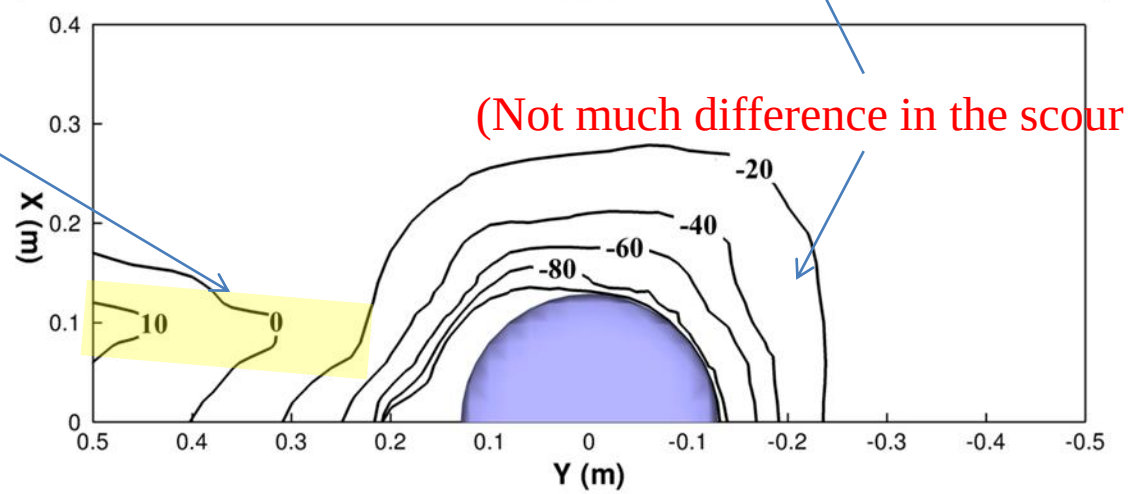

(Not much difference in the scour hole)

5. Simulation on the failure of Shuan-Yuan Bridge

in the event of 2009 Typhoon Morakot

The undular waves imply the uneven soft bottom

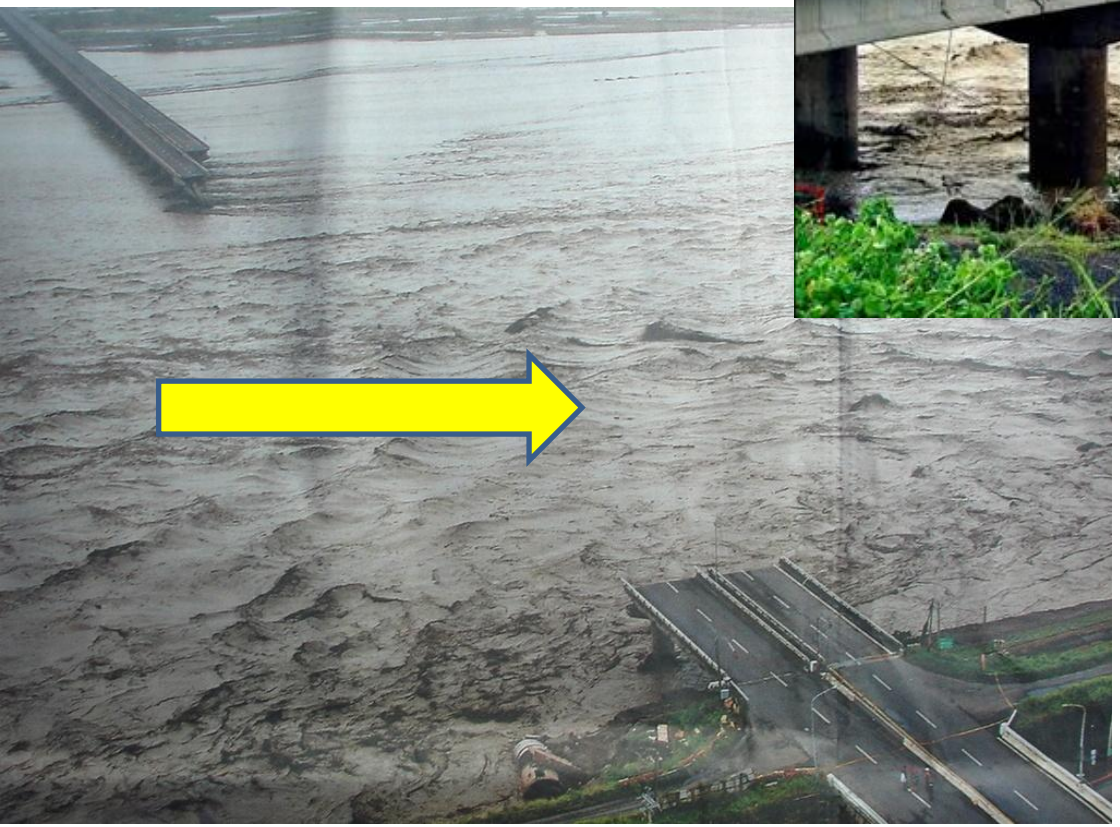

3D Local scour induced by the strong flood

mud_vof =0.05

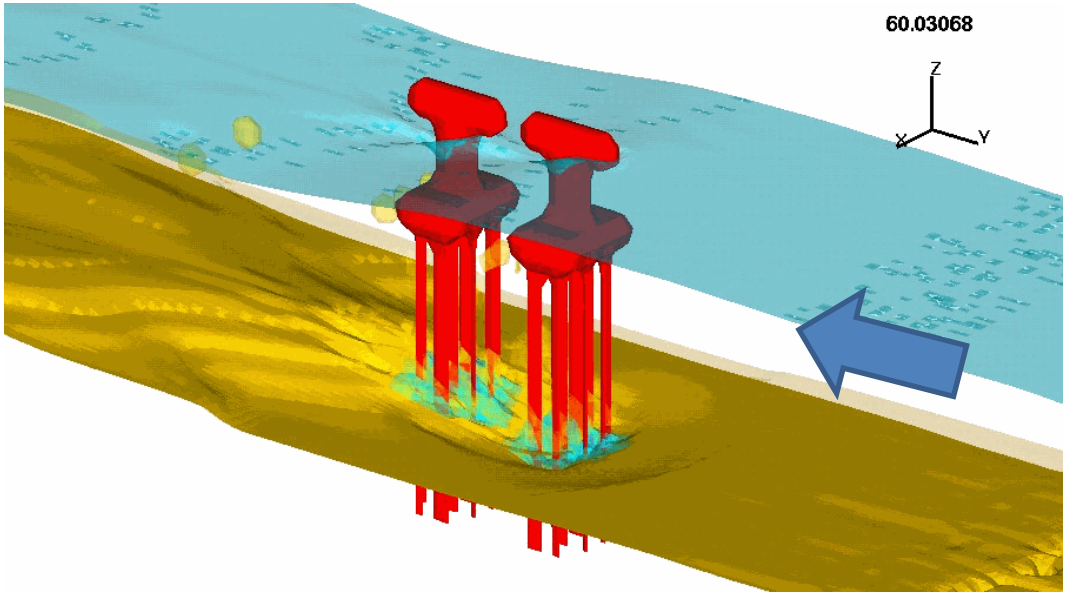

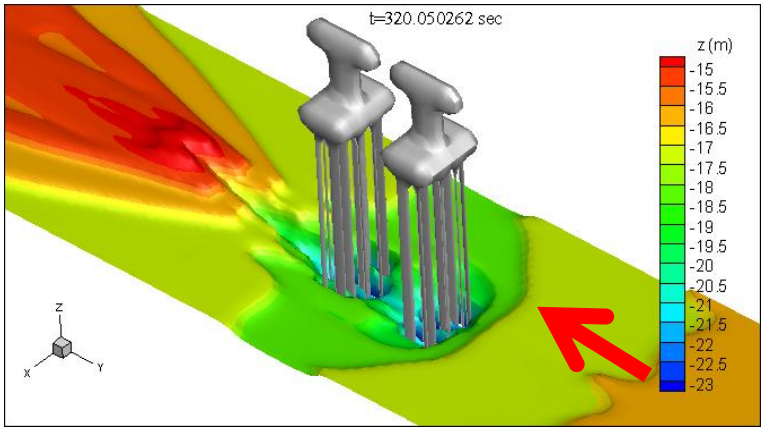

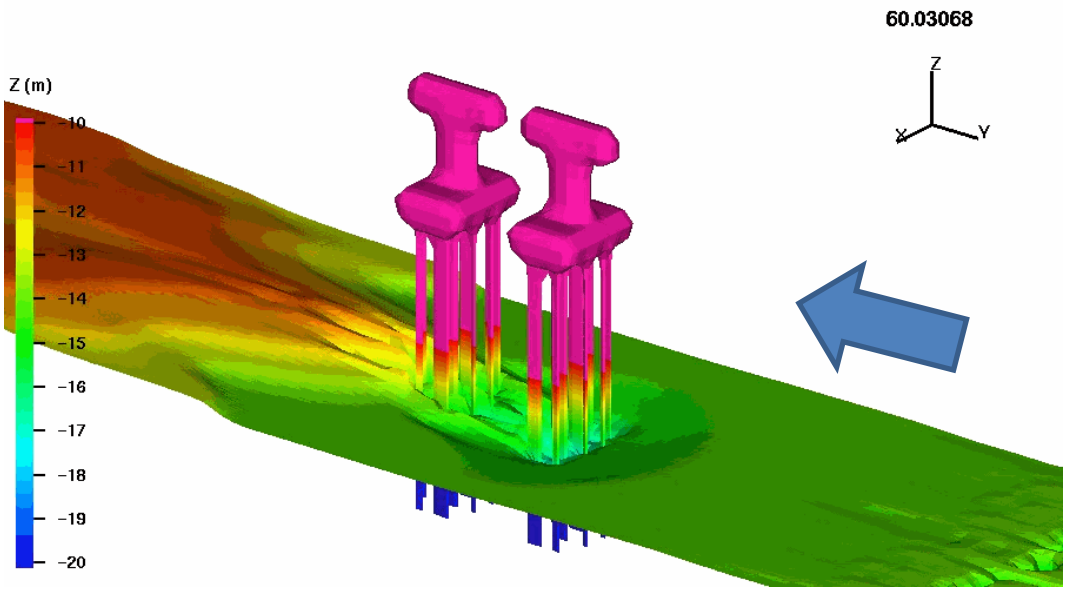

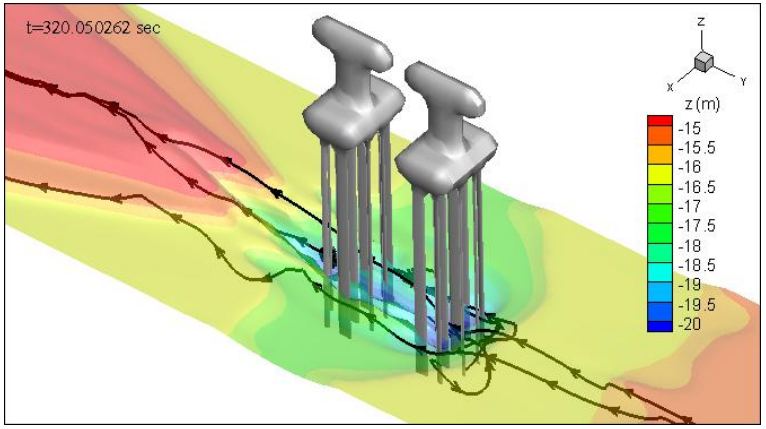

Comparison to the Field Survey Data

Maximum Scour Depth:

Right in front of the bridge piers:

Field survey: about 23 m.

Numerical: 23 m.

30 m upstream away from the bridge piers:

Field survey: 15 m

Numerical: 15 m

地電阻法

（Electrical Resistivity Tomography, ERT）

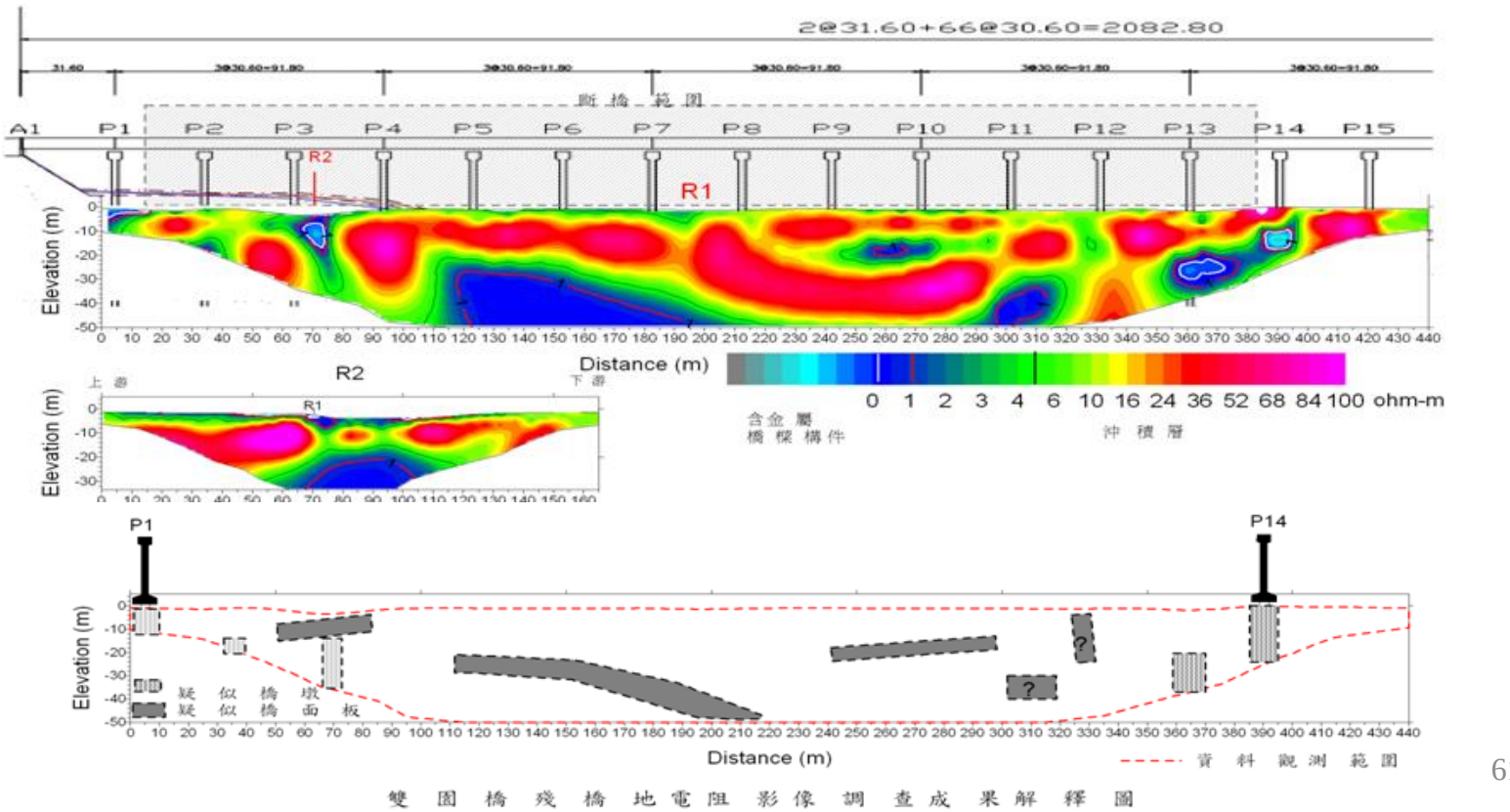

計算域設置

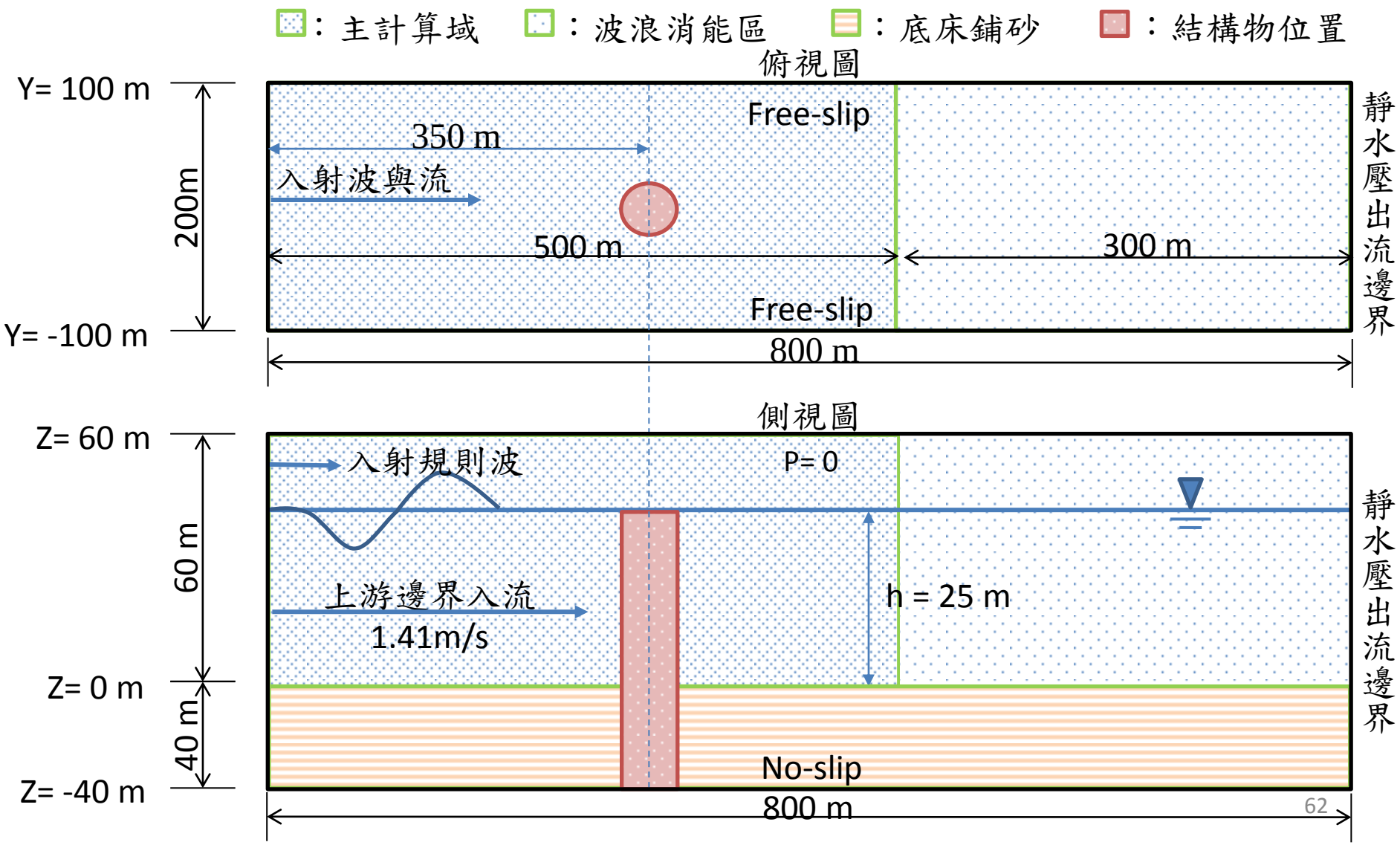
：主計算域
：波浪消能區
：底床鋪砂
：結構物位置
俯視圖
Y= 100 m
Y= -100 m
200m
350 m
入射波與流
Free-slip
500 m
300 m
Free-slip
800 m
靜水壓出流邊界
側視圖
Z= 60 m
Z= 0 m
Z= -40 m
60 m
40 m
入射規則波
P= 0
上游邊界入流
1.41m/s
h = 25 m
No-slip
800 m
靜水壓出流邊界

不同海流攻角之比較：0° V.S. 45°

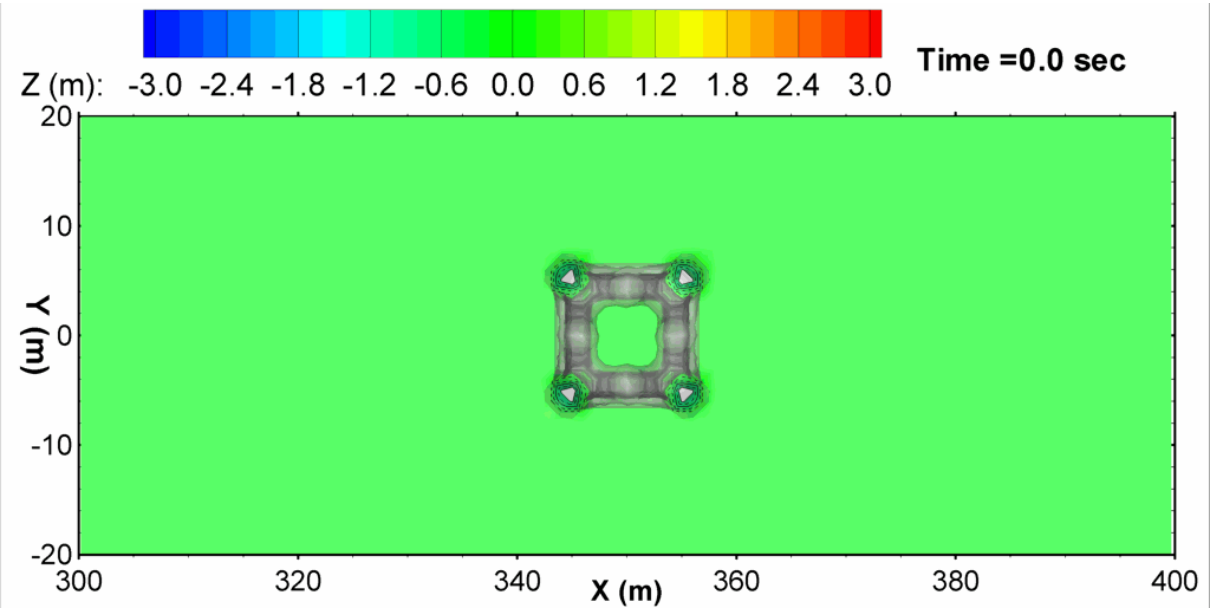

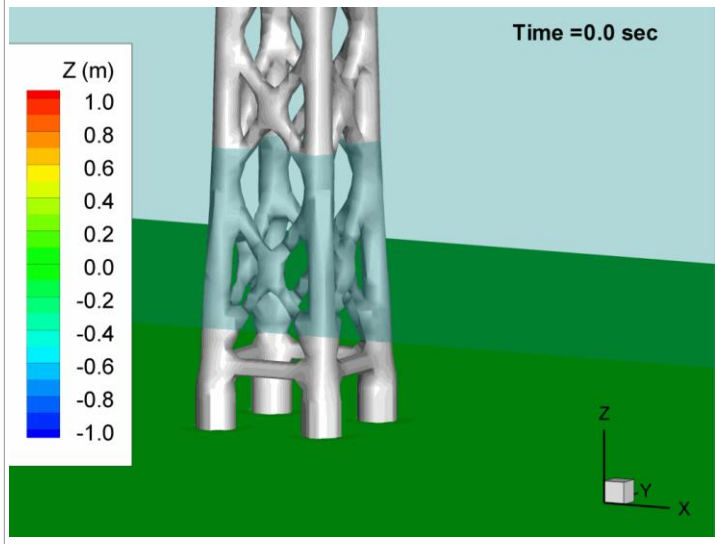

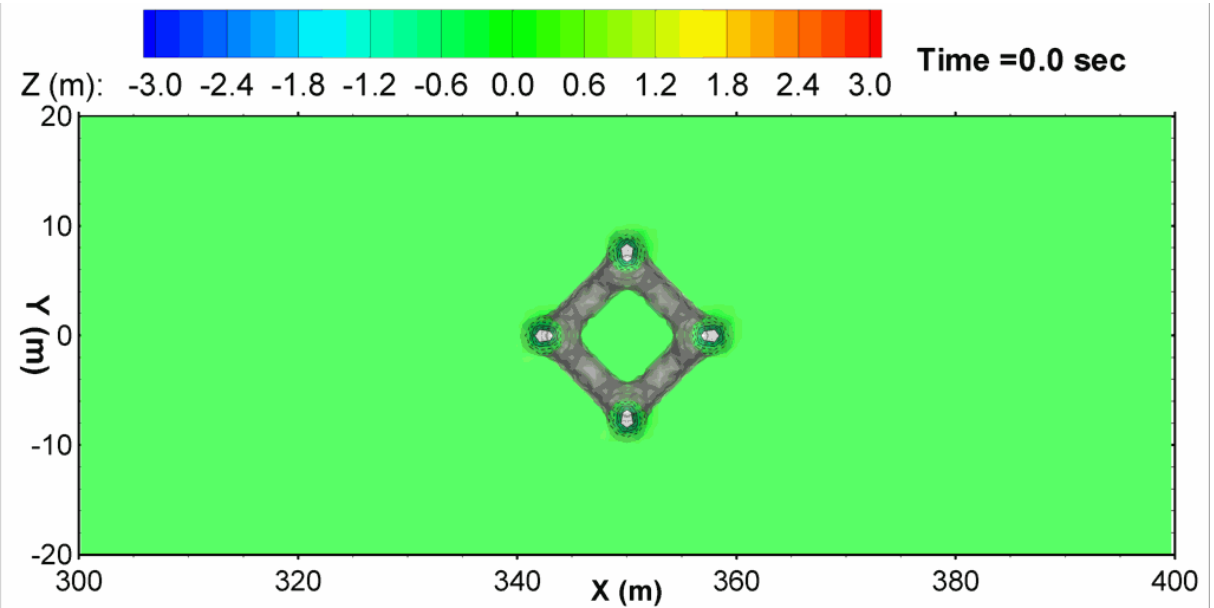

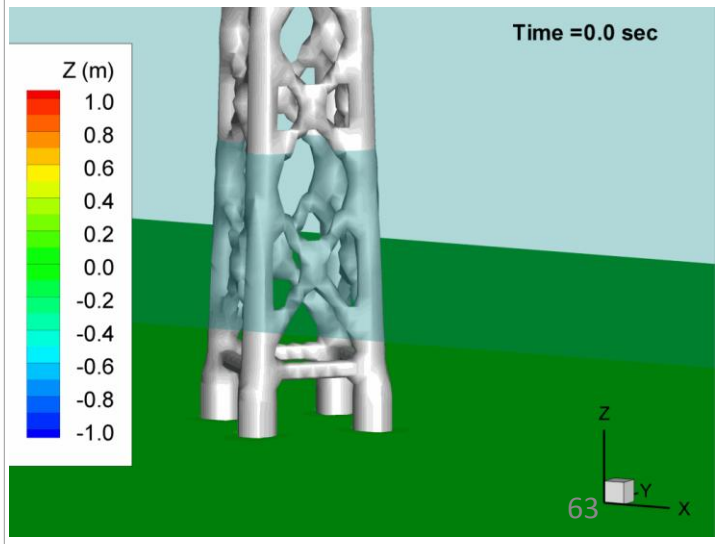

Advance visualization collaboration in DMCC with Leibniz Supercomputing Center (lrz), with Dr. Dieter Kranzlmueller and his crews

Move on to the next stage, for a real case,

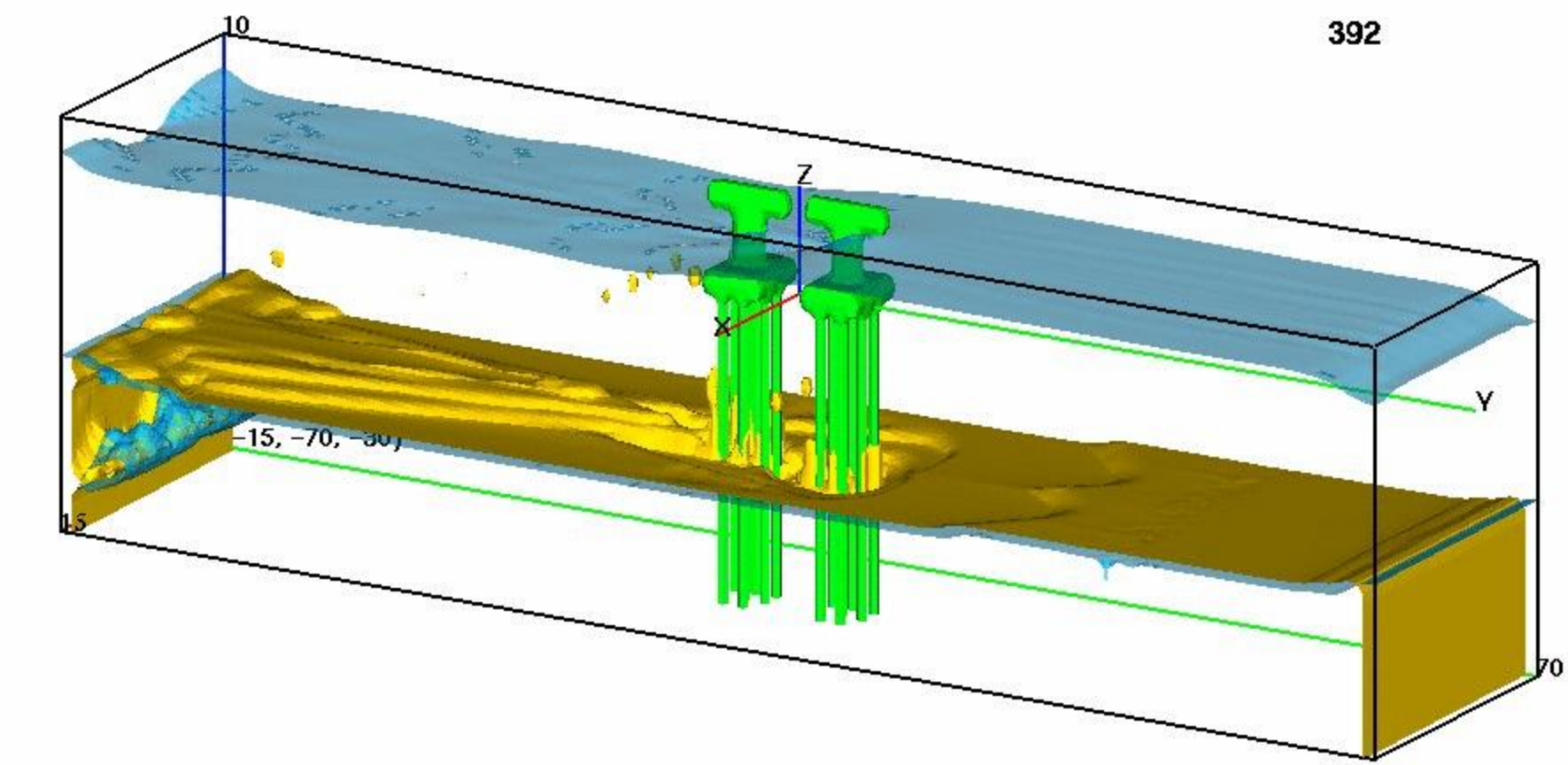

(Shuang Yuan Bridge, x-axis mirrored)
Water vof = 0.5
Bridge vof = 0.3
Mud vof = 0.1 (in order to see suspension)

Simulation done by YuHung

DMCC advanced visualization

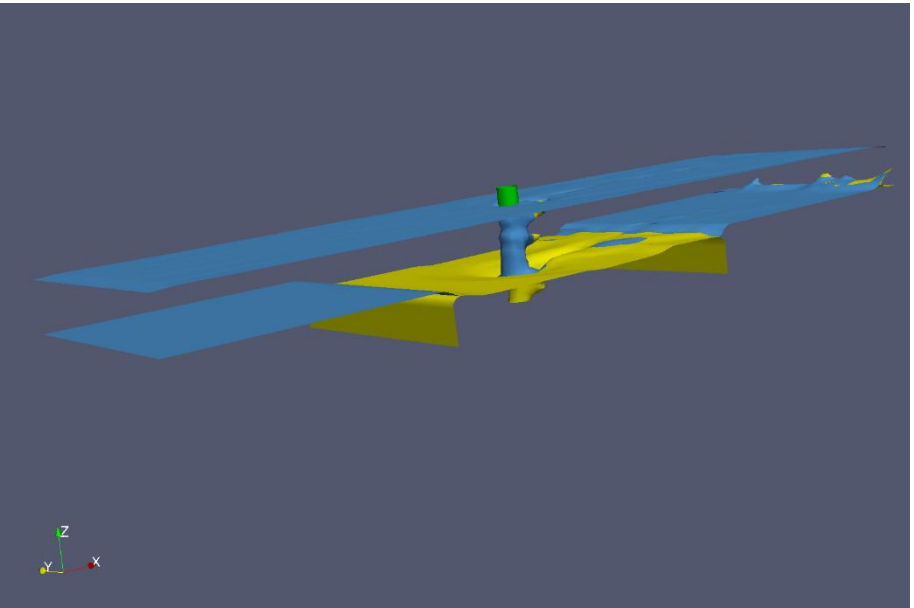

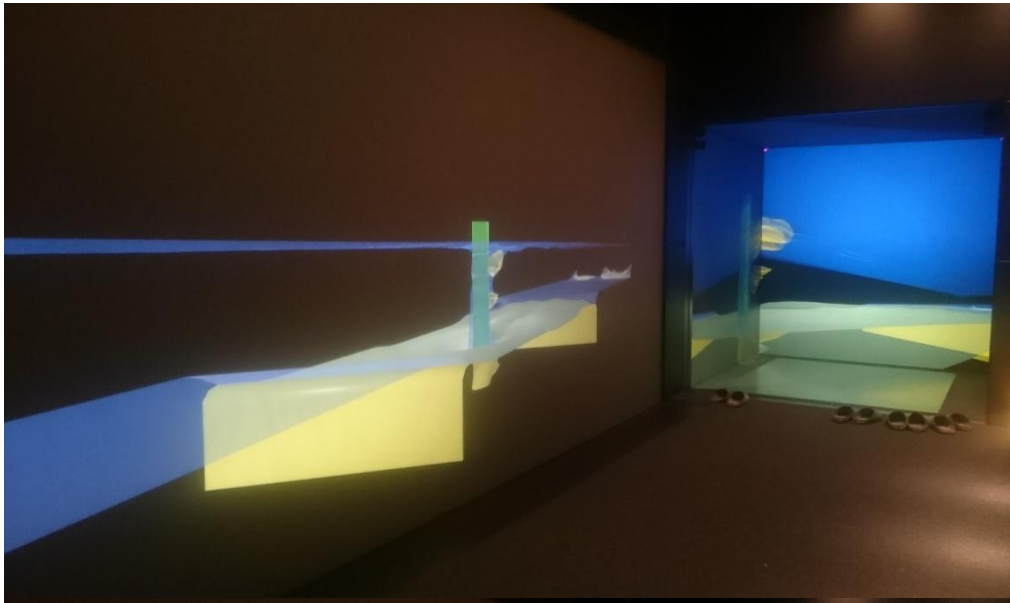

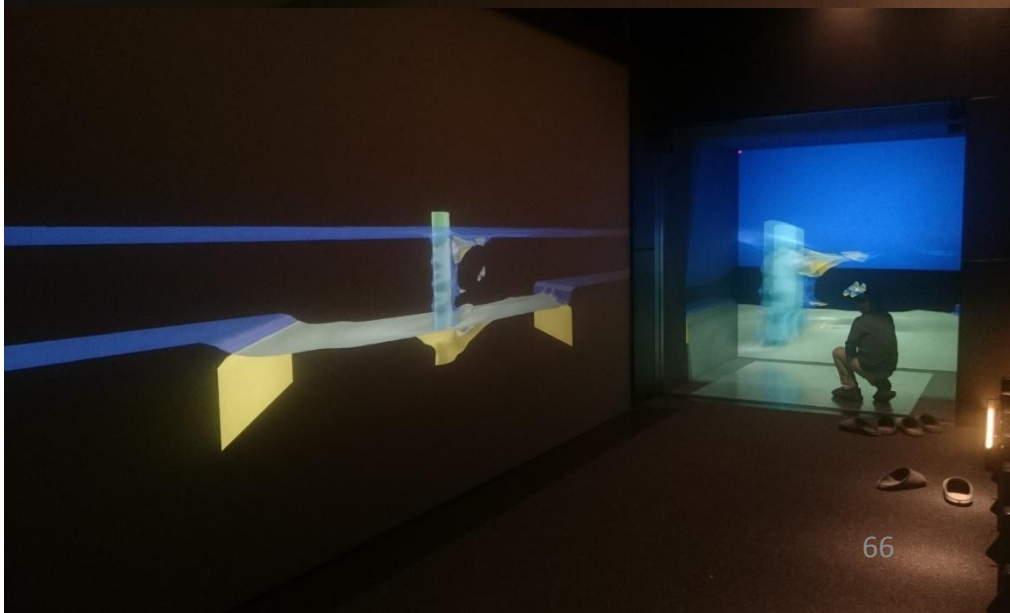

DMCC advanced visualization (short film)

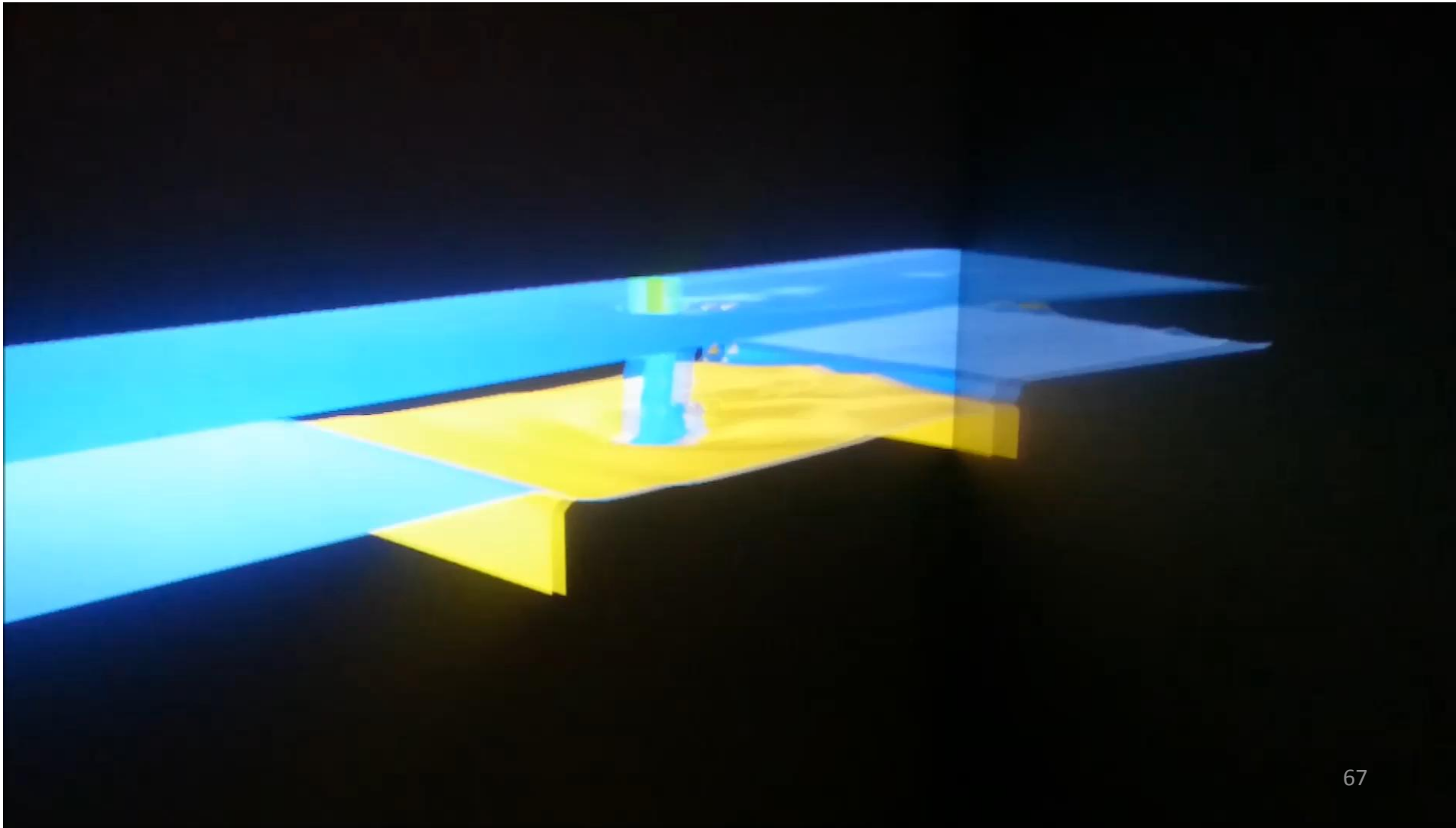

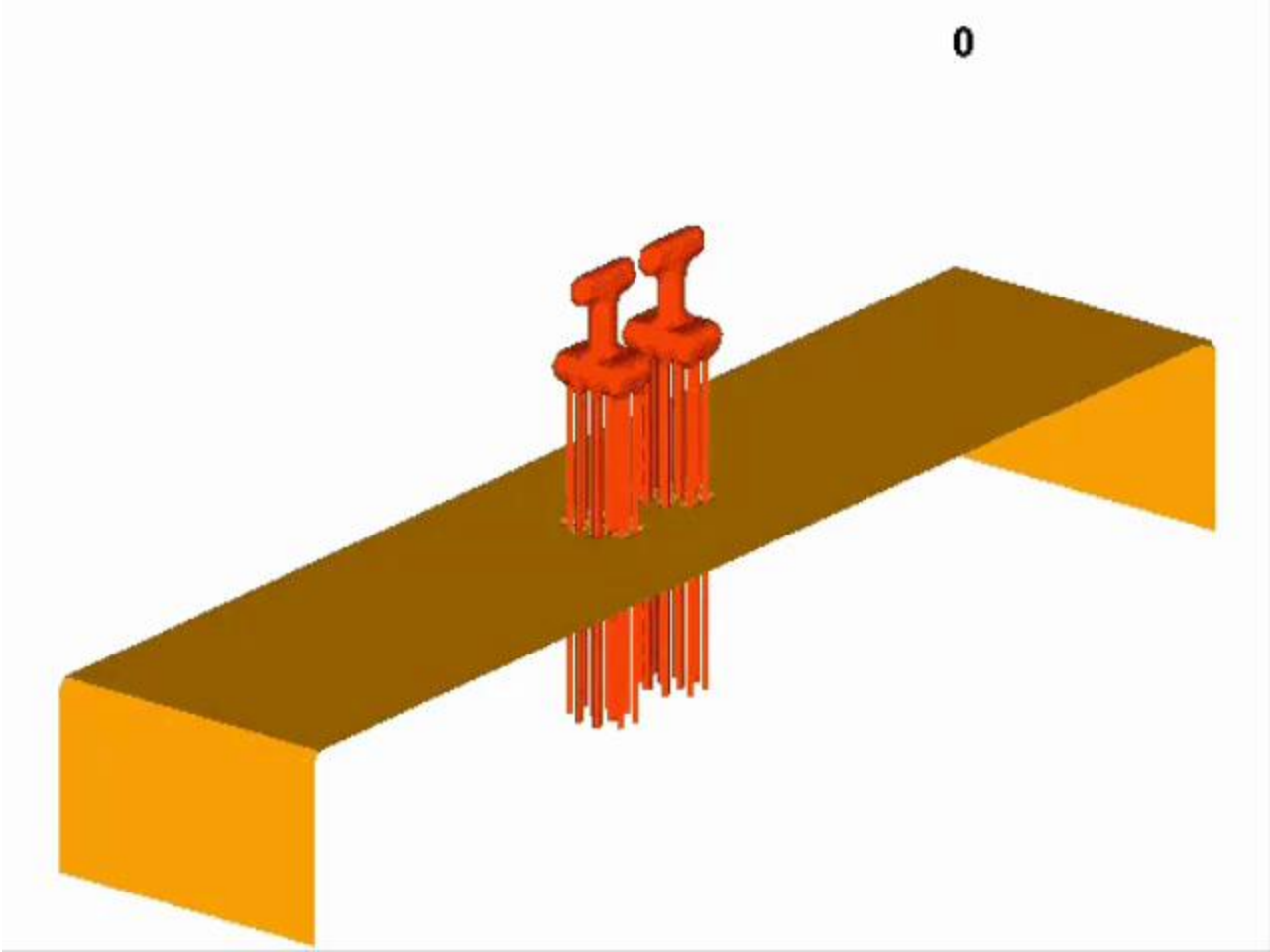
0

Dirty harbor in Japan?

T2 (Manila Trench 1) (Animation)

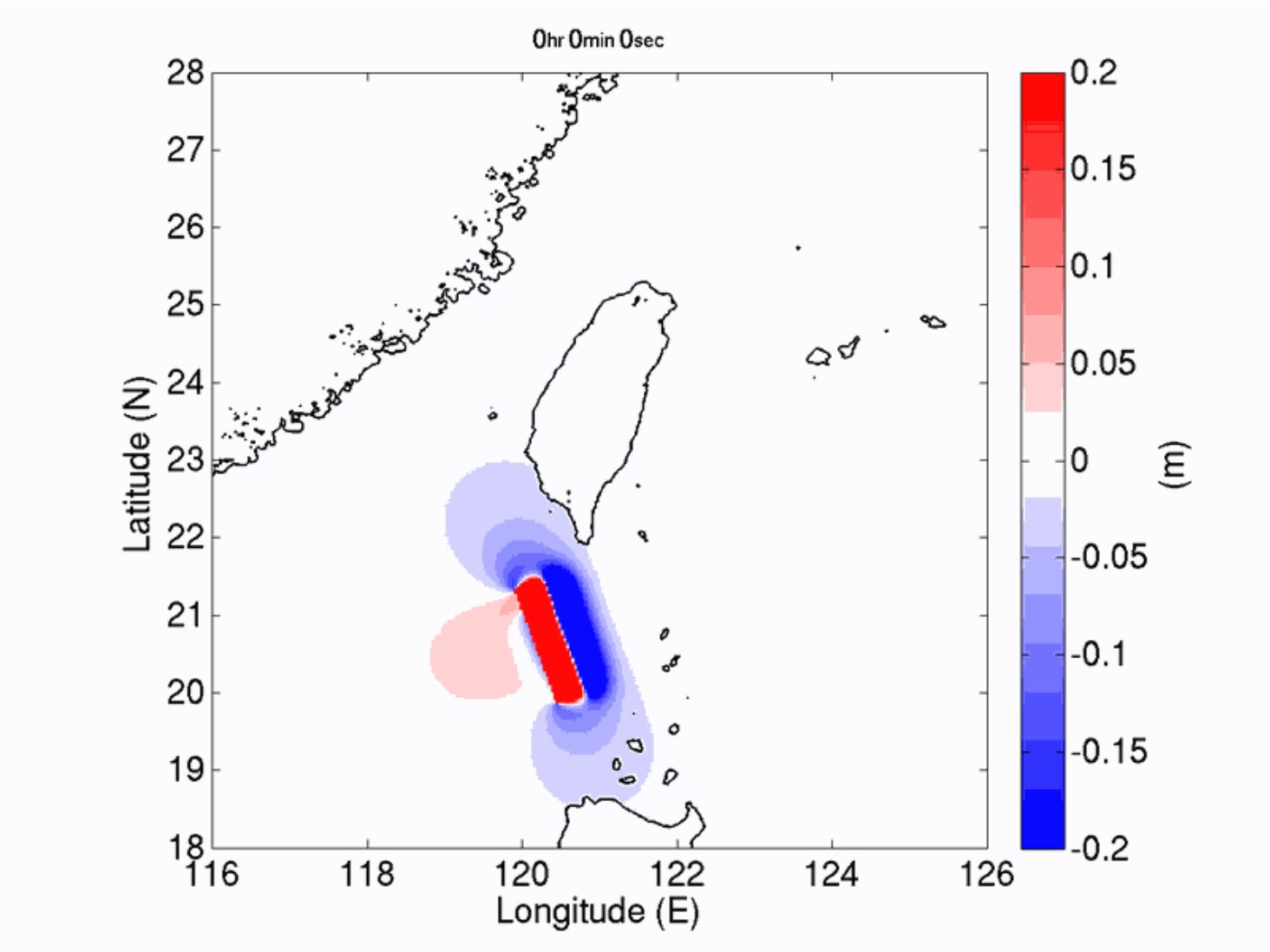

T02, Inundation and Maximum Runup Height

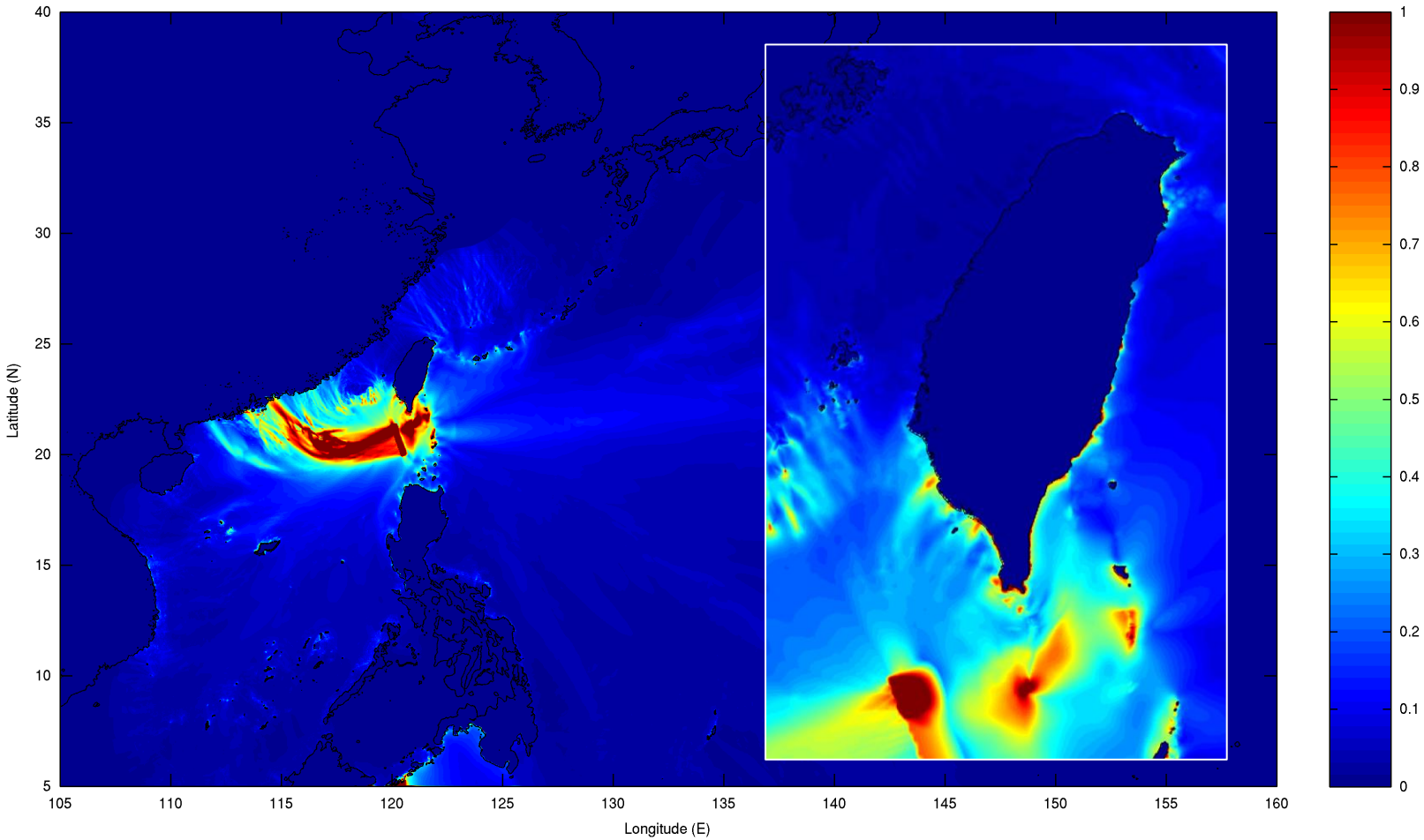

T02, Nearshore Inundation and Maximum Runup Height

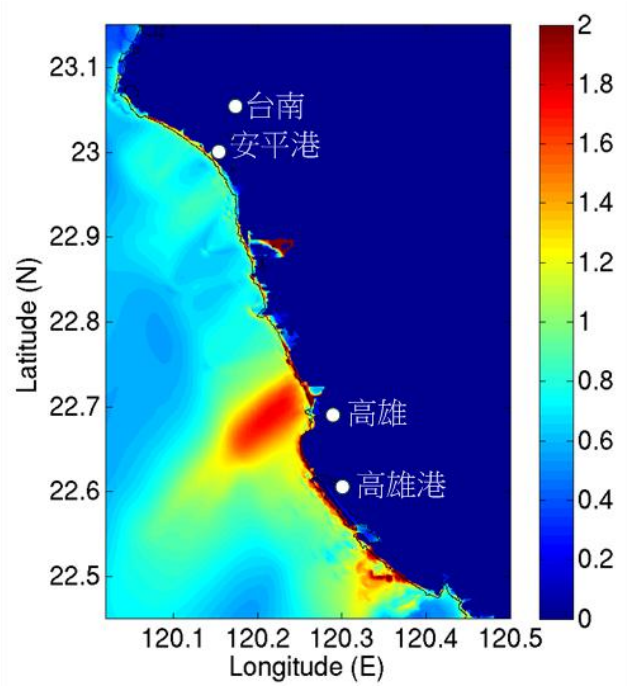

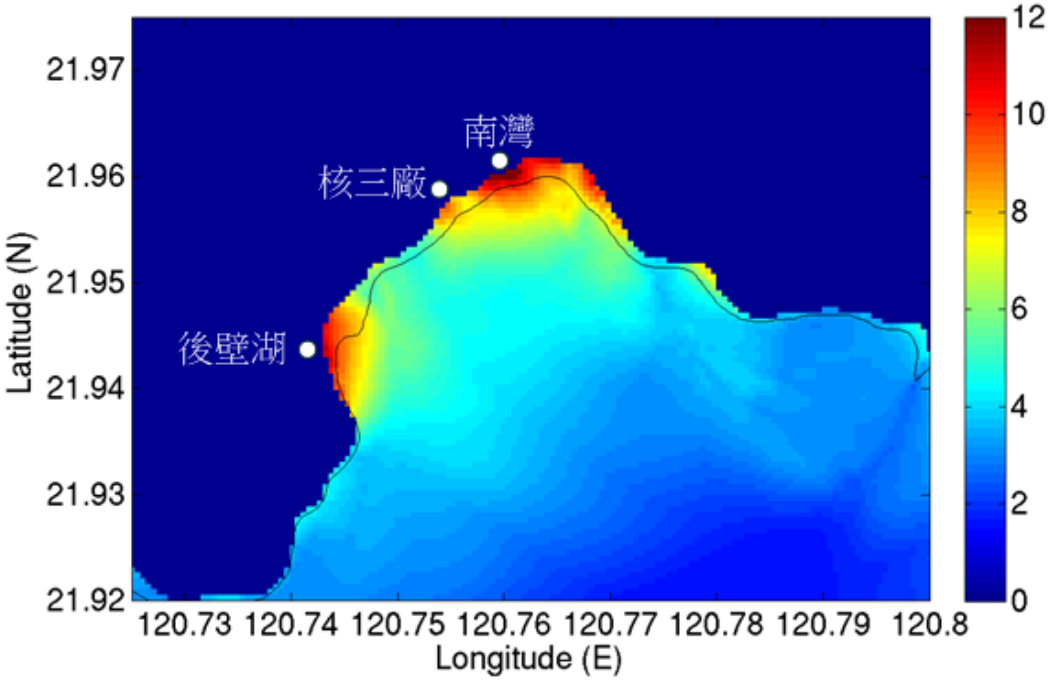

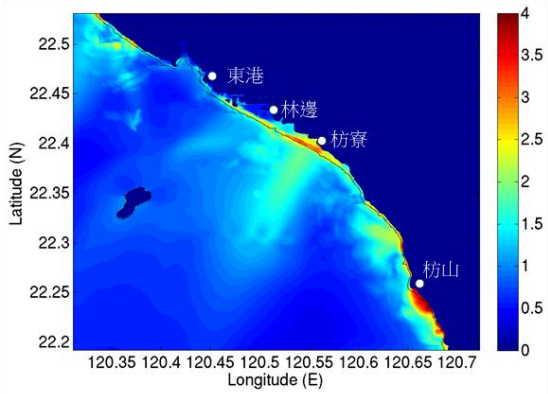

核三廠溯昇高達10~12公尺，墾丁南灣達18公尺

The First National-wide Tsunami Drill in Taiwan in 2014/9/19

台灣電力公司

核一、二及三廠增設防海嘯牆規劃設計

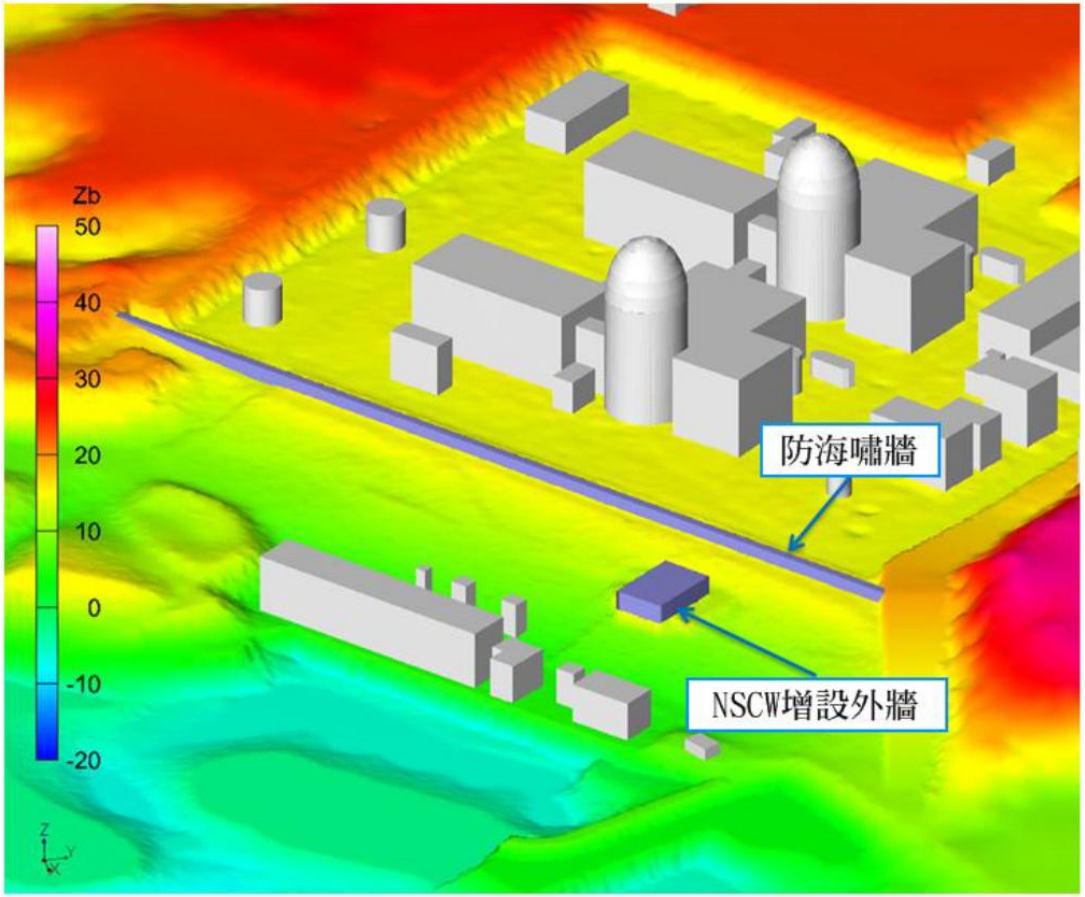

Conclusion

- Discontinuous Bi-viscous Model (DBM) is able to describe mud slide and the development of 3D scour hole.
- Quadratic DBM is able to describe mud and sediment motions.
- Combining with VOF model, we are able to simulate the complex local scour problem with only 3 property parameters.
- Very accurate results are presented.
- This model can be used on many practical problems, such as landslide, mudslide, local scour problems.

- Thanks for listening. Any questions for Prof. WU?吳祚任？

Storm Surge Modeling

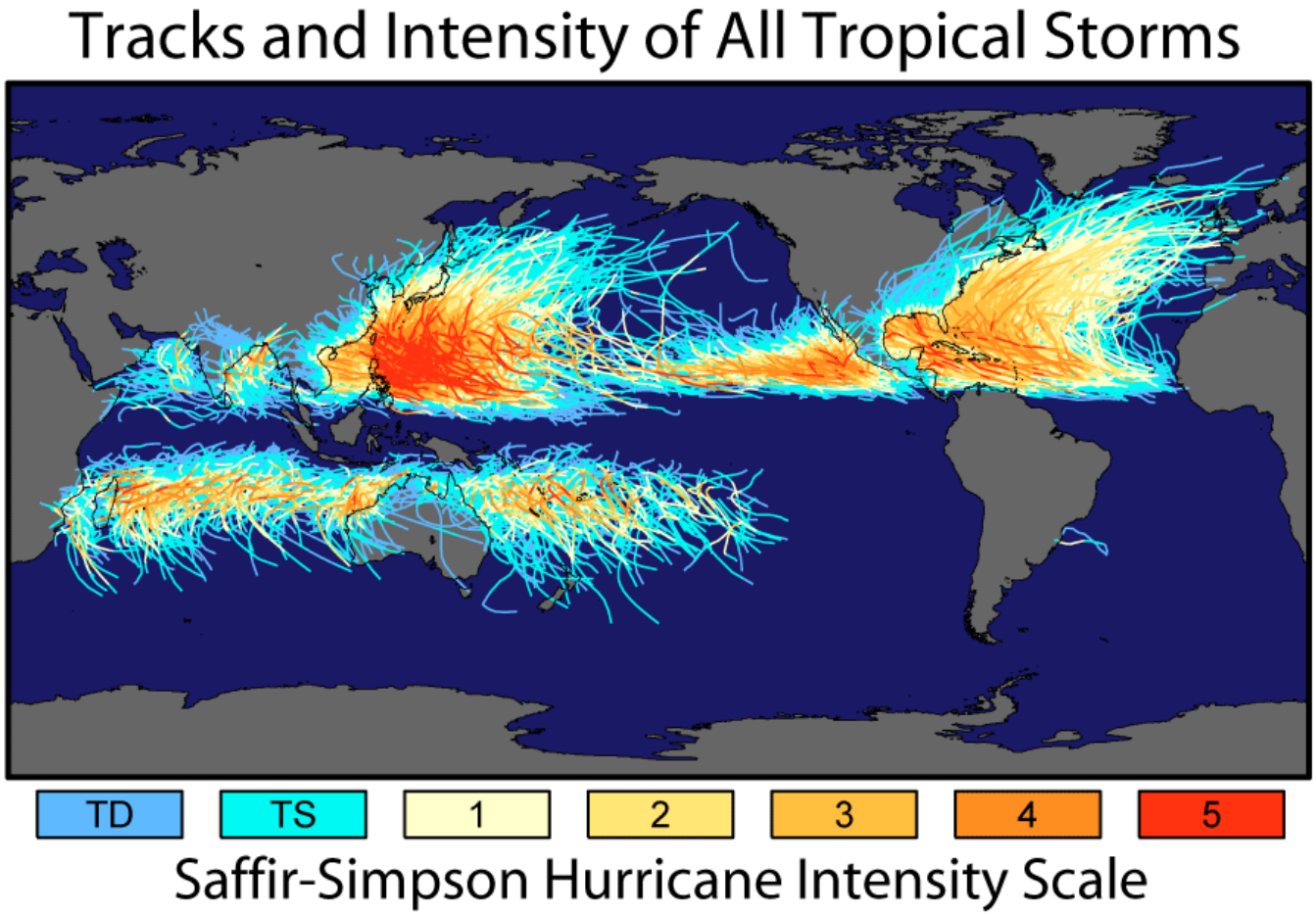

http://eoimages.gsfc.nasa.gov/images/imagerecords/7000/7079/tropical_cyclone_map.gif

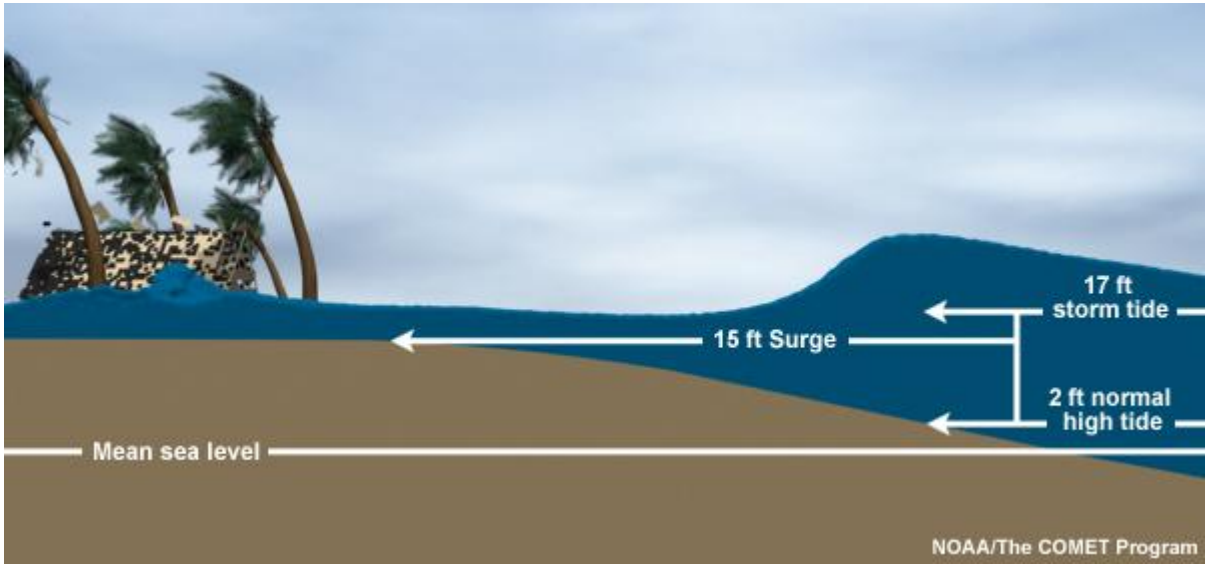

Storm Surge vs. Storm Tide

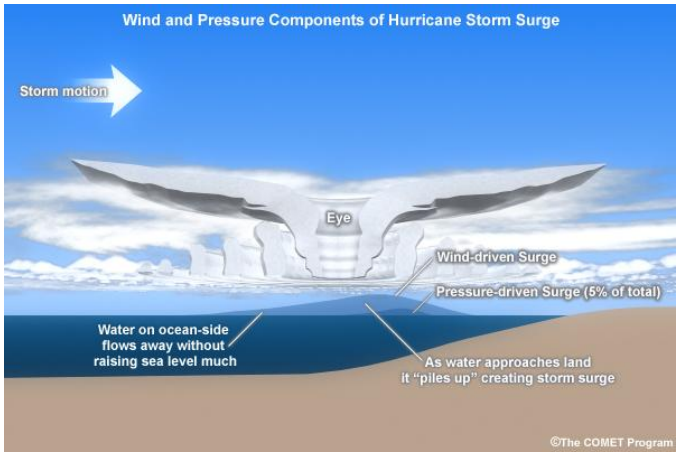

Wind and Pressure Components of Hurricane Storm Surge

COMCOT Storm Surge Fast Calculation System

(Cornell Multi-grid Coupled Tsunami Model – Storm Surge)

Nonlinear Shallow Water Equations in Spherical Coordinate

$$\frac{\partial \eta}{\partial t} + \frac{1}{R\cos\varphi}\left\{\frac{\partial P}{\partial \psi} + \frac{\partial}{\partial \varphi}(\cos\varphi \cdot Q)\right\} = 0$$

$$\frac{\partial P}{\partial t} + \frac{1}{R\cos\varphi}\frac{\partial}{\partial \psi}\left(\frac{P^2}{H}\right) + \frac{1}{R}\frac{\partial}{\partial \varphi}\left(\frac{PQ}{H}\right) + \frac{gH}{R\cos\varphi}\frac{\partial \eta}{\partial \psi} - fQ + F_\psi^b = -\frac{H}{\rho_w R\cos\varphi}\frac{\partial P_a}{\partial \psi} + \frac{F_\psi^s}{\rho_w}$$

$$\frac{\partial Q}{\partial t} + \frac{1}{R\cos\varphi}\frac{\partial}{\partial \psi}\left(\frac{PQ}{H}\right) + \frac{1}{R}\frac{\partial}{\partial \varphi}\left(\frac{Q^2}{H}\right) + \frac{gH}{R}\frac{\partial \eta}{\partial \varphi} + fP + F_\varphi^b = -\frac{H}{\rho_w R}\frac{\partial P_a}{\partial \psi} + \frac{F_\varphi^s}{\rho_w}$$

- Solve shallow water equations on both spherical and Cartesian coordinate systems
- Explicit leapfrog Finite Difference Method for stable and high speed calculation
- Multi/Nested-grid system for multiple shallow water wave scales
- Moving Boundary Scheme for inundation
- High-speed efficiency

• Moving Boundary Scheme

Moving boundary scheme was also introduced in COMCOT to model the run-up and run-down. The instant "shoreline" is defined as the interface between a dry grid and wet grid and volume flux normal to the interface is assigned to zero.

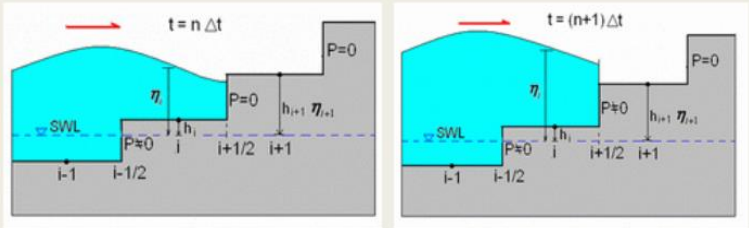

Fig.02 Moving Boundary Scheme

Coupled with TPXO global tide model

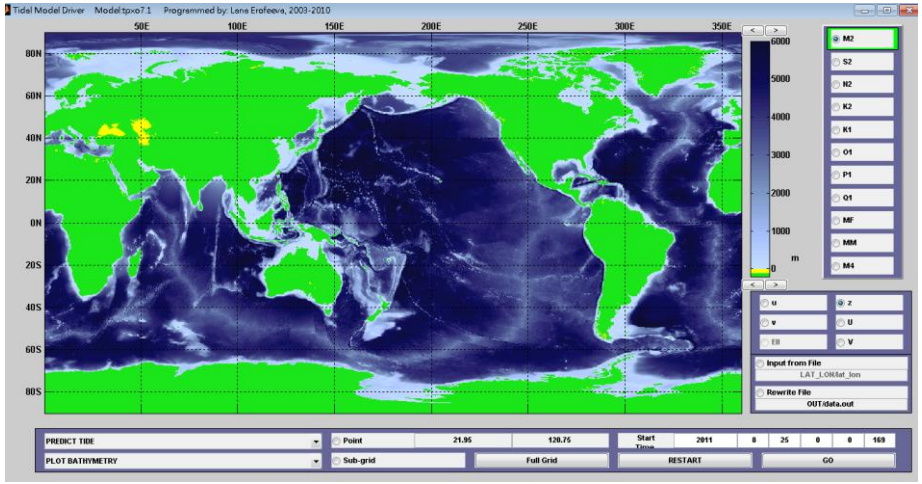

TPXO操作介面

The tides are provided as complex amplitudes of earth-relative sea-surface elevation for eight primary (M2, S2, N2, K2, K1, O1, P1, Q1), two long period (Mf,Mm) and 3 non-linear (M4, MS4, MN4) harmonic constituents, on a 1440x721, 1/4 degree resolution full global grid (for versions 6.* and later).

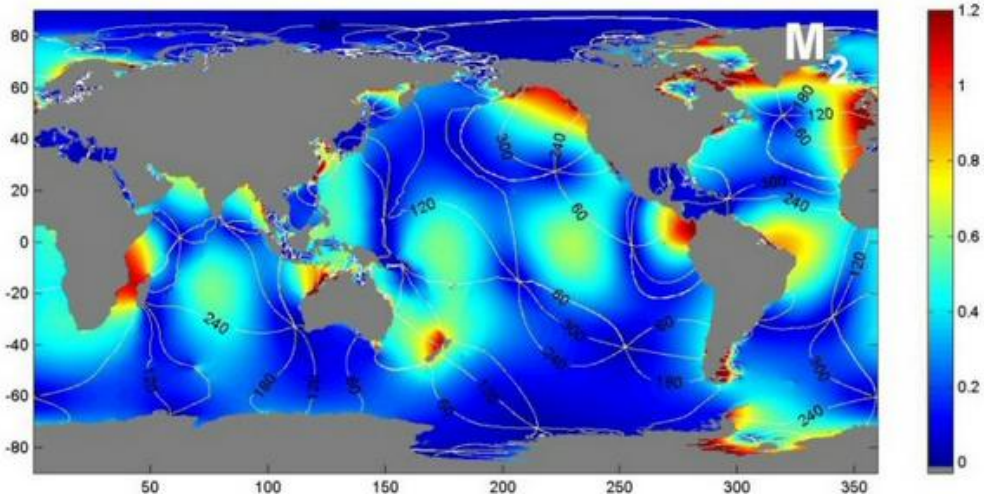

提供各種不同分潮資訊，以M2分潮為例

A TOPEX/POSEIDON global tidal model (TPXO.2) and barotropic tidal currents determined from long-range acoustic transmissions

Brian D. Dushaw[1], Gary D. Egbert[2], Peter F. Worcester[3], Bruce D. Cornuelle[3], Bruce M. Howe[1] and Kurt Metzger[4]

[1]*Applied Physics Laboratory, College of Ocean and Fishery Sciences, University of Washington, Seattle, WA, U.S.A.*
[2]*College of Oceanic and Atmospheric Sciences, Oregon State University, Corvallis, OR, U.S.A.*
[3]*Scripps Institution of Oceanography, La Jolla, CA, U.S.A.*
[4]*Department of Electrical Engineering and Computer Science, University of Michigan, Ann Arbor, MI, U.S.A.*

Abstract – Tidal currents derived from the TPXO.2 global tidal model of Egbert, Bennett, and Foreman are compared with those determined from long-range reciprocal acoustic transmissions. Amplitudes and phases of tidal constituents in the western North Atlantic are derived from acoustic data obtained in 1991–1992 using a pentagonal array of transceivers. Small, spatially coherent differences between the measured and modeled tidal harmonic constants mostly result from smoothing assumptions made in the model and errors caused in the model currents by complicated topography to the southwest of the acoustical array. Acoustically measured harmonic constants (amplitude, phase) of M_2 tidal vorticity ($3–8 \times 10^{-9}$ s^{-1}, 210–310°) agree with those derived from the TPXO.2 model ($2–5 \times 10^{-9}$ s^{-1}, 250–300°), whereas harmonic constants of about ($1–2 \times 10^{-9}$ s^{-1}, 350–360°) are theoretically expected from the equations of motion. Harmonic constants in the North Pacific Ocean are determined using acoustic data from a triangular transceiver array deployed in 1987. These constants are consistent with those given by the TPXO.2 tidal model within the uncertainties. Tidal current harmonic constants determined from current meters do not generally provide a critical test of tidal models. The tidal currents have been estimated to high accuracy using long-range reciprocal acoustic transmissions; these estimates will be useful constraints on future global tidal models.

(Dushaw et al., 1997)

High resolution at nearshore region

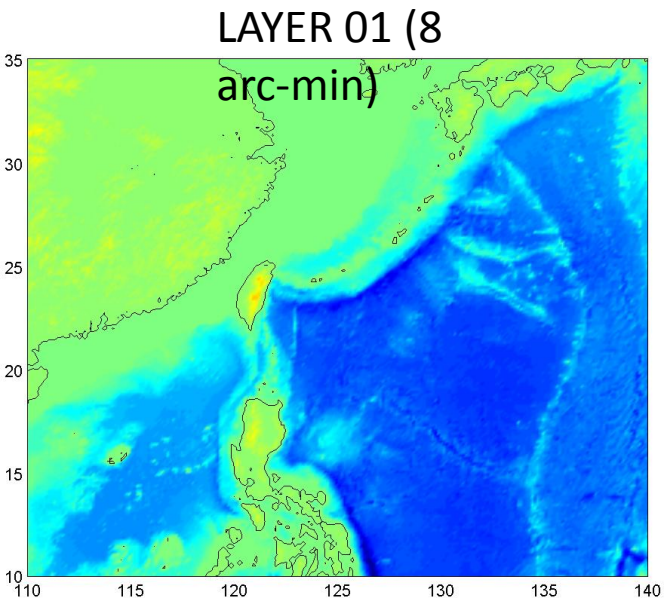

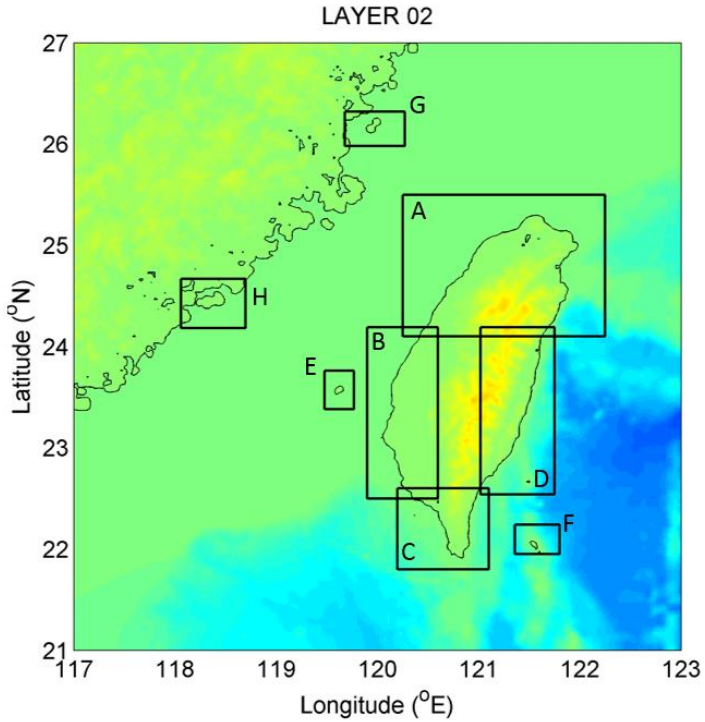

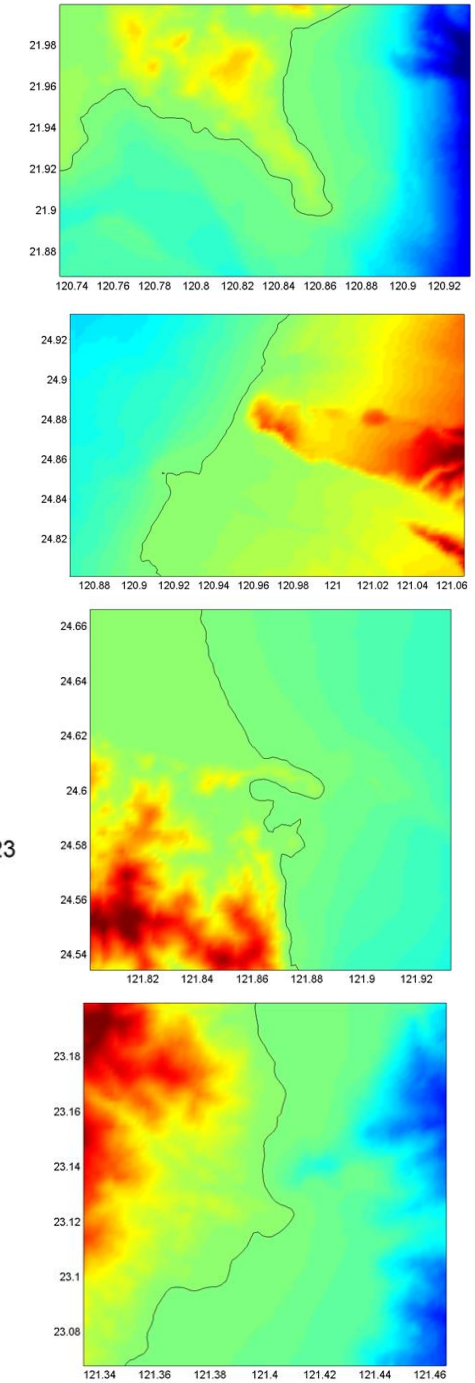

計算網格編號	經度方向範圍（oE）	緯度方向範圍（oN）	解析度
LAYER 01	110.0 – 134.0	10.0 – 35.0	8 arc-min
LAYER 02-A	120.25 - 122.25	24.10 - 25.50	4 arc-min
LAYER 02-B	119.90 -120.60	22.50 - 24.19	4 arc-min
LAYER 02-C	120.20 -121.10	21.80 - 22.60	4 arc-min
LAYER 02-D	121.02 -121.75	22.54 - 24.19	4 arc-min
LAYER 02-E	119.48 -119.77	23.38 - 23.76	2 arc-min
LAYER 02-F	121.36 -121.80	21.95 - 22.24	1 arc-min
LAYER 02-G	119.68 - 120.27	25.98 - 26.32	2 arc-min
LAYER 02-H	118.06 - 118.70	24.18 - 24.67	2 arc-min
LAYER 03（南灣）	120.725 - 120.990	21.862 - 22.029	0.01 arc-min
LAYER 03（新竹）	120.837 - 121.085	24.765 - 24.951	0.01 arc-min
LAYER 03（蘇澳）	121.812 - 121.945	24.509 - 24.675	0.01 arc-min
LAYER 03（成功）	121.297 - 121.524	23.014 - 23.254	0.01 arc-min

Validation on the tide height

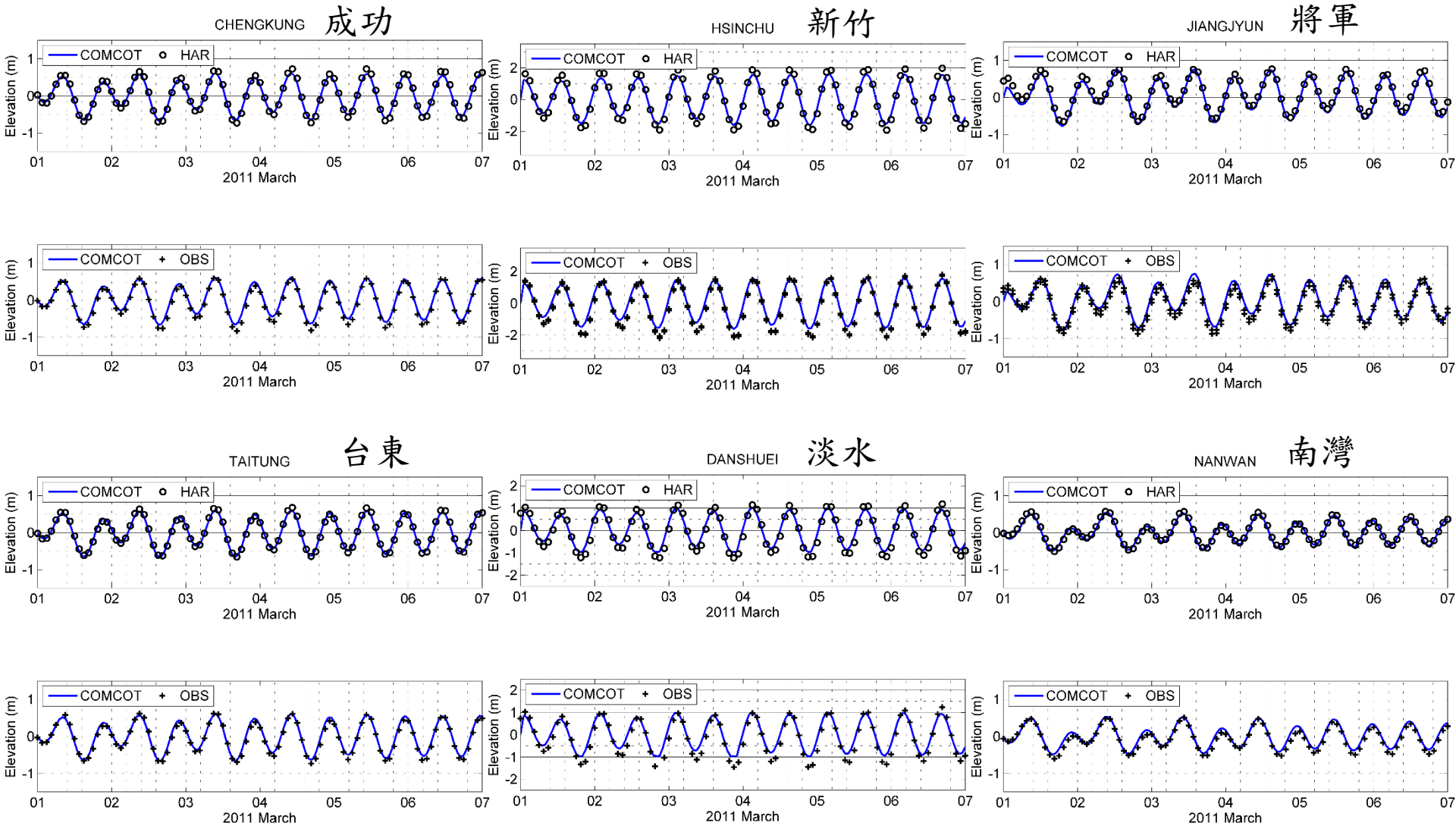

2013 Typhoon Fitow (第一類路徑)

- 颱風菲特（Typhoon Fitow）於2013年9月27日於帛琉北部海面上生成，以西北方向朝臺灣北部海面前進；於2013年10月3日轉變為中度颱風，7日由福建、浙江交界進入中國大陸，最後於10月7日轉變為熱帶性低氣壓；為第1類侵臺路徑。

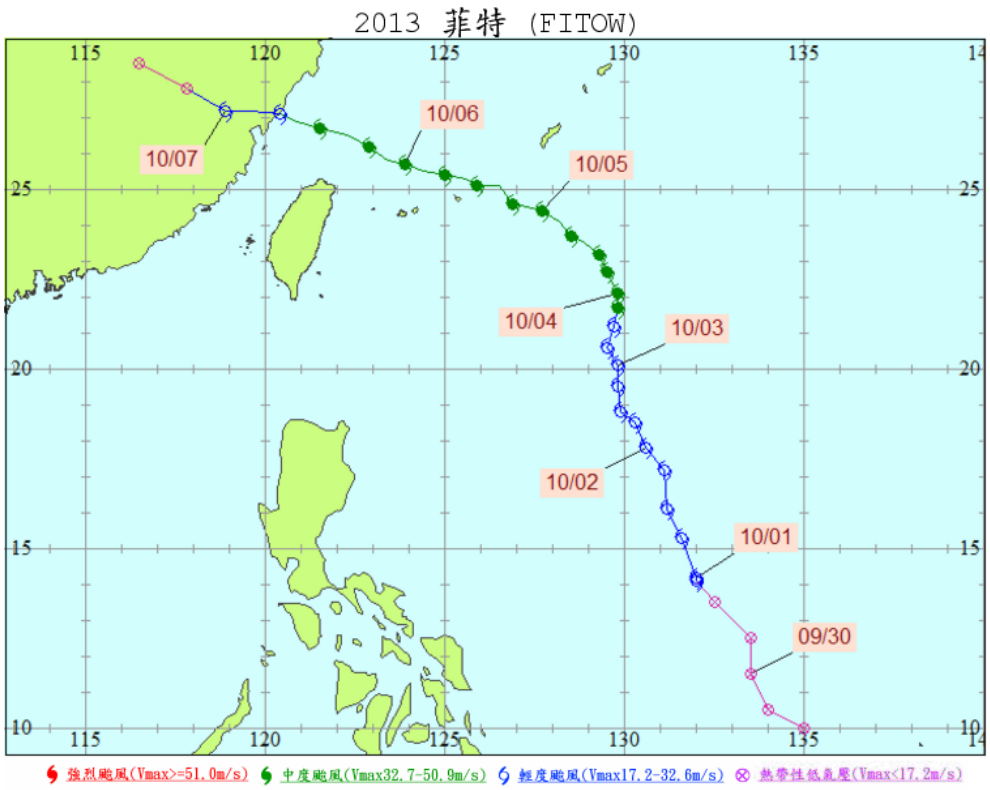

取自中央氣象局 颱風資料庫

2013 Typhoon Fitow

2013.10.01 00:00 – 2013.10.07 00:00 (UTC+0)

Total Time :518400 sec (~7 days)
Time Step : 8 sec
Resolution : 8/4/0.1 arc-min

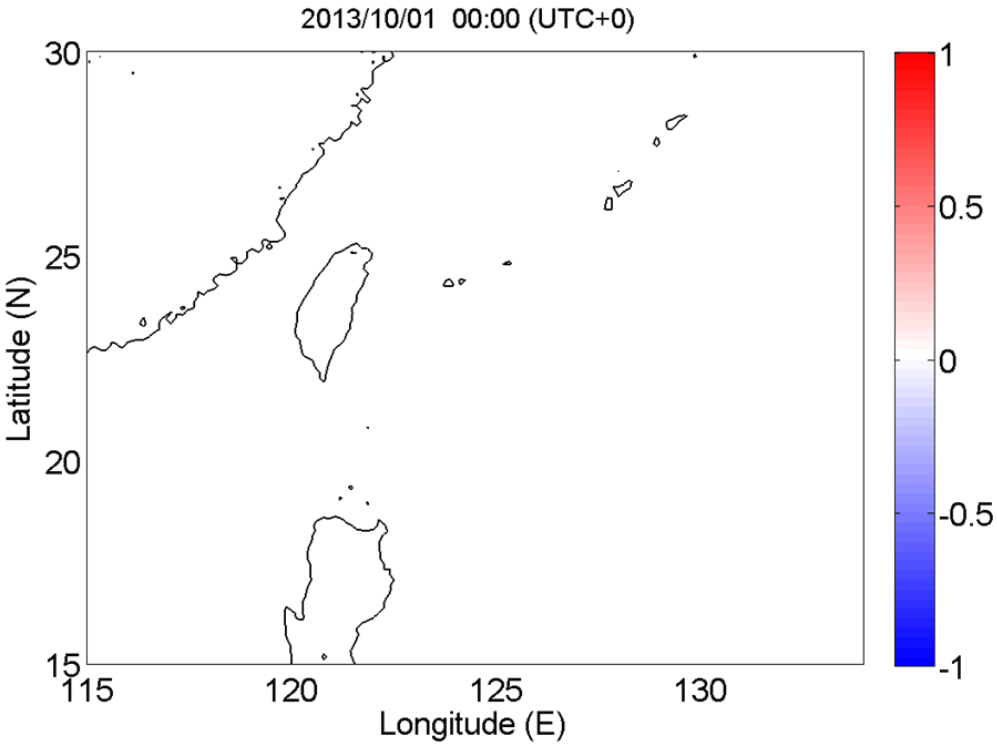

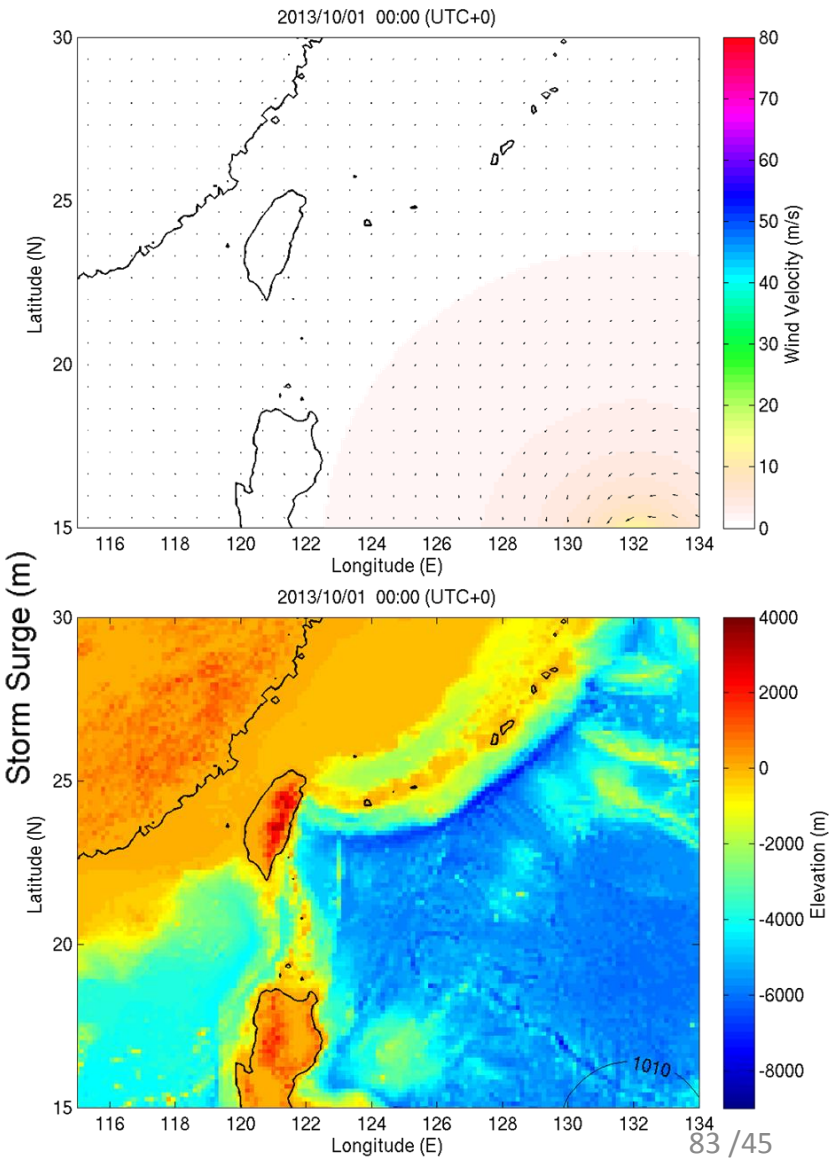

2013 Typhoon Fitow

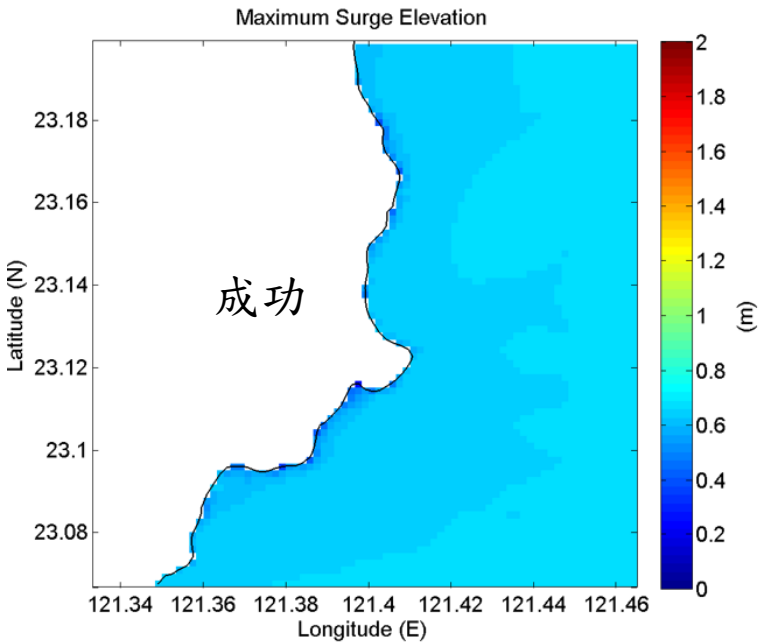

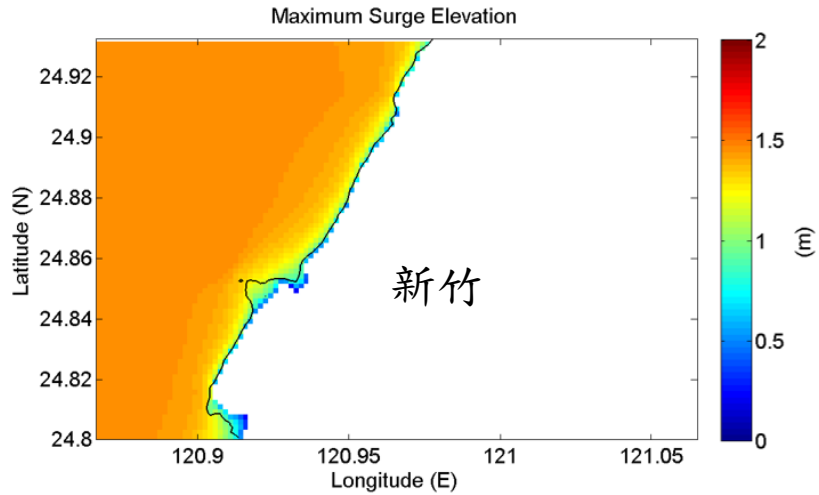

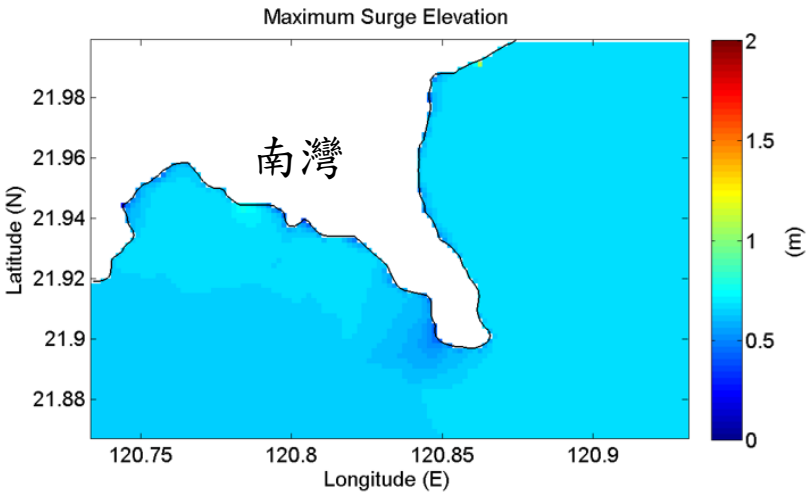

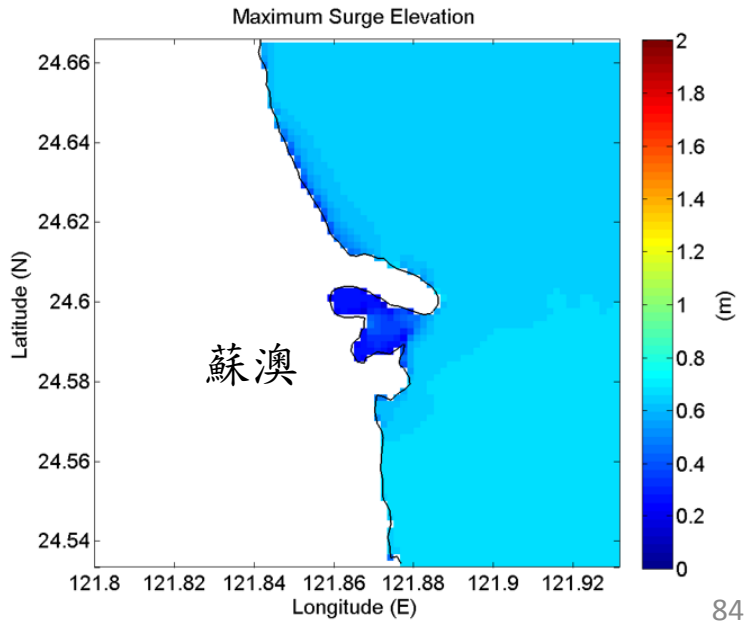

潮位計資料比對（菲特颱風）